DUAL FUNCTIONALIZED LIPOSOMES FOR CO-DELIVERY OF ANTI-CANCER CHEMOTHERAPEUTICS FOR TREATMENT OF BRAIN TUMOR

A Dissertation
Submitted to the Graduate Faculty
of the
North Dakota State University
of Agriculture and Applied Science

By

Sushant Lakkadwala

In Partial Fulfillment of the Requirements
for the Degree of
DOCTOR OF PHILOSOPHY

Major Department:
Pharmaceutical Sciences

March 2019

Fargo, North Dakota

North Dakota State University
Graduate School

Title

Dual functionalized liposomes for co-delivery of anti-cancer chemotherapeutics for treatment of brain tumor

By

Sushant Lakkadwala

The Supervisory Committee certifies that this ***disquisition*** complies with North Dakota State University's regulations and meets the accepted standards for the degree of

DOCTOR OF PHILOSOPHY

SUPERVISORY COMMITTEE:

Dr. Jagdish Singh
Chair

Dr. Chengwen Sun

Dr. Yagna Jarajapu

Dr. Megan Orr

Approved:

03/27/2019
Date

Dr. Jagdish Singh
Department Chair

ABSTRACT

Glioblastoma is a hostile brain tumor associated with high infiltration leading to poor prognosis. Currently available treatment options are insufficient to increase median survival time. The combination therapy has emerged as an efficient way to deliver chemotherapeutics for treatment of glioblastoma. It provides collaborative approach of targeting cancer cells by acting *via* multiple mechanisms, thereby reducing drug resistance. However, the presence of selective and impermeable blood brain barrier (BBB) restricts the delivery of chemotherapeutic drugs into the brain. To overcome this limitation, we designed a dual functionalized liposomes by modifying their surface with transferrin (Tf) and a cell penetrating peptide (CPP) for receptor and adsorptive mediated transcytosis, respectively. In this study, we used various CPPs based on their physicochemical properties (TAT, penetratin, QLPVM and PFVYLI) and investigated the influence of insertion of CPP to Tf-liposomes on cytotoxic potential, cellular uptake, hemocompatibility and transport across the BBB both *in vitro* and *in vivo.* In addition, anti-tumor efficacy of dual functionalized liposomes was evaluated *in vitro* as well as *in vivo*. The liposomes were encapsulated with chemotherapeutics agents, doxorubicin and erlotinib for delivery to brain. Co-delivery of doxorubicin and erlotinib loaded Tf-CPP liposomes revealed significantly ($p < 0.05$) higher translocation more than 12 % across the co-culture endothelial barrier resulting in regression of tumor in the *in vitro* brain tumor model. The biodistribution of Tf-CPP liposomes demonstrated more than 10 and 2.7 fold increase in doxorubicin and erlotinib accumulation in mice brain, respectively compared to free drugs. Histological evaluation of tissue sections showed no signs of toxicity. In addition, Tf-Pen liposomes showed excellent antitumor efficacy by regressing ~90% of tumor in mice brain with significant increase in the median survival time (36 days). In conclusion, we have developed a high efficiency liposomal drug delivery carrier that can

cross the BBB and co-deliver doxorubicin and erlotinib to desired target tumor site *in vivo* in mice, thereby 1) increased concentration of chemotherapeutics in brain, 2) regression in glioblastoma tumor size, 3) reducing the possibility of drug resistance in cancer cells, without eliciting undesired toxicity.

ACKNOWLEDGEMENTS

First of all, I would like to express my deepest appreciation to my advisor, Dr. Jagdish Singh, for providing me an opportunity to be a part of his research group. His continuous support, guidance, constant motivation, patience and immense experience helped me during my PhD. Without his guidance and persistent help this dissertation would not have been possible.

I would also like to thank my committee members, Dr. Chengwen Sun, Dr. Yagna Jarajapu and Dr. Megan Orr for their support, motivation, encouragement and guidance.

I would like to convey my sincere thanks to my seniors, lab colleagues and fellow graduate student, Dr. Buddhadev Layek, Dr. Neha Singh, Dr. Tiecheng Zhong, Dr. Amrita Banerjee, Bruna Rodrigues, Divya Sharma, Sanjay Arora, Riddhi Trivedi, Shrinidh Joshi and Harshit Shah for their help and support. I also like to thank my friends Anurag Goswami, Kshitij Sharma, Kritika Sharma.

I wish to acknowledge all the faculty, staff and students of the department of Pharmaceutical Sciences for helping me directly or indirectly during my research.

I specially would like to acknowledge the help, support, assistance from Janet Krom, Diana Kowalski and Jean Trautmann during my studies at NDSU.

I gratefully acknowledge financial supports from the National Institutes of Health, the Department of Pharmaceutical Sciences, NDSU, and the North Dakota Established Program to Stimulate Competitive Research (ND EPSCoR).

Last but not the least, I would like to thank my family members, especially my brother and also my in-laws for their constant support, love, sacrifice, and understanding. Most importantly, I would like to thank my wife, Dr. Mithila Fadia for her love, support, sacrifice and always standing by me during my good and bad times.

DEDICATION

Dedicated to my mother,

Late Mrs. Lata Lakkadwala

and my father,

Mr. Ashok Lakkadwala.

TABLE OF CONTENTS

LIST OF TABLES

LIST OF FIGURES

LIST OF ABBREVIATIONS

5-FU 5-Fluorouracil

ADT..... Adsorptive mediated transcytosis

ANOVA..... Analysis of variance

BBB..... Blood brain Barrier

BCA..... Bicinchoninic acid

bEnd.3 ..... Brain endothelial cells

CHOL ..... Cholesterol

CHS ..... Cholesteryl hemisuccinate

CNS ..... Central nervous system

CPPs ..... Cell penetrating peptides

DMEM ..... Dulbecco's modified eagle medium

DMF ..... Dimethylformamide

DOPE 1, 2-dioleoyl-sn-glycero-3-phosphoethanolamine

DOTAP..... 1, 2-dioleoyl-3-trimethylammonium-propane chloride

DOX ..... Doxorubicin

DPBS..... Dulbecco's phosphate buffered saline

DSPE-$PEG_{(2000)}$-COOH..... 1,2-distearoyl-sn-glycero-3- phosphoethanolamine-N-[carboxy(polyethylene glycol)-2000]

EDC..... 1-Ethyl-3-(3-dimethylaminopropyl) carbodiimide

EE..... Entrapment efficiency

EGFR..... Epidermal growth factor receptor

ERLO ..... Erlotinib

EVOM2 ..... Epithelial voltohm meter

FBS..... Fetal bovine serum

FITC	Fluorescein isothiocyanate
GBM	Glioblastoma multiforme
H&E	Hematoxylin-eosin
HEPES	4-(2-hydroxyethyl)-1-piperazineethanesulfonic acid
HPLC	High performance liquid chromatography
kDa	kilo Dalton
MDPs	Multidrug resistance proteins
MTT	3-(4,5-dimethylthiazol-2-yl)-2,5-diphenyltetrazolium bromide
MWCO	Molecular weight cut off
Na-F	Sodium fluorescein
NHS	N-hydroxysuccinimide
NHS-PEG(2000)-DSPE	3-(N-succinimidyloxyglutaryl) aminopropyl, polyethyleneglycol-carbamyl distearoylphosphatidyl-ethanolamine
OCT	Optimal cutting temperature
PARP	Poly ADP ribose polymerase
PBS	Phosphate buffered saline
PDI	poly dispersity index
PEG	Polyethylene glycol
PET	Polyethylene terephthalate
PLGA	Poly (D, L-lactide-co-glycolide) 50:50
RMT	Receptor mediated transcytosis
RPM	Revolutions per minute
TEER	Transendothelial electrical resistance
TfR	Transferrin receptor

U87.. Glioblastoma cells

CHAPTER 1. INTRODUCTION

Drug delivery to brain has been a challenge for scientists due to major three hurdles: Blood brain barrier (BBB), the blood cerebrospinal fluid barrier and the blood tumor barrier. However, application of nanomedicine have shown improvement in delivering drug moieties across the BBB into the brain. The selectivity and impermeability of the BBB prevent the brain against unwanted substances including drug molecules. Regardless of advancement in the field of drug development in recent years and our understanding of molecular and receptor expression on the BBB, still a challenge for many of the untreated CNS associated diseases. This challenge can be overcome by a deliberated effort in understanding of physiology as well as its permeability under disease conditions. It is also important to understand the responses to physical and chemical stimuli as well as different receptors present of the BBB. The understanding of all these approaches give an insight into using a ligand mediated drug delivery into the brain.

Blood Brain barrier is a dynamic barrier with low and selective permeability of molecules in the brain. There are five major factors which control and restrict the entry of unwanted substances in the brain:

1. decreased rate of pinocytosis due to the absence of fenestra in the barrier, which restricts the entry of molecules from the luminal side of the barrier [1–3].
2. the intricate complexes between transmembrane proteins and cytoplasmic proteins of adjacent endothelial cells form a tight junction, which thereby sealing the intracellular gap between the adjacent endothelial cells. This tight junction is further supported by the presence of astrocytes and pericytes [4].
3. a combination effect of astrocyte, pericytes, neuron, astrocytic perivascular end feet and macrophages on the BBB prevents the uptake of molecules in the brain [5–7].

4. the second line of protection from unwanted substances by an enzymatic barrier.
5. the presence of various efflux transporters such as p-glycoprotein (p-gp), multidrug resistance proteins (MDPs) remove the molecules from the endothelial cells before translocating into the brain parenchyma [8,9].

Moreover, the BBB has a lot of other functions apart from restricting unwanted substances into brain. The BBB involves not only in protecting brain but also regulates in secretion of functional and informational molecules in translocation into brain [10]. Three major strategies were tested to overcome the BBB and deliver drugs to the brain which includes: disruption of BBB, transcellular diffuse and active transport.

1.1. Strategies to deliver drugs to brain

In past few years, receptor and adsorptive mediated transcytosis have emerged as a new approach in transporting therapeutics to brain. Due to rapid progress in the field of molecular biology has increased the understanding of BBB, brain and various brain disorders. It has been found that multidisciplinary approaches of biology, nanotechnology and biophysics have important role in achieving this goal. There are few common strategies which can be used to deliver therapeutics to the brain.

1.1.1. Drug transport across the BBB through tight junctions

In past years, there have been rapid increase in understanding of molecules which are involved in the formation of tight junctions. Such knowledge helps in discovery of modulators which can be used for opening of BBB. These modulators could be chemical, biological or physical stimuli such as ultrasound or magnetic fields [11–13]. The paracellular approach has been studies in opening tight junctions which includes: 1) this is a phenomena majorly associated with many brain diseases such as brain tumors, Alzheimer's disease, stoke etc. and stimuli. 2) increased

paracellular transport leads the translocation of small hydrophilic molecules across the BBB. 3) opening of tight junctions helps in increase in transport of macromolecules and delivery carrier such as liposomes, nanoparticles, micelles into the brain. 4) temporarily disrupting the BBB by using physical stimuli such as ultra sound or magnetic fields increase the delivery of drugs into the brain.

Cereport, a synthetic peptide has been studied for enabling the transport of drug through paracellular route [14–17]. It temporarily disrupts the tight junction, thereby enhancing the transport of various drugs including carboplatin, loperamide, and acyclovir through changes in cAMP and cGMP second messenger systems in human brain microvascular endothelial cells [14,15,18–20]. In addition, virus can also be used as a biological stimuli to open the tight junction. It can act through upregulation of chemokines for infiltration of inflammatory cells into the CNS [21]. Cyclodextrins are known for capability to increase the water solubility of hydrophobic molecules by forming inclusion molecular complexes [22]. According to the previously published report, cyclodextrins extract cholesterol from endothelial cells resulting in temporarily opening of tight junction [23]. There have been several studies published demonstrating the use of energy dependent physical stimuli, such as ultrasound, electromagnetic fields, to open the tight junctions [12,13]. Ultrasound is a non-invasive method to open the tight junctions locally without damage to the neurons [12,24]. In addition, microwaves exposure can increase the permeability of the BBB though thermal effects and enhancing the transport of drugs into the CNS whereas electromagnetic fields though regulation of protein kinase C signaling [25,26].

1.1.2. Drug transport through transporters

One the most successful strategies in recent years is the use of transporters to delivery drug molecules across the BBB. These transporters are present on the BBB to transport nutrients such

as proteins, peptides, glucose, nucleic acids [27]. However, the use of such transporters for drug delivery is limited to peptide drugs. Levadopa has molecular structure mimicking the endogenous nutrient, which is hydrophilic in nature and has precursor of dopamine used for the treatment of Parkinson's disease. It competes to large neutral amino acid carrier *via* carboxyl and alpha-amino groups present in levodopa [28]. However, this strategy is less preferred due to interference of the transport of nutrients.

1.1.3. Drug transport through adsorptive mediated transcytosis (ADT)

In recent years, there have been substantial evidence demonstrating the use of cationic proteins and peptides for the delivery of drugs across the BBB into the brain [29]. Cell penetrating peptides (CPPs) are a group of short cationic peptides with amphiphilic properties. They are known for their ability to translocate across the cell membranes and deliver drugs into cells [30]. These CPPs show some common qualities even though difference in their sequence and length [31]. This includes: amphipathic nature, cationic charge, hydrophobicity and helical moment, their capability to interact with cell membranes and formation of secondary structure upon interaction with lipids [31]. The mechanisms behind the uptake of these CPPs are receptor and energy-independent process. However, endocytosis is the major mechanism for some CPPs. The internalization of SynB is a temperature and energy dependent process through Adsorptive mediated transcytosis (AMT) [32]. However, the uptake of HIV-1 (trans-activating transcriptor) TAT is majorly through lipid raft-mediated micropinocytosis which is motivated by cell surface binding of TAT [33].

The major application of CPPs is established on the coupling of CPPs to the biologically active cargo to translocate into the cells. The coupling could be covalent or non-covalent bond. A numerous variety of active cargoes including proteins, peptides, small molecules, DNA fragments, liposomes and nanoparticles have been delivered into cells through CPPs [30]. For instance, SynB3

has been studied by a group for the brain uptake of various chemotherapeutic agents including doxorubicin, paclitaxel and dalargin both *in vivo* and *in vitro* BBB model [34]. They reported an increase in the brain uptake of chemotherapeutic agents by several folds. Moreover, HIV-1 TAT has been used by several groups demonstrated that TAT could potentially increase the translocation of nanoparticle or liposomes into the brain, thereby delivering chemotherapeutic agents [35,36]. Sharma and group demonstrated enhanced penetration of Transferrin-TAT liposomes in brains of adult Sprague Dawley rats [35]. In another study performed by Xia et al. showed the significantly high uptake of penetratin coupled PEG-poly lactic acid nanoparticles in rat brains [36]. Adsorptive mediated transcytosis facilitates the accumulation of hydrophobic drugs into the brain however, due to its non-specificity these CPPs can go into non-targeting organs and lead to toxicity and immunogenicity.

1.1.4. Drug transport through receptor mediated transcytosis (RMT)

AMT of drugs is limited due to its non-specific nature of accumulation in non-targeting organs. However, this can be overcome by the use of receptor mediated transcytosis (RMT). RMT is a process of active targeting of the BBB. There are several receptors expressed on the surface of brain endothelium which could be exploited for the delivery of chemotherapeutic agents [35,37,38]. Drug delivery cargoes can be modified with the targeting ligands which can further be translocated across the BBB into the brain. The approach of RMT is known as the molecular Trojan horse approach [39,40]. In case of disease condition, certain receptors are up-regulated which further increase the chance of active targeting of therapeutic molecules to the specific target site. For instance, transferrin receptors are up-regulated on the surface of brain endothelium in case of brain tumor disease condition. The transport of delivery cargo *via* RMT involves three major steps: 1) endocytosis of targeting ligand-cargo to the luminal side of the cell after binding to its

receptor. 2) transport through the cytoplasm. 3) exocytosis of the ligand-cargo to the abluminal side of the cell [40].

There are various receptors expressed on the surface of the BBB which can be used to delivery drugs into the brain such as insulin, transferrin, low density lipoprotein recptor-1 and -2, diphtheria toxin receptors. Insulin receptor has been widely studied for the delivery of drugs and genes into the brain [41,42]. Pardridge et al. conjugated a radiolabeled amyloid-beta-peptide to monoclonal antibody (mAb) which binds to the insulin receptor [41]. This acts as a diagnostic probe for Alzheimer's disease. Nonetheless, this strategy is considered risky due to its completion with glucose. Transferrin receptor (TfR) has been most widely studied and characterized RMT approach for the delivery of drugs across the BBB into the brain [35,44]. However, this receptor is not unique to the brain endothelium. Majorly, there are two ways to exploiting TfR for translocation of drugs into the brain. They are: use of specific antibody against the TfR (such as OX-26) and endogenous transferrin (Tf) as targeting ligand. However, this approach of using Tf as a targeting ligand is not advisable due to the competition between endogenous Tf and exogenous Tf conjugated cargo which is limiting factor for TfR. The limiting factors of RMT approach involves are the endosomal entrapment and receptor saturation.

1.2. Approaches used in this research

1.2.1. Liposomes used as delivery carrier across the BBB

Liposomes are the bilayer vesicles prepared from phospholipids. These nanoparticles are considered as non-toxic due to the phospholipids used in preparation have structural similarity to the cell membrane [44]. The liposomal drug delivery carrier provides substantial advantages including their ability to protect loaded agents in circulation and ease of surface modifications over other nanoparticles [45,46]. The surface modification of liposomes by polyethylene glycol (PEG)

prevents them from taken up by phagocytes as well as increase their half-life by preventing their tendency to exchange lipids with cell membrane [44]. The PEGylated liposomes reduce the nonspecific interactions of liposomes and plasma clearance, thereby increasing the circulation time due to its steric repulsion effect [44]. These PEGylated liposomes are desired to be used for the drug delivery drugs for active targeting of drug delivery cargo including modification with proteins, peptides and antibodies [47–49]. Liposomes can be functionalized with one or more ligands for enhancing the delivery of drugs to the specific target site.

1.2.2. Receptor mediated transcytosis: transferrin receptor (TfR)

The rapid change in the development of the drug delivery aspect has resulted in delivery of drug to target-specific site to the brain. The target-specific approach of delivering drug helps in increase in the therapeutic index of drugs. Furthermore, polymer- and liposome-based drug delivery demonstrate abilities to serve site specific targeting. The transferrin receptor (TfR) is one of the most widely studied receptors for the receptor mediated transcytosis drug delivery systems. The transferring receptor is a 90 kDa of two subunits cell membrane glycoprotein and 760 amino acid residue [50]. The major function of TfR is to regulate cellular uptake of iron. It acts as a gatekeeper on the cell membrane and allows the endocytosis of iron from a plasma protein, transferrin in the circulation [51–53]. Although, the interaction of iron with the transferrin receptor is not direct. The main route of Iron transport in the body from the sites of absorption, storage, and utilization is through transferrin. Two molecules of iron bind with the transferrin very tightly but reversibly. TfR is expressed not only on blood brain barrier but also on erythrocytes, intestinal cells, hepatocytes [54].

Transferrin is a natural protein and which could be used for a major site-specific targeting. It is biodegradable, non-immunogenic, and non-toxic. Important aspect of using transferrin as a

site specific targeting agent is due to presence of its receptor on the cell surface in high density. Proliferating malignant cells which overexpress TfR have shown potential for the delivery of proteins, anticancer drugs, and therapeutic genes to the brain using this transferrin pathway. A study performed by Ulbrich and co-workers, they coupled transferrin to human serum albumin nanoparticles for the delivery of loperamide across the BBB [55]. Rooy et al. coupled five different ligands to liposomes including transferrin, and R17-217 [56]. They studied the ability of target ligands coupled liposomes to the brain. There are several factors which could influence the performance of targeted drug delivery system such factors are particle size, surface properties, and conformation of the targeting ligand. To completely understand the function and performance of the targeted ligand on different nanocarriers more studies would be needed.

1.2.3. Cell penetrating peptides (CPPs)

CPPs are the group of short cationic amphiphilic peptides, consisting of < 30 amino acids [30]. The translocation of CPPs through various biological membrane make them distinguish from one another. In the past few years, the application CPPs has been evaluated for the delivery of various carriers such proteins, peptides, nucleic acids, liposomes, nanoparticles across the cell membranes [57–60]. CPPs offer several advantages such as low toxicity, dose dependent efficiency, cell type independent efficiency, flexibility on selection of delivery carrier, high internalization, ease of synthesis and potential of sequence modification [61]. The specific peptide sequences has conferred with the ability to penetrate the cell membrane, they are called protein transduction domains [62]. These peptide sequences have basic amino acids which carry cell penetrating properties. Due to their ability to translocate across the cell membrane has evoked the interest using CPPs for delivering drugs. CPPs can be classified into three categories based on their origin, which includes protein-derived, chimeric derived, and synthetic derived [63–66]. Based on

the physicochemical properties, these CPPs are again divided into cationic, amphipathic, and hydrophobic CPPs [31,67–69]. Various CPPs include penetrating, HIV-1 TAT, QLPVM and PFVYLI have been coupled to delivery carrier to enhance the translocation of delivery carrier across the cell membranes.

1.2.3.1. Penetratin

Penetratin (Pen) is an amphiphilic cationic peptide which facilitates internalization of delivery carriers. This peptide is derived from 60 residue Antennapedia homeodomain, a naturally occurring protein. Pen is 16 amino acids sequence from 43-58 residue of the third α-helix of the homeodomain which is important for the translocation activity [70]. The translocation of delivery carrier depends on the net charge and amphiphilic nature of the peptide regardless of the initial binding of the peptide to the cell membrane [71,72]. Penetratin forms an inverted micelle structure in the cell membrane after binding to negatively charged phospholipids present in the cell membrane [73]. A study has been published which demonstrates that the translocation of penetratin takes place by interacting with negatively charged lipids in the cell membrane from hydrophilic to hydrophobic environment through charge neutralization [74]. Several studies have demonstrated the significantly ($p < 0.05$) higher liposomal transport of Tf and penetratin modified liposomes both *in vitro* and *in vivo* [35,37].

1.2.3.2. HIV-1 TAT

TAT is a cationic peptide with more hydrophilic amino acids residues and derived from the trans-activating protein of the HIV type-1 [75,76]. This peptide has been shown efficient delivery of cargoes from nanoparticles to proteins, peptides and nucleic acids [30]. In recent years, TAT has been widely studied for the delivery of drugs and nucleic acids. Domain 4 of the original HIV-1 TAT contains a highly basic regions which contributes to the nucleolar localization [77]. A

study demonstrated the potential of TAT conjugated Qdots in translocation across the endothelial cells into the brain parenchyma [78]. The mechanism of the translocation of TAT is through the energy-dependent macropinocytes [33]. In another study performed by Liu et al. showed the efficient transport of TAT-PEG-b-cholesterol nanoparticles both *in vitro* and *in vivo* across the BBB and further translocated around the nucleus of neurons [79].

1.2.3.3. QLPVM

The penta peptide QLPVM has more hydrophobic amino acid residues and derived from Bax-binding domain of Ku70 protein [80,81]. It has been studied for enhanced cell penetration and cell death inhibition properties [82].

1.2.3.4. PFVYLI

PFVYLI (PFV), is a synthetic peptide with only six amino acids, which represents the c-terminal portion of C105Y [17]. This hydrophobic peptide sequence has shown potential in intracellular transport of delivery carriers. A study demonstrated the co-delivery of doxorubicin and erlotinib through Tf-PFVYLI conjugated liposomes. The results showed the higher cellular uptake of drugs in glioblastoma cell lines and significantly ($p < 0.05$) higher transport across the *in vitro* endothelial co-culture barrier [43]. Another study demonstrated an efficient delivery of doxorubicin from PFVYLI conjugated liposomes in cancer therapy [83]. The mechanism involved in translocation is through lipid raft and clathrin mediated endocytosis mechanism in an energy dependent manner [83].

1.2.4. Combination drug therapy

Combination drug therapy is the most effective treatment option for cancer which combines two or more chemotherapeutic drugs and has a potential to enhance the therapeutic efficacy. This therapy provides several advantages by targeting different mechanisms, reduce drug

resistance and offer therapeutic benefits, thereby decreasing tumor growth and metastatic potential of cancer cells. Drug resistance to chemotherapeutic agents, such as doxorubicin, is a common clinical problem limiting their effectiveness, especially as a single agent. Data suggests that conventional therapies exert their cytotoxic activities primarily by inducing apoptosis in tumor cells however, resistant cells adopt mechanisms to evade these apoptotic pathways [84]. Recently, characterization of the adaptive kinome response in the context of Epidermal Growth Factor Receptor (EGFR) therapy has shown that EGFR inhibition promotes the expression of compensatory kinases to allow for continued proliferative signaling in the cell, diminishing the growth inhibitory effect of the drug [85]. Thus, the proposed co-administering of doxorubicin and EGFR inhibitor (erlotinib) is suggested to be an effective approach for attenuating GBM progression *in vivo*.

1.3. Statement of the problem and research objectives

Glioblastoma multiforme (GBM) is an aggressive malignant brain tumor arising from astrocytes. The median survival time of the patients from this tumor is less than 15 months with a 5-year survival rate of less than 3 % after diagnosis [86,87]. This is due to rapid growth of tumor cells and their aggressive infiltration into other parts of brain. Currently, therapeutic treatments available for brain tumor are divided into surgical resection, radiation and chemotherapy. Removal of tumor completely by surgical resection is not possible due to its ability to invade and progress in different parts of the brain [88]. Chemotherapy is the major treatment modality which functions by damaging DNA of cancerous cells. However, intravenous administration of chemotherapeutics does not reach the brain in desired concentration due to the presence of a protective barrier called blood brain barrier (BBB). In addition, incompetent tumor targeting of these chemotherapeutic agents leads to several detrimental and toxic effects on healthy brain tissue [89,90]. Therefore, it

is crucially important to develop a delivery system with efficient glioblastoma targeting ability which is able to translocate well in high concentration across the BBB as well as deliver the chemotherapeutic agents to the core of glioblastoma tumor including migrating cells [91]. Expression of several receptors on the BBB facilitate the transcytosis of amino acids, glucose, or nucleic acids into brain, which can be used to deliver a carrier with chemotherapeutic agents into the brain tissue [37,38,43,92]. Overexpression of transferrin receptors (TfRs) on the surface of brain endothelial cells as well as on glioblastoma cells can be exploited to deliver chemotherapeutic agents in high concentration across the BBB to glioblastoma tumor [93,94].

Lipid based nanoparticles e.g. liposomes, being functionally versatile and have ability to be engineered for targeting these receptors, make them as potential carriers for drug delivery [90]. Receptor targeted drug delivery systems have been studied to enhance the targeting effect. However, the delivery of molecules through receptor targeted is restricted by receptor saturation, thereby limiting the transport across the BBB and lowers the effect of chemotherapeutics [95]. Therefore, we have conjugated two ligands to liposomes (i) transferrin (Tf), a receptor targeting serum glycoprotein [93] (ii) a cell penetrating peptide (HIV-1 TAT, penetratin, QLPVM, PFVYLI). Doxorubicin (Dox) is effective in treating glioblastoma but as a single chemotherapeutic agent, it is prone to develop drug resistance in cancer cells thereby limiting their effectiveness which is a common clinical problem. To overcome this limitation, an epidermal growth factor receptor (EGFR) inhibitor, erlotinib (Erlo) can be used along with doxorubicin. EGFR inhibitor promotes the expression of compensatory kinases to allow for continued proliferative signaling in the cell, diminishing the growth inhibitory effect of the drug [85]. Thus, the proposed co-administering of doxorubicin and EFGR inhibitor (erlotinib) is suggested to be an effective approach for attenuating glioblastoma progression *in vivo*. The **long-term goal** of this proposed

research is to develop a liposomal drug delivery system for the efficient co-delivery of doxorubicin and erlotinib to brain for the treatment of glioblastoma. We **hypothesize** that doxorubicin and erlotinib loaded liposomes surface modified with Tf and CPP will increase their translocation across the BBB and co-deliver desired chemotherapeutics into glioblastoma tumor in brain *via* receptor mediated transcytosis and enhanced cell penetration, will achieve glioblastoma tumor regression, both *in vitro* and *in vivo* (Figure 1). We tested our hypothesis through the following specific aims:

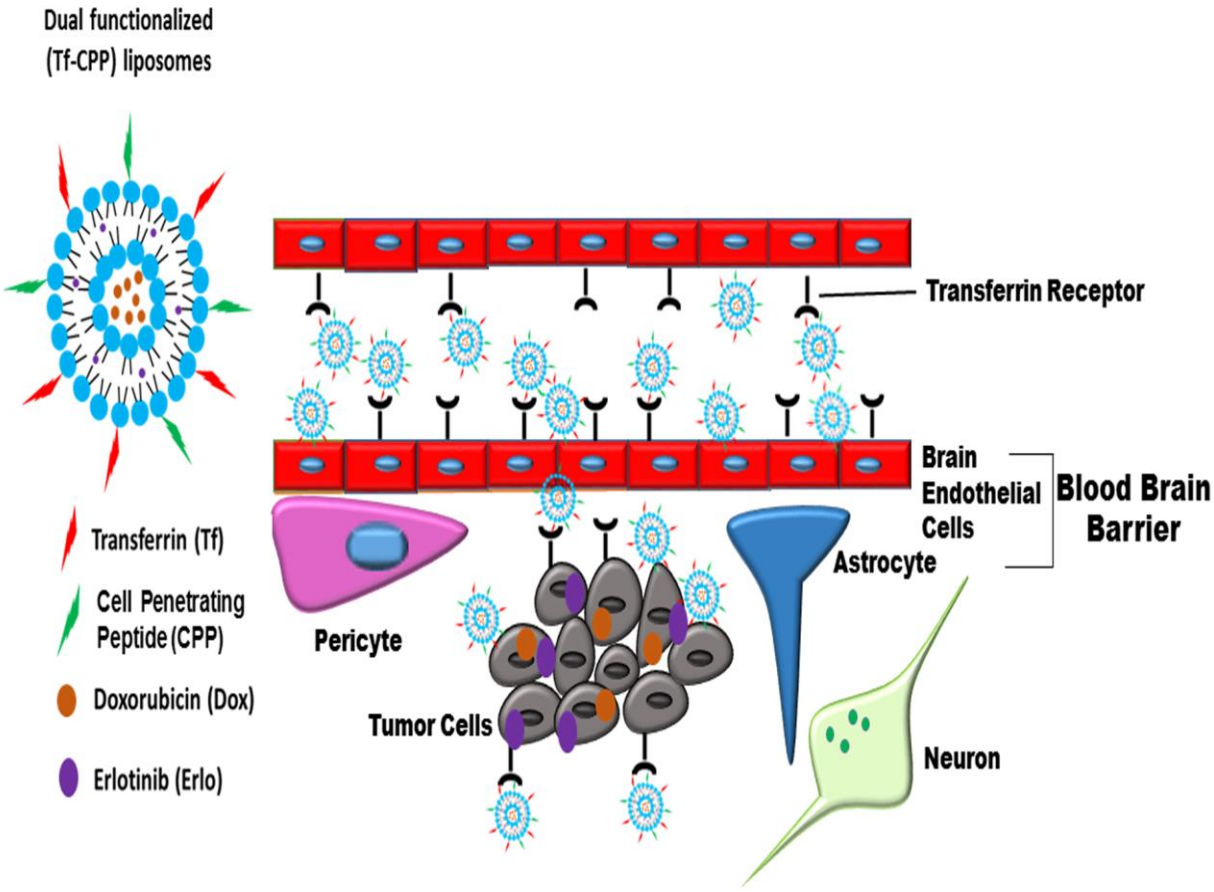

Figure 1. Schematic showing translocation of Dox and Erlo loaded Tf-CPP liposomes across the BBB, followed by endocytosis into glioblastoma tumor cells.

1.3.1. Specific aim 1: synthesis and characterization of Tf and CPP coupled liposomes loaded with doxorubicin and erlotinib

DSPE-PEG-NHS was used to couple transferrin and CPP through nucleophilic substitution reaction. The coupling efficiency was characterized by micro Bicinchoninic Acid assay (micro BCA). CPP-liposomes was prepared using thin film hydration. Moreover, post-insertion technique was employed to prepare dual-functionalized liposomes by mixing CPP-liposomes with Tf-micelles. Various types of CPPs were used based on their physico-chemical properties, i.e. hydrophilic (HIV-1 TAT), amphiphilic (penetratin), and hydrophobic (QLPVM and PFVYLI). These dual-functionalized liposomes were characterized for particle size and zeta potential by dynamic light scattering. Dox was entrapped into liposomes through pH gradient method. Dox and Erlo entrapment into liposomes was quantified using HPLC. The biocompatibility of dual-functionalized liposomes was studied in glioblastoma (U87), brain endothelial cells (bEnd.3) and glial cells by MTT assay. Additionally, the liposomes were also evaluated for hemolysis and cellular uptake.

1.3.2. Specific aim 2: design an in vitro brain tumor model to study the transport of liposomes across barrier layer and investigate the anti-tumor efficacy of liposomal formulation on the tumor growth

We designed an *in vitro* brain tumor model by growing glioblastoma cells in the chitosan-PLGA porous scaffold. The seeding efficiency was determined using MTT assay. The growth of tumor inside PLGA-chitosan scaffold was assessed using hematoxylin-eosin staining. The transport of liposomes was evaluated across the endothelial co-culture barrier layer having brain endothelial cells and primary glial cells on the opposite sides of the culture inserts, into the tumor cells inside porous scaffold. Additionally, the regression of tumor inside scaffold was studied by

determining the viability of tumor cells by using MTT assay after Dox and Erlo loaded Tf-CPP liposomes treatment thereby evaluating the anti-tumor efficacy of liposomal formulations, *in vitro*.

1.3.3. Specific aim 3: to study *in vivo* biodistribution, biocompatibility, and antitumor activity of doxorubicin and erlotinib loaded Tf-CPP-liposomes in glioblastoma bearing mice

The biocompatibility of liposomes was evaluated by analyzing the histological sections of different organs including liver, kidneys, spleen, lungs, brain and heart for the presence of toxicities, necrosis, inflammation, fibrosis and any signs of lesions using hematoxylin-eosin staining. The biodistribution of lissamine rhodamine labeled as well as drugs (Dox and Erlo) loaded liposomes was evaluated in nude mice. Due to the complex pathology of brain, it is important to investigate antitumor efficacy of liposomes in glioblastoma bearing mice. We developed glioblastoma tumor in mice brain. The anti-tumor efficacy of liposomes was determined by measuring tumor size and plotting Kaplan-Meier survival curves. Ki67 and cleaved PARP immunofluorescence staining were performed to study the effects of liposomal formulations on cell proliferation and induction of apoptosis, respectively.

CHAPTER 2. MATERIALS AND METHODS

2.1. Materials

1,2-dioleoyl-3-trimethylammonium-propane chloride (DOTAP), 1,2-distearoyl-sn-glycero-3- phosphoethanolamine-N-[carboxy(polyethylene glycol)-2000] (DSPE-PEG-COOH), 1,2-dioleoyl-snglycero-3-phosphoethanolamine-N-(lissamine rhodamine B sulfonyl) (DOPE-lissamine rhodamine), and 1,2-dioleoyl-sn-glycero-3-phosphoethanolamine (DOPE) were procured from Avanti Polar Limited (Birmingham, Alabama). 3-(N-succinimidyloxyglutaryl) aminopropyl, polyethyleneglycol-carbamyl distearoylphosphatidyl-ethanolamine (NHS-$PEG_{(2000)}$-DSPE) was obtained from Biochempeg Scientific Inc. (Watertown, Massachusetts). Doxorubicin HCl was purchased from MedChem Express (Monmouth Junction, New Jersey). Erlotinib was bought from Cambridge Chemicals (Woburn, Massachusetts). Transferrin (Tf), Cholesterol (Chol) and Chitosan (50 kDa) were obtained from Sigma-Aldrich Company (St. Louis, Missouri). Penetratin (Pen), HIV-1 TAT (TAT), QLPVM, PFVYLI (PFV) were obtained from Zhejiang Ontores Biotechnologies Co., Ltd (Zhejiang, China). Fetal bovine serum (FBS) was procured from Omega scientific Inc. (Tarzana, California). Dulbecco's modified eagle medium (DMEM) and Dulbecco's phosphate buffered saline (DPBS) were purchased from Mediatech Inc. (Manassas, Virginia). 3-(4, 5-dimethylthiazol-2-yl)-2, 5- diphenyltetrazolium bromide (MTT) was purchased from Alfa Aesar (Ward Hill, Massachusetts). Polyethylene terephthalate (PET) thincerts, cell culture inserts were bought from Greiner Bio-One International (Monroe, North Carolina). Poly (D, L-lactide-co-glycolide) 50:50 was purchased from Polyscitech (West Lafayette, Indiana). All the chemicals used were of analytical grade. Glioblastoma (U87) and Brain endothelial cells (bEnd.3) were procured from American Type Culture Collection (ATCC, Rockville, Maryland).

2.2. Experimental methods

2.2.1. Coupling of penetratin to DSPE-PEG$_{(2000)}$-COOH

Penetratin (Pen) was coupled through the reaction of carboxyl group of DSPE-PEG$_{(2000)}$-COOH and the amine group of penetratin in the presence of EDC/NHS. Briefly, DSPE-PEG$_{(2000)}$-COOH was suspended in HEPES buffered saline pH 5.0 to form micelles. This suspension was treated for 60 mins with 360 µl of both 0.5 M EDC and 0.5 M NHS per 10 µl of DSPE-PEG$_{(2000)}$-COOH to activate carboxyl group of DSPE-PEG$_{(2000)}$-COOH. Excess EDC/NHS were removed using dialysis membrane MWCO 1,000 Da. Furthermore, the pH was adjusted to 7.4 using 0.1 N sodium hydroxide. Penetratin was added to the suspension in the molar ratio 1:3 (Pen: DSPE-PEG) and stirred overnight at room temperature. Uncoupled penetratin was removed through dialysis membrane MWCO 3.5 kDa. The coupling efficiency was determined by micro bicinchoninic acid (BCA) assay in accordance with manufacturer's protocol. Penetratin was used as a standard and DSPE-PEG$_{(2000)}$-COOH was used as a control for the studies.

2.2.2. Coupling of transferrin to DSPE-PEG$_{(2000)}$-COOH

The coupling of transferrin (Tf) to DSPE-PEG$_{(2000)}$-COOH was performed through EDC/NHS reaction, as previously described [48,92]. Tf (125 µg /µ mole of the lipid) was added to the activated DSPE-PEG$_{(2000)}$-COOH and stirred for 8 h at room temperature. The unbound transferrin was separated using sephadex G-100 column. The coupling efficiency was determined using micro BCA assay. Briefly, 100 µl of liposome suspension was mixed with 400 µl of methanol and this mixture was vortexed and centrifuged at 9,000 x g for 30 s. Further, 200 µl of chloroform was added to this mixture and vortexed and centrifuged at 9,000 x g for 30 s. The phase was separated by adding 300 µl of water to this mixture. Thereafter, the mixture was vortexed and centrifuged at 9,000 x g for 1 min. The upper phase was discarded and 300 µl of methanol was

added to the interphase between chloroform and protein precipitate, that was followed by centrifugation at 9,000 x g for 2 mins. The supernatant layer was removed and precipitated protein pellet was air dried. The pellet was dissolved in 100 µl of phosphate buffered saline (PBS), pH 7.4 and analyzed for coupling efficiency using micro BCA assay in accordance with manufacturer's protocol [48,96].

2.2.3. Synthesis of DSPE-PEG$_{(2000)}$-CPP

The coupling of CPP was performed using nucleophilic substitution reaction to the distal end of activated NHS-PEG$_{2000}$-DSPE. Briefly, NHS-PEG$_{2000}$-DSPE and CPP at a molar ratio of 3:1 were dissolved in an anhydrous dimethylformamide (DMF) and adjusted pH to 8-9 using triethylamine. The reactant mixture was stirred for 3 days at room temperature. Further, the resulting product was dialyzed using dialysis membrane MWCO 3.5kDa for 48 h to remove free uncoupled CPP. The dialysate was lyophilized and stored at -20 °C until used. The coupling of Pen and TAT were determined using micro bicinchoninic acid (BCA) assay in accordance with manufacturer's protocol whereas the coupling of QLPVM and PFV were confirmed using high performance liquid chromatography (HPLC). CPPs and DSPE-PEG$_{(2000)}$-NHS were used as standard and control, respectively for the studies.

2.2.4. Synthesis of DSPE-PEG$_{(2000)}$-Tf

Tf was coupled to the terminal end of DSPE-PEG$_{(2000)}$-NHS using nucleophilic substitution, as described in the previous section [35,43,48]. Briefly, DSPE-PEG$_{(2000)}$-NHS and Tf (125 µg /µ mole of lipid) were dissolved in an anhydrous DMF. Using triethylamine, the pH was adjusted to 8-9. The mixture was stirred using magnetic stirrer for 24 h at room temperature. The resultant product was passed through G-100 sephadex column to separate uncoupled transferrin. The coupling efficiency was evaluated using micro BCA assay, as per described in the previously

published article [43]. Tf and DSPE-$PEG_{(2000)}$-NHS were used as standard and control, respectively for the studies.

2.2.5. Preparation of dual functionalized liposomes

The dual-functionalized liposomes were prepared using post-insertion technique [92]. Briefly, DSPE-$PEG_{(2000)}$-Pen and other phospholipids, in the following molar ratio: DOTAP/DOPE/CHS/CPP-$PEG_{(2000)}$-DSPE (43.5:43.5:5:4 mole %) were dissolved in chloroform: methanol (2:1; v/v). The solvent of the mixture was evaporated using rotavapor (Buchi Rotavapor RII, New Castle, DE) to form a thin lipid film. Pen coupled liposomes were prepared by hydrating the dried lipid thin film with HEPES buffered saline, pH 7.4. Furthermore, the Pen-liposomes were stirred overnight with DSPE-$PEG_{(2000)}$-Tf micelles at room temperature to form dual functionalized liposomes (Tf-Pen-conjugated liposomes). The free DSPE-$PEG_{(2000)}$-Tf micelles were removed from Tf-Pen-liposomes by passing the liposomes through sephadex G-100 column.

For preparation of lissamine-rhodamine labeled liposomes, 0.5 mole % of lissamine rhodamine coupled DOPE was dissolved as a liposomal membrane marker along with other lipids in chloroform: methanol (2:1; v/v) and evaporated to form a thin lipid film. For coumarin-6 labeled liposomes, 0.5 mole % of coumarin-6 was added to the lipid mixture prior to the formation of thin lipid film.

2.2.6. 5-Fluorouracil loading

5-FU was loaded into liposomes using pH gradient method as previously reported [97]. Briefly, the thin film was hydrated using 300 mM sodium carbonate pH 9.6, to form Pen-conjugated liposomes, followed by stirring with DSPE-$PEG_{(2000)}$-Tf micelles. To create pH gradient, the formulations were passed through sephadex G-100 pre-equilibrated with HEPES buffered saline pH 7.4. The drug 5-FU was added to the liposomal formulation and incubated at

50ºC for 1 h. The 5-FU loaded liposomes were then cooled down to room temperature and passed through sephadex G-100 column to separate unentrapped drug. Entrapment efficiency was quantified using high performance liquid chromatography (HPLC) (Agilent Technologies 1120 Compact LC). Briefly, 100 µl of liposomal formulation before and after passing through the column was dispersed in 200 µl of D.I. water with 100 µl of methanol and 100 µl of 0.5% triton X-100. The analysis of 5-FU was determined at a wavelength of 264 nm using C-18 column (Thermoscientific Hypersil BDS, 5 µm, 250 x 4.6 mm) and mobile phase containing 0.2 M potassium phosphate monobasic: acetonitrile (98:2) with a flow rate of 0.750 mL/min at room temperature.

2.2.7. Preparation of dual functionalized liposomes (Tf-Pen, Tf-TAT, Tf-QLPVM and Tf-PFV) and drug loading

CPP-liposomes were prepared using thin film hydration method while post-insertion method was used to formulate dual-functionalized liposomes [35,37,43]. Briefly, DSPE-$PEG_{(2000)}$-CPP, erlotinib and other phospholipids at a molar ratio of 45:45:2:4 (mole %) were dissolved in chloroform: methanol (2:1, v/v). Dried lipid film was formed after evaporating the solvent mixture using rotary evaporator (Buchi Rotavapor RII, New Castle, DE). Further, the film was hydrated with 300 mM citric acid buffer pH 5.0 to form CPP-liposomes. Then, DSPE-$PEG_{(2000)}$-Tf micelles were added to this and stirred on magnetic stirrer overnight at room temperature to form Tf-CPP coupled liposomes. pH gradient was used to encapsulate doxorubicin into liposomes. The external pH was exchanged by titrating the liposomes with 300 mM sodium carbonate. Then, doxorubicin was added to the liposomes and incubated for 1 h at 50 °C. After cooling, the liposomes were pass through G-100 sephadex column to separate unentrapped Dox and Erlo.

The percent entrapment efficiency of drugs was determined as per previously published reports [35,43]. Briefly, the liposomal formulations before and after passing through column were lysed using methanol and triton X-100 (0.5% v/v). Then, the lysed dispersion was centrifuged for 10 min at 3000 rpm. The supernatant from liposomal lysate was injected into high performance liquid chromatography (HPLC) to quantify the entrapment efficiency of drugs. Analysis of Dox was performed using C-18 column (Thermoscientific Hypersil Gold, 5 µm, 250 x 4.6 mm) at a wavelength 234 nm with some modifications [43]. The mobile phase comprised of 0.2 M phosphate buffer, pH 5.5: acetonitrile (70:30) with a flow rate of 1 ml/min at room temperature. With some modifications, Erlo was analyzed using C-8 column (Thermoscientific Hypersil BDS, 5 µm, 250 x 4.6 mm) at a wavelength of 246 nm. The mobile phase consisting of 0.2 M potassium phosphate, pH 3.0: acetonitrile (50:50) with a flow rate of 0.750 ml/min at room temperature [43].

2.2.8. Characterization of liposomal nanoparticles

The hydrodynamic diameter and zeta potential analysis of the liposomes were conducted after appropriately diluted with phosphate buffer saline (PBS) at 25 °C by zetasizer ZS 90 (Malvern Instruments, Worcestershire, UK). The cuvettes filled with samples were placed in the path of 5 mW He−Ne laser of wavelength 633 nm and the data was collected at a scattering angle of 90°.

2.2.9. *In vitro* release of 5-FU

In vitro release studies of 5-FU were performed by diluting liposomes in PBS, pH 7.4 with 10% FBS. Briefly, 5-FU encapsulated liposomes were placed inside tightly sealed dialysis tube (MWCO 6,000-8,000 Da) and immersed in 50 ml of PBS (pH 7.4) and incubated at 37 ± 0.5 °C with mild oscillation of 50 rpm. At predetermined time points, 1 ml of samples were taken and replaced with 1 ml of fresh PBS (pH 7.4). The samples were analyzed using HPLC, as described previously for evaluation of 5-FU loading.

2.2.10. *In vitro* release of doxorubicin and erlotinib

In vitro release studies of doxorubicin and erlotinib were performed by diluting liposomes in phosphate buffer saline (PBS, pH 7.4) with 10% FBS. The drugs encapsulated liposomes were placed into a dialysis tube (MWCO 6000-8000) and tightly sealed. Then, the dialysis tube was immersed into 50 ml of phosphate buffer saline (PBS, pH 7.4) and incubated at $37 \pm 0.5°C$ with mild oscillation of 50 rpm. At predetermined intervals, 1 ml of samples were taken and replaced with same volume of fresh PBS (pH 7.4). The samples were analyzed using HPLC, as described above for evaluation of doxorubicin and erlotinib loading.

2.2.11. *In vitro* cytotoxicity

In vitro cytotoxicity was performed to evaluate the biocompatibility of liposomes. The cytotoxic potential of liposomes (plain, Tf, Pen, Tf-Pen) was evaluated in glioblastoma (U87) and brain endothelial (bEnd.3) lines using MTT assay at varying phospholipid concentrations. Similarly, the biocompatibility of Tf-CPP liposomes (Tf-Pen, Tf-TAT, Tf-QLPVM, and Tf-PFV) was evaluated in U87, bEnd.3, and glial cells using MTT as per previously published reports. Briefly, 1,000 cells per well were seeded in 96 well plates in 200 µl of DMEM supplemented with 10% FBS and 1% pen-strep and incubated at 37 °C under 5% CO_2 atmosphere. After attachment for 24 h, cells were incubated with different phospholipid concentrations of either plain, Tf, CPPs (Pen, TAT, QLPVM, and PVF), Tf-CPP liposomes for 2 h in serum free media. Subsequently, the formulation was removed and cells were further incubated at 37 °C under 5% CO_2 atmosphere for 48 h, with fresh serum containing media. After 48 h, the viability of cells was evaluated using MTT assay. Untreated cells were considered as control group under the same cell culture conditions.

2.2.12. Cellular uptake assessment

Cellular uptake of 5-FU loaded liposomes (plain, Tf, Pen, Tf-Pen) was studied in U87 and bEnd.3, while cellular uptake of Dox and Erlo loaded liposomes (plain, Tf, CPPs, and Tf-CPP) was quantified in U87, bEnd.3 and glial cells. For qualitative determination, cell were incubated with lissamine rhodamine labeled liposomes and observed under fluorescence microscope as per previous reports. Briefly, cells (U87, bEnd.3 and glial) were seeded at a density of 6 X 10^5 cells per well in 6 well plate and incubated at 37 °C under 5% CO_2 atmosphere. After 24 h, cells were incubated for 2 h with different drugs loaded liposomal formulations (plain, Tf, CPP and Tf-Pen) at a concentration of 200 nMoles of phospholipid. Then, the formulation was removed and the cells were washed and rinsed with DPBS, pH 7.4. For qualitative uptake, the nucleus of cells was stained with 1 ml of Hoechst 33342 (1 µg/mL). The cells were observed under Leica DMi8 fluorescence microscope (Leica Microsystems Inc., Buffalo Grove, IL). For quantitative estimation of Dox and Erlo uptake, triton X-100 (0.5% v/v) was used to lyse the cells. Then, methanol was added to the cell lysate to extract drugs. The solution was centrifuged at 4 °C for 10 min at 10,000 rpm and the supernatant was injected in HPLC and analysis was performed. Same procedure was followed to extract 5-FU. Cellular uptake of 5-FU in cells was determined as described above for determination of 5-FU loading, while uptake of Dox and Erlo was quantified as described above for evaluation of doxorubicin and erlotinib loading [43].

2.2.13. Apoptosis study

Apoptosis induction by liposomal formulations in U87 cells was quantified by FITC-annexin-V/PI double staining assay. Briefly, U87 cells were seeded in 6 well plates at a density of 1 x 10^6 cells per well. 24 h after seeding, cells were treated with different 5-FU loaded liposomes (200 nMoles of phospholipid concentration in each well) and free 5-FU for 5 h. Similarly, various

Dox and Erlo loaded liposomes (plain, Tf, PFV and Tf-PFV) and free Dox and Erlo were also incubated for 5 hours followed by replacement of formulations with fresh complete medium and incubated for an additional 24 h at 37ºC. Subsequently, the cells were trypsinized, collected, and stained with Annexin V-FITC apoptosis detection kit. The cells were assessed using BD Accuri C6 flow cytometer (BD Biosciences Accuri cytometers, San Jose, CA) in accordance with manufacturer's protocol.

2.2.14. Penetration ability into U87 spheroids

U87 spheroids were grown using liquid overlay system to study the penetration ability of dual-functionalized liposomes [98]. Briefly, low melting point agarose was added into DPBS and heated to 80ºC for 30 mins to form 2% (w/v) solution. Each well of 24 well plate was coated with 150 µl of the prepared agarose. After cooling to ambient temperature, 1 x 10^3 U87 cells were seeded into each well of the 24 well plate. The plates were allowed to agitate for 5 mins and incubated at 37 ºC, followed by supplementation with DMEM containing 10% FBS and 1% penicillin-streptomycin for 6 days. The media was changed every other day. U87 spheroids were treated with different coumarin-6 loaded liposomal formulations (200 nMoles of phospholipid concentration) at 37 ºC for 12 h. Subsequently, the spheroids were washed with cold DPBS and subjected to imaging using FV300 confocal laser scanning microscope (Olympus, Melville, NY). The z-stage images were obtained by scanning the different layers of the spheroids from the top to the equatorial plane.

2.2.15. Hemolysis study

Hemolysis study demonstrates the interaction between the negatively charged membrane of erythrocytes and liposomes, which may cause hemolysis. The liposomes are meant to be injected intravenously, therefore, it is important to evaluate *in vitro* hemocompatibility prior to *in*

vivo studies. Briefly, blood sample was collected from an adult rat into EDTA containing tubes. Then, the blood containing tube was centrifuged for 10 min at 2000 rpm to separate erythrocytes and washed thrice with sterile PBS, pH 7.4. With predetermined number of erythrocytes (1.5 x 10^7) were incubated with different phospholipid concentrations of liposomes (plain, Tf, CPPs and Tf-CPP) for 60 min at 37 °C. Again, the samples were centrifuged at 2000 rpm for 10 min. The absorbance of the supernatant was determined at 540 nm using spectrophotometer (SpectraMax® M5, Molecular devices, Sunnyvale, CA). Hemolysis of 0% and 100% after treatment with PBS and triton X-100 were taken as controls, respectively. The percent hemolysis was determined by using the following equation:[37,43]

$$\text{Percent hemolysis} = [(OD_{(treatment)} - OD_{(PBS)})/ OD_{(Triton\ x\text{-}100)}] \times 100$$

Where $OD_{(treatment)}$, $OD_{(PBS)}$ and $OD_{(T)}$ are the optical densities of treatment groups, PBS and triton X-100, respectively.

2.2.16. Design of *in vitro* endothelial barrier

The *in vitro* endothelial barrier was constructed by combination of bEnd.3 cells on luminal side and primary glial cells on abluminal side of the culture insert. Briefly, primary glial cells (15,000 cells/cm^2) in DMEM with 20% FBS were seeded on the bottom side of the culture insert overnight to allow adherence of the cells to the culture insert's membrane [92]. Following day, brain endothelial cells (37,500 cells/cm^2) were seeded on the inside of culture inserts, placed in a 24 well plate and were cultured for 6 days to form a tight barrier [98]. The media was replaced every 2 days and cells were checked for confluence. The integrity of the barrier was determined by measuring the flux of sodium fluorescein (Na-F) across the endothelial barrier layer and transendothelial electrical resistance (TEER) using EVOM2 with STX2 (World Precision Instruments, Sarasota, FL), as previously reported [92,98]. Briefly, the culture inserts with both

bEnd.3 and glial cells (co-culture) or only endothelial cells (monolayer) were placed in 24 well plates with 1 ml of DPBS in the lower compartment. In the upper compartment of the culture inserts, the medium was replaced with 500 µl containing 10 µg/ml Na-F. The samples were taken at specific time points by transferring the culture inserts to new wells containing 1 ml of DPBS. The paracellular transport was evaluated by measuring the fluorescence intensity of Na-F from the upper and lower compartment using spectrophotometer microplate reader at excitation/emission wavelengths of 485/535 nm respectively (SpectraMax® M5, Molecular devices, Sunnyvale, CA). The endothelial permeability coefficient (P_e) was calculated by measuring the flux across cell free inserts for both models, as per previously published reports [92,99,100].

2.2.17. Preparation of PLGA-chitosan scaffold

Emulsion freeze drying technique was used to prepare porous PLGA-chitosan scaffold [35,100]. Briefly, poly (D, L-lactide-co-glycolide) (50:50) (PLGA) at a concentration of 0.2 g/ml was dissolved in dichloromethane. Separately, 500 mg of chitosan and 150 mg of polyvinyl alcohol (PVA) were dissolved in 10 ml of acetic acid buffer pH 4.5. To this mixture, previously prepared PLGA solution was added at a rate of 2 ml/min with constant stirring to form an emulsified paste. 500 µl of 0.1% w/v collagen solution in 0.1 M acetic acid was added to the paste. Further, the paste was poured into rod-shaped mold and freeze dried. Then, this was cut into 2mm thick circular discs.

2.2.18. Growth of tumor cells inside PLGA-chitosan scaffold

To provide strength, the scaffolds were treated with 5 M sodium hydroxide and washed thrice with DPBS to remove excess sodium hydroxide. The scaffolds were then treated with 70% ethanol and washed with sterile DPBS pH 7.4. Thereafter, the scaffolds were soaked in DMEM supplemented with 30% FBS overnight before seeding tumor cells on them. The surface of the

scaffold was seeded with 5 x 10^5 U87 cells and incubated for 6 h, followed by subsequent addition of fresh media containing 30% FBS. The cells in the scaffold were cultured for 21 days to form 3D tumors on the scaffold. At different time points, the sections of the scaffold containing U87 tumor cells were embedded in OCT and frozen. The frozen scaffold was subsequently sectioned using cryostat and mounted on polylysine coated slides and the cell growth was monitored using hematoxylin eosin staining. The seeding efficiency was determined by MTT assay, as per previously published report [101].

2.2.19. Transport of coumarin-6 loaded liposomes across *in vitro* brain tumor model

The *in vitro* brain tumor model was prepared by placing the culture insert (seeded with bEnd.3 on upper side and primary glial cells on the bottom of the insert membrane) above the glioblastoma tumor grown scaffold on day 14 and the entire unit was further cultured for 7 days. This model mimics *in vivo* conditions, where the liposomal formulation prior to reaching the target U87 tumor inside the scaffold must cross the endothelial barrier. The transport of coumarin-6 loaded liposomes (plain, Tf, Pen, and Tf-Pen) was quantified across the *in vitro* brain tumor model by placing them in sterile DPBS containing 10% FBS to mimic the *in vivo* environment. The culture insert with bEnd.3 and glial cells were placed on U87 tumor grown scaffold in 24 well plates containing 1 ml DPBS supplemented with 10% FBS in the lower compartment. In the upper compartment of inserts, the medium was replaced with the coumarin-6 loaded liposomal suspension (200 nMoles) in 500 µl of fresh serum containing buffer. Samples were taken at specific time points of 1, 2, 4, 6, 12 and 24 h by transferring the culture inserts to new wells containing 1 ml DPBS with serum. Following transport, the scaffolds were rinsed with DPBS and tumor cells on scaffold were lyzed by adding 50 µl of 0.5% triton X-100 followed by addition of 450 µl of methanol to extract coumarin-6. The lysate was evaluated by quantifying the

fluorescence intensity of coumarin-6 from the lower compartments using fluorescence SpectraMax® M5 spectrophometer microplate reader (excitation/emission wavelengths 465/502 nm respectively) to calculate the amount of coumarin-6 transport across the endothelial barrier.

2.2.20. Drug loaded Tf-CPP liposomes transport across *in vitro* brain tumor model

The liposomal transport was studied across *in vitro* brain tumor model, as per previously published report [37,43]. To develop the model, the culture insert containing bEnd.3 and glial cells (co-culture endothelial barrier) were placed above the U87 grown scaffold on day 14 and additional cultured for 7 more days. On day 21, the upper compartment of the co-culture endothelial barrier was treated with 200 nMoles of phospholipid concentration of different liposomal formulations (plain, Tf, CPPs, and Tf-CPP) in 500 µl of DPBS with 10% FBS and samples were taken at predetermined intervals. Following the transport, the tumor cells in the scaffold were lysed as per described above and the lysate was centrifuged at 10,000 rpm for 10 min at 4 °C. The transport of liposomes was analyzed in the same way as described above in the cellular uptake using HPLC. Fluorescence analysis of endothelial co-culture barrier after transport of lissamine-rhodamine labeled liposomes was performed. Concisely, the co-culture barrier insert membrane was carefully excised using a scalpel after 24 h treatment with liposomal nanoparticles and stained with Hoechst 33342. Further, the excised membrane was mounted on glass slide and covered with glass cover slip using cytoseal 60 mounting medium. The membrane sections were imaged on a Zeiss Axio observer Z1 LSM 700 confocal laser-scanning microscope (Peabody, MA). The images were processed using Imaris x64 9.0.2 software by Bitplane AG (Concord, MA).

2.2.21. Evaluation of efficacy of 5-FU loaded liposomes on tumor regression

The anti-tumor efficacy of 5-FU loaded liposomes was evaluated by adding different 5-FU loaded liposomes to the culture inserts seeded with brain endothelial and glial cells and placed on

tumor scaffold. The media surrounding the scaffold was replaced with 1 ml DPBS pH 7.4 containing serum. In the upper compartment of inserts, the medium was replaced with 5-FU encapsulated liposomal suspension (200 nMoles) and free 5-FU in 500 µl of fresh serum containing DPBS. The *in vitro* brain tumor model was treated for 24 h and the scaffolds were thereafter incubated for 6 more days in fresh DMEM with 30% FBS at 37ºC under 5% CO_2 atmosphere. The media of the scaffolds was changed every other day. The percent tumor cell viability was determined by using MTT assay. For fluorescence imaging, the scaffolds were stained using viability/cytotoxicity assay kit (Biotum Inc., Fremont, CA) according to manufacturer's protocol. Following that, the scaffolds were embedded in OCT and frozen. Subsequently, the frozen scaffolds were sectioned using cryostat and mounted on polylysine coated slides. The fluorescence images of scaffolds were assessed using Leica DMi8 fluorescence microscope (Leica Microsystems Inc., Buffalo Grove, IL).

2.2.22. Anti-tumor efficacy of Dox and Erlo loaded liposomes using *in vitro* brain tumor model

The antitumor efficacy of liposomes was performed in *in vitro* brain tumor model, as described in previously published report [37,43]. Briefly, the media in the upper compartment of the model was replaced with 200 nMoles of phospholipid concentration of different Dox and Erlo loaded liposomal nanoparticles (plain, Tf, CPPs and Tf-CPPs) in 500 µl of DPBS with 10% FBS and treated for 24 h. Following treatment, the scaffolds were further incubated with fresh DMEM supplemented with 30% FBS for 6 days at 37 °C under 5% CO_2 atmosphere. The media was changed in every two days. The percent cell viability of U87 tumor cells in scaffold was quantified by using MTT assay. This was further confirmed by performing fluorescence imaging of treatment scaffolds. The scaffolds were stained with live/dead cell staining (Biotum Inc., Fremont, CA) after

6 days of treatment, as per the manufacturer's protocol. Then, the scaffolds were snap frozen in OCT and 20 µm thick sections of scaffolds were cut using a cryostat. The slides were observed under Leica DMi8 fluorescence microscope (Leica Microsystems Inc., Buffalo Grove, IL) for the images.

2.2.23. Animal experiments in mice

All animal experiments were performed according to the animal protocol # 17074 approved by the Institutional Animal Care and Use Committee (IACUC) at North Dakota State University. Male/Female nude mice (nu/J; stock # 002019) were used for all animal experiments. Animals were purchased from the Jackson laboratory (Bar Harbor, ME). The animals were housed under controlled temperature conditions with 12 h dark and light cycles. The animals were allowed free access of water and food. The experiments were started after 7 days' acclimation period.

2.2.24. *In vivo* biodistribution and biocompatibility of liposomes

In vivo biodistribution of liposomes was performed qualitatively as well as quantitatively. Male/female mice were randomly divided into six groups each group consisted of 6 mice (3 males and 3 females). Each group was injected with either PBS, free doxorubicin, free erlotinib, doxorubicin and erlotinib loaded plain, Tf, CPPs, and Tf-CPPs loaded liposomes via tail vein at a dose of 15.2 µmoles/ kg of body weight, calculated based on *in vitro* biocompatibility studies. Animals injected with only PBS were considered as control group. After 24 h, animals were sacrificed and various organs including brain, heart, lungs, liver, spleen and kidneys were harvested and blood samples were withdrawn. The organs were washed with PBS, weighed and frozen at -80 °C until assayed. To determine the biodistribution of drugs, organs were homogenized and drugs were extracted in acetonitrile: methanol (9:1). Then, the extracted sample was centrifuged at 10,000 rpm for 15 min at 4 °C. The supernatant was evaporated using vacuum

evaporator. The residue extracted sample was reconstituted in methanol: PBS pH 5.5 (1:1) and vortexed followed by centrifugation of the sample at 4 °C for 15 min at 10,000 rpm to separate unwanted proteins. Quantification of drugs was accomplished by HPLC. The quantification of Dox was performed as described in doxorubicin loading, while the quantification of Erlo was performed as described in erlotinib loading with some modifications. The mobile phase consisted of 0.2 M potassium phosphate buffer pH 3.0: acetonitrile (52:48) with a flow rate of 0.600 ml/min at room temperature. All data were normalized and represented in units of percentage of injected dose per gram of the tissue (% ID/gram).

For qualitative distribution of liposomes, mice were injected with lissamine-rhodamine labeled liposomes via tail vein at a dose of 15.2 µmoles/ kg of body weight. At 24 h, mice were sacrificed and whole body as well as ex-vivo fluorescent images of the organs were acquired using Kodak *in vivo* imaging system FX (Carestream Health Inc., Rochester, NY). The system was equipped with a halogen lamp of 150 W as the excitation light source and rhodamine channel was used to acquire images. The organs were exposure for 2 min. The captured images were processed using Kodak molecular imaging software (4.0). For biocompatibility of liposomes, all the major organs including brain, heart, lungs, liver, spleen, and kidneys were harvested and fixed in 10% neutralized buffer formalin. Then, the organs were embedded in paraffin and sectioned for histopathological analysis with hematoxylin and eosin (H&E) staining. The tissue slides were carefully observed for any sign of toxicity.

2.2.25. Anti-tumor efficacy in mice

For orthotopic brain tumor model, male/female nude mice were anesthetized (using a mixture of oxygen 1 L/min and 4% of isoflurane for induction and later 1% for maintenance) and carefully placed on a stereotaxic apparatus (David Kopf Instruments, Tujunga, USA). A 10 mm

incision was made along the midline and a burr hole was drilled into the frontal lobe of the skull 1.6 mm to the right lateral and 0.7 mm anterior to the bregma using a high speed drill. With the help of a 27 Gauge Hamilton syringe 5 µl of DMEM containing 5 x 10^5 U87 cells were injected at the junction between the cortex and striatum at a depth of 3.0 mm from the outer border of cranium over a period of 10 min. The needle was kept in place for another 5 min after injection and then slowly removed to prevent a vacuum and cell build-up the needle track. The hole was covered with bone wax to prevent the leakage of cerebrospinal fluid and surgical clips were used to close the incision. After surgery, animals were regularly checked for any sign of pain and distress.

2.2.26. Tumor regression

After 10 days of tumor inoculation, the mice were randomly divided into 6 groups and each group consisted of 6 mice. Each group was injected with either PBS, free Dox-Erlo, Dox and Erlo loaded plain, Tf, Pen, and Tf-Pen loaded liposomes at a dose of 15.2 µmoles/ kg of body weight. Dose was administered *via* tail vein injection, every two days with a total of 3 doses per mouse. At day 16, mice were sacrificed and brains were surgically removed. Brains were fixed in 10% neutralized buffer formalin and embedded in paraffin. Hematoxylin and eosin (H&E) staining was performed on brain sections. Brain tumor diameter was measured and tumor area was calculated using the formula: $\pi\ (d/2)^2$. Where d corresponds to the diameter of tumor [102]. Percent body weight of mice were also measured.

2.2.27. Survival study

On day 10^{th} of tumor inoculation, the animals were randomly divided into 6 groups. Mice in each group were administered 3 doses of either PBS, free Dox-Erlo, Dox and Erlo loaded Plain, Tf, Pen, and Tf-Pen liposomes at a dose of 15.2 µmoles/ kg of body weight in every two days *via* tail vein injection. Survival time was calculated from the day of tumor inoculation (day 0) to the

day of death of mice. Kaplan-Meier survival curves were plotted for each group using Graphpad Prime 5.0 for windows (GraphPad Software, Inc., La Jolla, CA).

2.2.28. Immunofluorescence staining for proliferation and apoptosis

Brains were harvested from mice after treatments and fixed in 10% neutralized buffer formalin, paraffin-embedded, and sectioned (4 μm thick). The brain tissue sections were incubated with anti-Ki-67 antibody (1:500) (Abcam, Cambridge, MA) for cell proliferation and with anti-cleaved PARP antibody (1:800) (Abcam, Cambridge, MA) for cell apoptosis for 1 h. Thereafter, the tissue sections were incubated with goat anti-rabbit CF®633 (1:200) (Biotum, Inc., Fremont, CA). The slides were observed under Leica DMi8 fluorescence microscope (Leica Microsystems Inc., Buffalo Grove, IL).

2.2.29. Data analysis

All the quantitative data were demonstrated as a mean ± standard deviation (SD). Statistical significant analysis among groups were performed using either Student's t test, one or two-way ANOVA. A p value of less than 0.05 was considered statistically significant. All quantitative data analysis was performed using Graphpad Prime 5.0 for windows (GraphPad Software, Inc., La Jolla, CA).

CHAPTER 3. RESULTS AND DISCUSSION

3.1. Synthesis and characterization of liposomes

The distal end of the NHS-PEG_{2000}–DSPE was modified by Tf and CPPs *via* nucleophilic substitution reaction at room temperature. The activated NHS ester group of PEG derivatives reacts with primary amine groups in Tf and CPPs in slightly alkaline conditions (pH 8 – 9) to form stable amide bonds. The coupling was confirmed using micro BCA assay and HPLC, which showed more than 75 % of coupling efficiency. The dual-functionalized liposomes were prepared by post-insertion technique, which efficiently inserts active ligands into preformed liposomes, thereby eliminates the probability of degradation of encapsulated agents by reacting with coupling agents [103,104]. In addition, the post-insertion technique is a spontaneous process, where hydrophobic part of lipid membrane interacts with hydrophobic part of PEG derivatives [105]. The post-insertion technique is majorly used for the insertion of large targeting protein to the liposomes which may eliminate the chances of protein conformational changes and decrease in targeting efficiency [106,107]. The incorporation of CPP-$PEG_{(2000)}$-DSPE with other lipids directly in the formation of liposomes, gives accuracy and reproducibility in production of stable liposomes as well as helps in controlling the amount of CPP in the formulation [107,108]. As listed in Table 1, the mean particle size and zeta potential of Tf-Pen-conjugated liposomes were less than 200 nm and ~ 3 mV, respectively. The average size of plain liposomes and Tf-Pen-conjugated liposomes was 172.52 ± 6.71 and 178.12 ± 4.67, respectively. Therefore, the coupling of transferrin and penetratin to the liposomes showed no significant difference ($p > 0.05$) in the particle size of the liposomes. In addition, the zeta potential of plain and Tf-Pen-conjugated liposomes was observed to be 4.86 ± 2.15 mV and 2.12 ± 1.56 mV, respectively. The size of Tf-Pen, Tf-TAT, Tf-QLPVM and Tf-PFV were also below 200 nm (Table 2). The results showed that

coupling of transferrin protein to the liposomes changed the zeta potential to a net negative value, which is because of presence of negative charges on transferrin. However, the Tf-CPP liposomes carry near neutral zeta potential (0-15 mV), which could be attributed to counter balancing of the negative charge of transferrin with the positive charge of CPP. The near neutral charge of dual functionalized liposomes is anticipated to prevent elimination by macrophage system [109,110]. The coupling efficiency of transferrin and penetratin as determined by micro BCA assay, was 56.1 ± 2.83 % and 62.81 ± 5.29%, respectively.

pH gradient method was used to ensure high entrapment of 5-FU.[97] The use of 300 mM sodium carbonate pH 9.6 is to protonate 5-FU intra-liposomally, which leads to further diffusion of the neutral unionized 5-FU from outside, according to concentration gradient. In order to achieve high entrapment, the core of the liposomes must be highly buffered to sustain the pH gradient to accumulate more 5-FU. The 5-FU encapsulation efficiencies of plain, Tf, Pen, and Tf-Pen liposomes were quantified as 25.08 ± 2.33%, 25.67 ± 1.47%, 24.98 ± 1.59%, and 25.61 ± 1.13%, respectively and showed no significant difference ($p > 0.05$) amongst the formulations. This might be because 5-FU is a small, membrane permeable and highly water soluble drug molecule. The retention of such a small and water soluble molecule in the hydrophilic core of liposomes is therefore quite difficult. In addition, no interference was seen in the entrapment of 5-FU due to presence of penetratin and transferrin on the liposomal surface. The *in vitro* release of 5-FU from liposomes was studied to examine the drug release property of liposomes in 10% FBS. The results showed that the percent cumulative release was 79.16 ± 2.69%, 62.16 ± 0.97%, 75.05 ± 5.22%, and 71.90 ± 2.71% from plain, Tf, Pen, and Tf-Pen liposomes, respectively over a period of 8 h (Figure 2). Whereas the *in vitro* release profile of Dox and Erlo loaded Tf-PFV liposomes

were studied in 10% FBS. The percent cumulative release for Dox and Erlo was more than 37% and 41% for liposomes, respectively, over the period of 24 h (Figure 3).

The pH gradient method was used to entrap Dox into liposomes. The hydration of thin film of lipids with 300 mM citric acid pH 5.0, protonates Dox intra-liposomally. According to concentration gradient, the protonation of Dox by acidic buffer further helps in diffusion of the unionized Dox from outside. The core needs to be highly buffered to endure the pH gradient for the high entrapment of Dox. Erlo is entrapped in the exterior lipid bilayer due to its strong hydrophobicity. The entrapment efficiencies of Dox and Erlo for all liposomal formulations were approximately 65% and 53%, respectively (Table 2). The surface modification of liposomes did not significantly ($p > 0.05$) affect the entrapment of drugs.

Table 1. Particle size distribution and zeta potential of various liposomal formulations

Liposomes	Particle size (nm)	PDI[a]	Zeta Potential (mV)
Plain	172.52 ± 6.71	0.20 ±0.01	4.86 ± 2.15
Tf	176.42 ± 5.86	0.27 ± 0.08	-8.11 ± 3.68
Pen	176.80 ± 1.84	0.25 ± 0.04	7.66 ± 1.23
Tf-Pen	178.12 ± 4.67	0.27 ± 0.09	2.12 ± 1.56

[a] Polydispersity index (PDI). The data represented as mean ± SD, (n=4).

Table 2. Particle size distribution, polydispersity index, zeta potential and entrapment efficiency of various liposomal formulations

Liposomes	Particle size (nm)	PDI[a]	Zeta Potential (mV)	Dox EE[b] (%)	Erlo EE[b] (%)
Plain	174.45 ± 10.24	0.17 ± 0.02	5.85 ± 2.37	64.80 ± 1.98	53.79 ± 1.48
Tf	177.45 ± 3.69	0.21 ± 0.02	-6.50 ± 1.08	65.32 ± 2.67	53.84 ± 1.10
Pen	177.98 ± 4.46	0.22 ± 0.02	16.25 ± 0.49	65.89 ± 2.85	53.94 ± 1.46
Tf-Pen	177.95 ± 7.04	0.19 ± 0.03	10.43 ± 0.50	65.80 ± 1.13	52.57 ± 1.70
TAT	173.60 ± 1.57	0.26 ± 0.02	20.35 ± 2.06	66.91 ± 2.54	52.67 ± 2.28
Tf-TAT	174.90 ± 4.45	0.25 ± 0.03	15.03 ± 3.94	65.72 ± 3.57	54.61 ± 1.18
QLPVM	171.90 ± 2.45	0.20 ± 0.04	19.27 ± 4.66	65.06 ± 1.20	51.82 ± 1.46
Tf-QLPVM	175.57 ± 4.57	0.25 ± 0.02	14.87 ± 0.53	66.47 ± 1.87	53.37 ± 1.10
PFV	158.70 ± 1.45	0.21 ± 0.02	14.16 ± 1.48	65.08 ± 1.10	53.92 ± 1.97
Tf-PFV	161.90 ± 4.60	0.23 ± 0.01	7.66 ± 0.87	65.26 ± 1.89	53.99 ± 1.63

[a] Polydispersity index (PDI). [b] Entrapment efficiency (EE). The data represented as mean ± SD, (n=4).

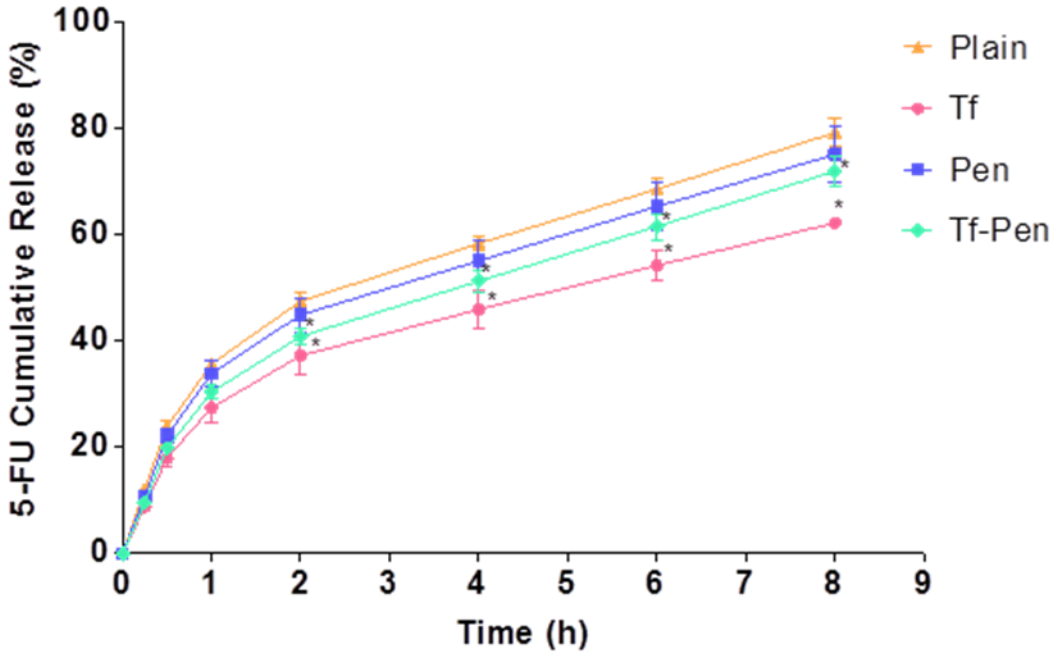

Figure 2. Percent cumulative 5-FU release from plain, Tf, Pen, and Tf-Pen liposomes. Statistically significant ($p < 0.05$) differences is shown as (*) with plain liposomes. Data represented as mean ± S.D. (n=4).

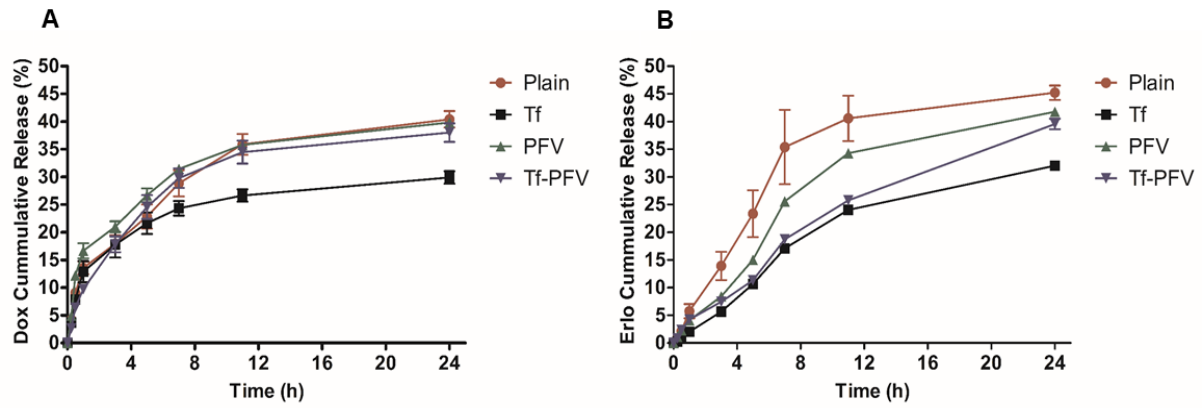

Figure 3. Percent cumulative (A) Dox and (B) Erlo release from plain, Tf, PFV, and Tf-PFV liposomes. Data represented as mean ± S.D. (n=3).

3.2. *In vitro* biocompatibility studies

The cytotoxicity was determined using MTT assay in glioblastoma (U87) and brain endothelial (bEnd.3) cells. It is important for a delivery carrier to be biocompatible at a desired concentration and should also have the ability to deliver the encapsulated agent. The cytotoxicity results revealed cell viability of more than 85%, relative to the untreated control group ($p<0.05$), after exposure to Tf-Pen-conjugated liposomes up to a phospholipid concentration of 200 nMoles, which demonstrates that liposomes are non-toxic and biocompatible with glioblastoma and brain endothelial cells (Figure 4). However, the cytotoxicity increased at higher phospholipid concentrations, which can be attributed to the presence of cationic peptide at the surface of liposomes. As depicted in Figure 4, the cell viabilities at 600 nMoles lipid concentration were found to be 66.83 ± 1.56% and 68.96 ± 2.15% in U87 and bEnd.3 cells, respectively. The cell viability of positively charged pen-conjugated liposomes was lower compared to the negatively charge Tf-conjugated liposomes, Tf-pen liposomes, and plain liposomes, irrespective of the type of cells. However, Tf-conjugated liposomes demonstrated greater cell viability as compared to Tf-Pen liposomes because of the negative charge of transferrin.

Similarly, *In vitro* biocompatibility of CPP and Tf-CPP liposomes were performed in U87, bEnd.3 and glial cell lines using MTT assay to demonstrate that liposomes are biocompatible and non-toxic. After exposure to different phospholipid concentrations of liposomes, MTT assay revealed the cell viability was more than 85%, relative to the untreated control group, up to a phospholipid concentration of 200 nMoles (Figure 5, 6 and 7). In case of all three cell lines, the viability decreased as the concentration of phospholipid increased regardless of cell types. The viability at 600 nMoles were observed to be less than 69% for U87, bEnd.3 and glial cells, respectively. At higher phospholipid concentration, the cell viabilities were observed to be lowered with Tf-QLPVM liposomes in all cell lines. This can be attributed in relation to the hydrophobic nature of QLPVM, which increases the interaction of this peptide with plasma membrane, resulting in increased membrane destabilization and permeabilization through binding to intracellular targets [111,112]. The cell viabilities of CPP coupled liposomes were lower compared to Tf coupled, plain and Tf-CPP liposomes in all three cell lines. This is can be due to their higher cationic charge.

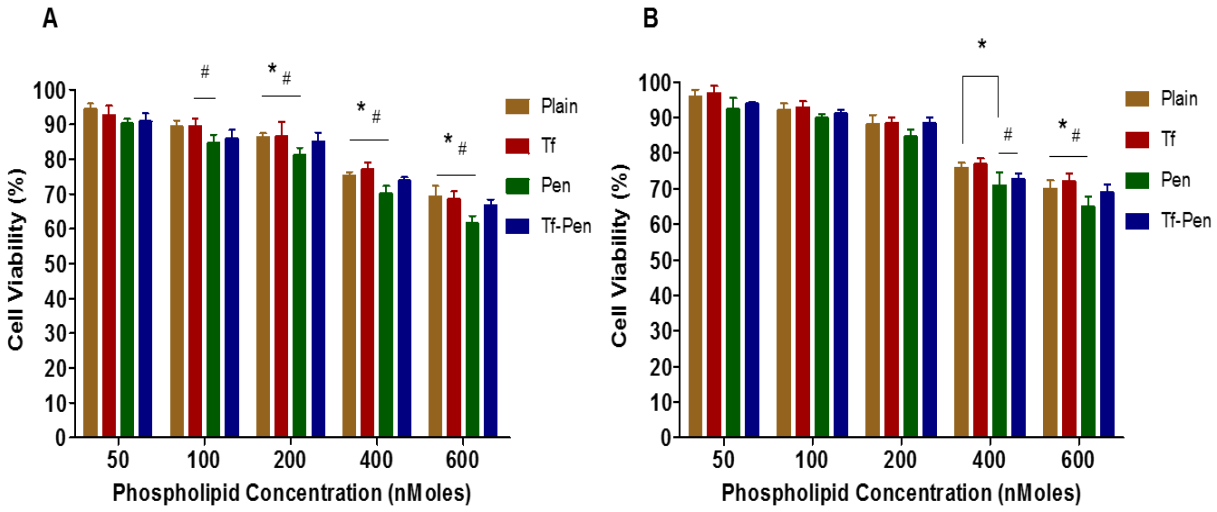

Figure 4. *In vitro* cell viabilities of (A) U87and (B) bEnd.3 cells after exposure to different phospholipid concentrations of plain, Tf, Pen, and Tf-Pen liposomes. Statistically significant ($p < 0.05$) differences is shown as (*) with plain liposomes and (#) with Tf-liposomes. Data represented as mean ± S.D., (n=4).

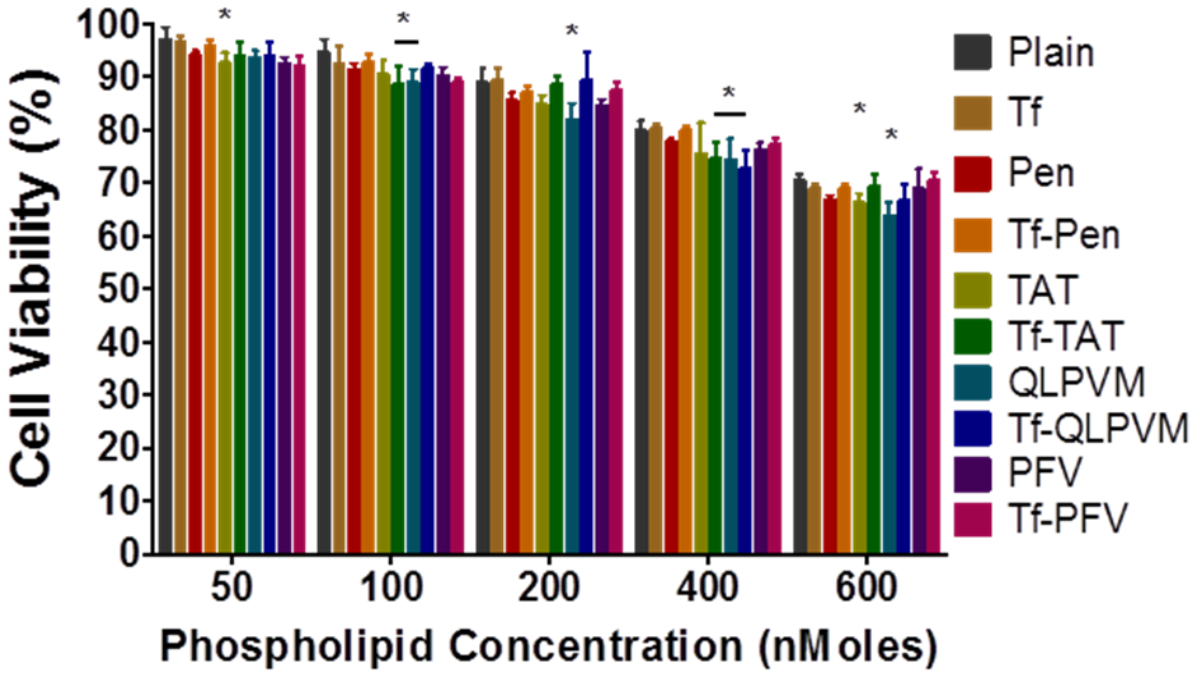

Figure 5. Graphical representation of the viabilities of U87 cells after exposure to various liposomes at varying phospholipid concentrations. The results are expressed as mean ± S.D. (n=4); *p<0.05 against plain liposomes at respective concentrations.

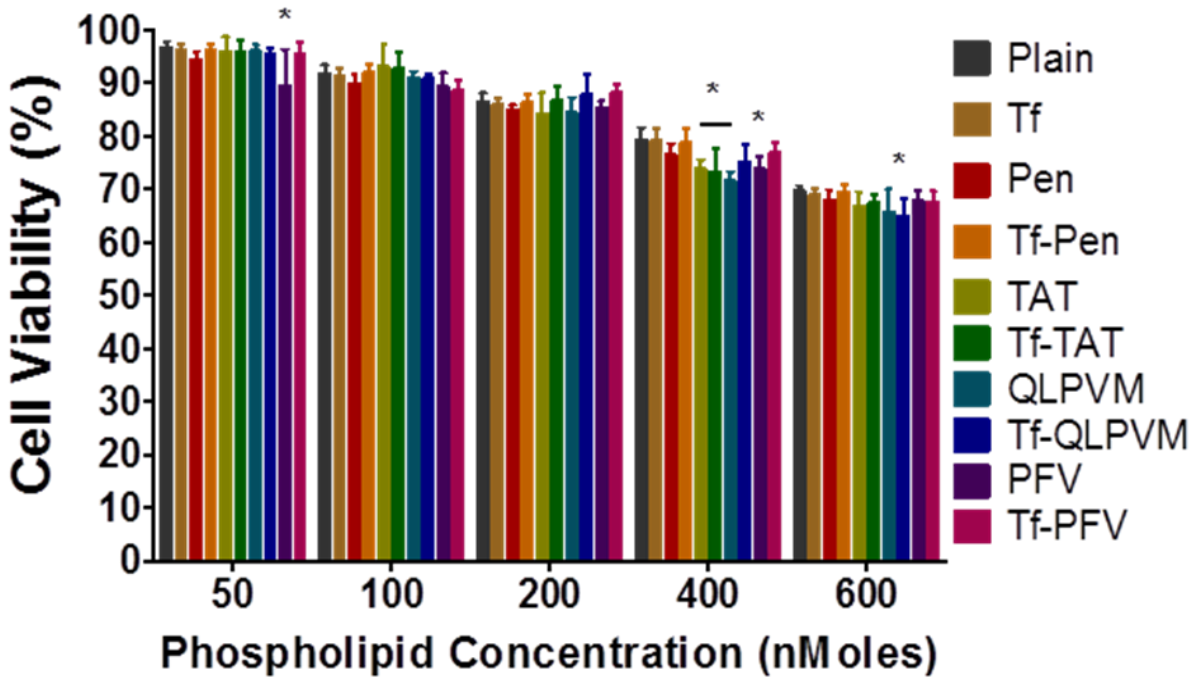

Figure 6. Graphical representation of the viabilities of bEnd.3 cells after exposure to various liposomes at varying phospholipid concentrations. The results are expressed as mean ± S.D. (n=4); *$p<0.05$ against plain liposomes at respective concentrations.

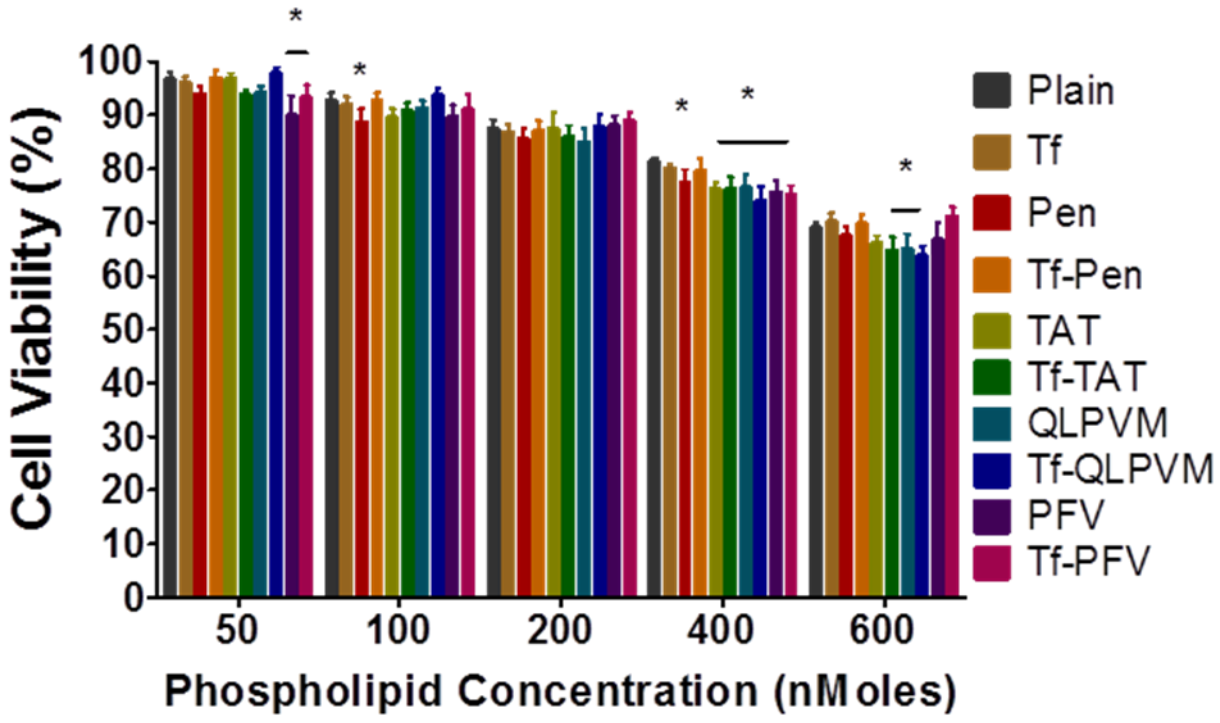

Figure 7. Graphical representation of the viabilities of glial cells after exposure to various liposomes at varying phospholipid concentrations. The results are expressed as mean ± S.D. (n=4); *p<0.05 against plain liposomes at respective concentrations.

3.3. Cellular uptake evaluation

The uptake of surface modified liposomes was studied quantitatively as well as qualitatively in U87 and bEnd.3 cells. Tf-Pen-conjugated liposomes labeled with lissamine rhodamine demonstrated maximum uptake as observed from the strong pattern of fluorescence throughout the cytoplasm as well in the nucleus, compared to plain liposomes that showed lowest uptake (Figures 8A and B). Moreover, Tf-conjugated liposomes showed higher uptake than Pen-conjugated liposomes and plain liposomes. The quantitative estimation of 5-FU uptake by the cells also showed higher uptake of dual functionalized liposomes, which confirmed the higher effectiveness of dual functionalized liposomes on cellular uptake over single ligand or plain liposomes (Figures 8C and D). The uptake of 5-FU loaded Tf-Pen-conjugated liposomes was found to be 66.64 ± 3.00% and 59.68 ± 4.55% in U87 and bEnd.3 cells, respectively, which was

significantly higher than single ligand (47.66 ± 1.78 % and 46.28 ± 2.39 % respectively for Tf and 45.91 ± 4.62 and 43.42 ± 2.31 respectively for Pen) or plain liposomes (31.51 ± 2.92% and 28.56 ± 3.29% respectively). This can be explained by the presence of cationic charge on penetratin which facilitated the binding and internalization of Tf-Pen-conjugated liposomes. It is reported that electrostatic interaction of positively charged penetratin with negatively charged heparin sulfate proteoglycans on the cell surface enables the internalization of penetratin through endocytic transcytosis [92]. This electrostatic interaction is postulated to facilitate cellular uptake of Pen-conjugated liposomes. However, the cellular uptake of Tf-conjugated liposomes was not significantly higher as compared to Pen-conjugated liposomes, which shows greater uptake via receptor-mediated transcytosis. Therefore, the cellular uptake of Tf-pen-conjugated liposomes is believed to be a combination effect of both initial binding of penetratin followed by Tf receptor mediated transcytosis that resulted in enhanced uptake of liposomes. The U87 cells showed higher cellular uptake of Tf-Pen-conjugated liposomes compared to bEnd.3 cells, illustrating a cell-type dependent liposomal uptake [35]. In summary, the results from the uptake study assessed the importance of dual targeting mechanism over single mechanism of receptor targeting or cell penetration.

The cellular uptake of different liposomal formulations (plain, Tf, CPPs, and Tf-CPPs) were evaluated quantitatively as well as qualitatively in three different cell lines following 2 h of incubation. The fluorescence images in Figure 9 shows the uptake of lissamine rhodamine labeled liposomes in all three cell lines. Tf-CPP liposomes showed strong fluorescence pattern all through cytoplasm and nucleus in comparison to single ligand or plain liposomes. Moreover, Tf liposomes displayed higher uptake than CPP liposomes and plain liposomes. As shown in Figure 10 and 11, the Dox and Erlo loaded liposomes demonstrated more than 66 % cellular uptake in all the three

types of cells. The quantitative estimation confirmed the efficacy of dual functionalization of liposomes over single. As compared to the cellular uptake of dual functionalized liposomes, the plain liposomes had only ~ 30 % of uptake, which demonstrated statistically significant ($p < 0.05$) difference. In addition, the dual functionalized liposomes exhibited significantly ($p < 0.05$) higher uptake as compared to single ligand liposomes. This can be described by dual mechanisms of liposomal uptake through both Tf receptors and enhanced cell penetration by CPPs, thereby believed to be a combination effect which enabled higher uptake of liposomes. In addition, the positively charged CPP coupled liposomes interacted electrostatically with negatively charged membrane and facilitated the uptake of liposomes through adsorptive mediated transcytosis [113]. Therefore, the rapid and higher uptake of Tf-CPP liposomes demonstrated synergistic effect of interacting with cell membrane followed by binding of Tf to Tf receptor, thereby leading to increase in cellular uptake in all three cell lines.

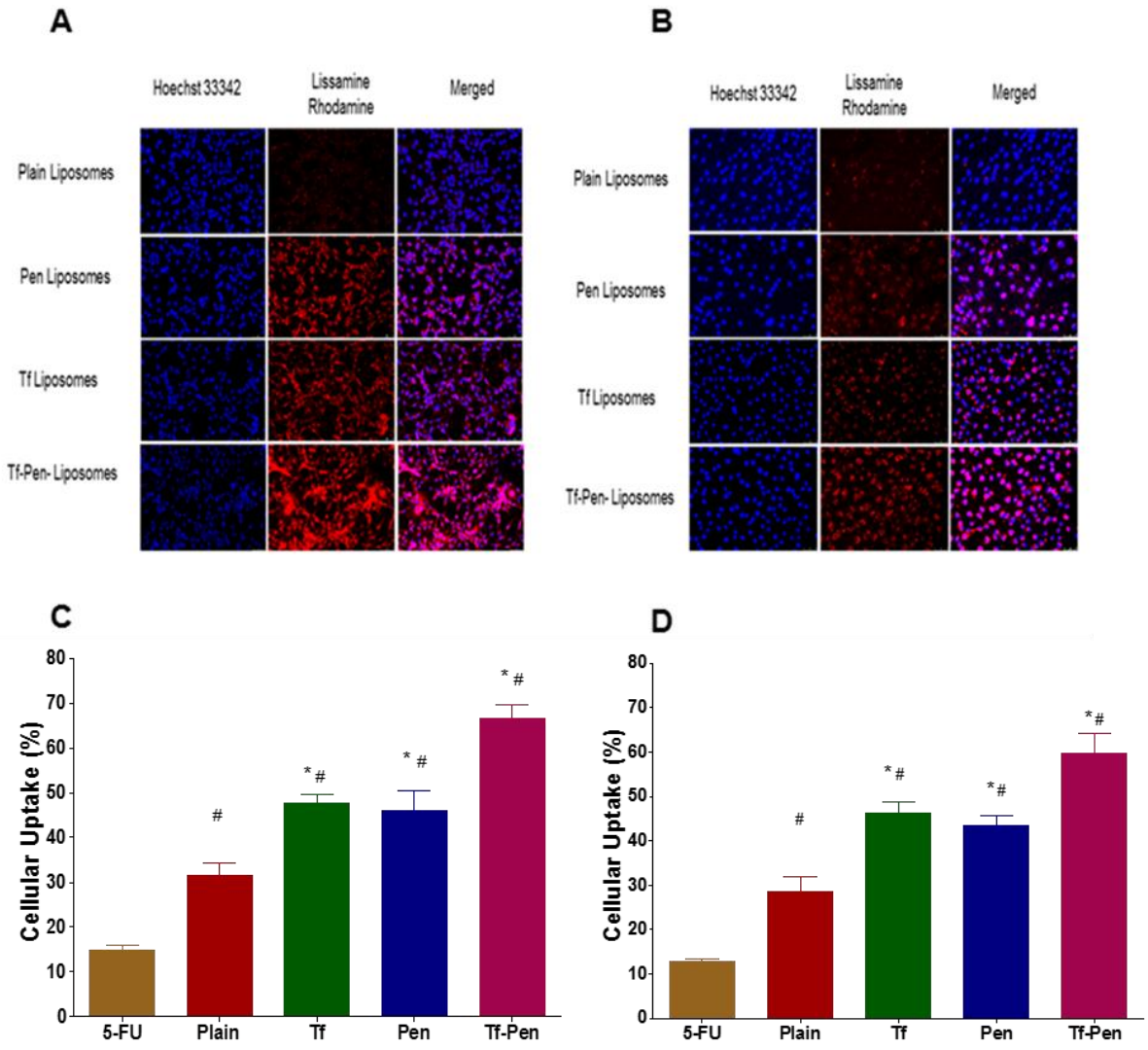

Figure 8. Fluorescence microscopic images (10X magnification) showed uptake of lissamine rhodamine labeled liposomes (excitation/emission wavelengths: 560/583 nm) in A) U87 and B) bEnd.3 cells after 2 h incubation. The nuclei of the cells were stained with Hoechst 33342 (excitation/emission wavelengths: 350/461 nm). The images show overlap of lissamine rhodamine labeled (red) and nuclei of the cells (blue). Graphs represent cellular uptake of 5-FU encapsulated liposomes in C) U87 and D) bEnd.3 cells after 2 h incubation. Data represented as mean ± SD, (n=4). Statistically significant ($p < 0.05$) differences is shown as (*) with plain liposomes and (#) with 5-FU.

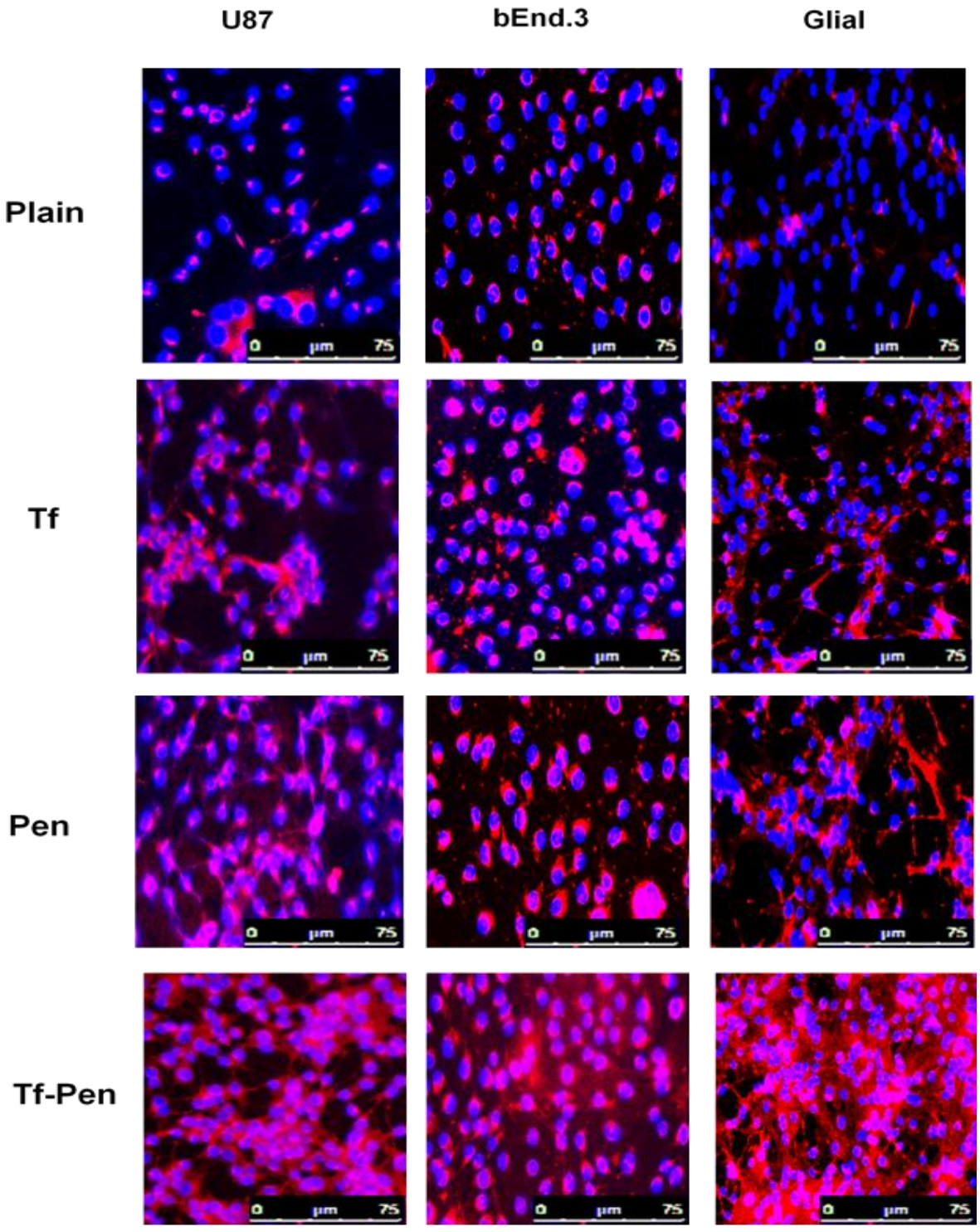

Figure 9. Fluorescence images showed uptake of lissamine rhodamine labeled liposomes after 2 h incubation in U87, bEnd.3 and Glial cells (red; excitation/emission wavelengths: 560/583 nm). Nuclei were stained with Hoechst 33342 (blue; excitation/emission wavelengths: 350/461 nm). Scale bar: 75 µm

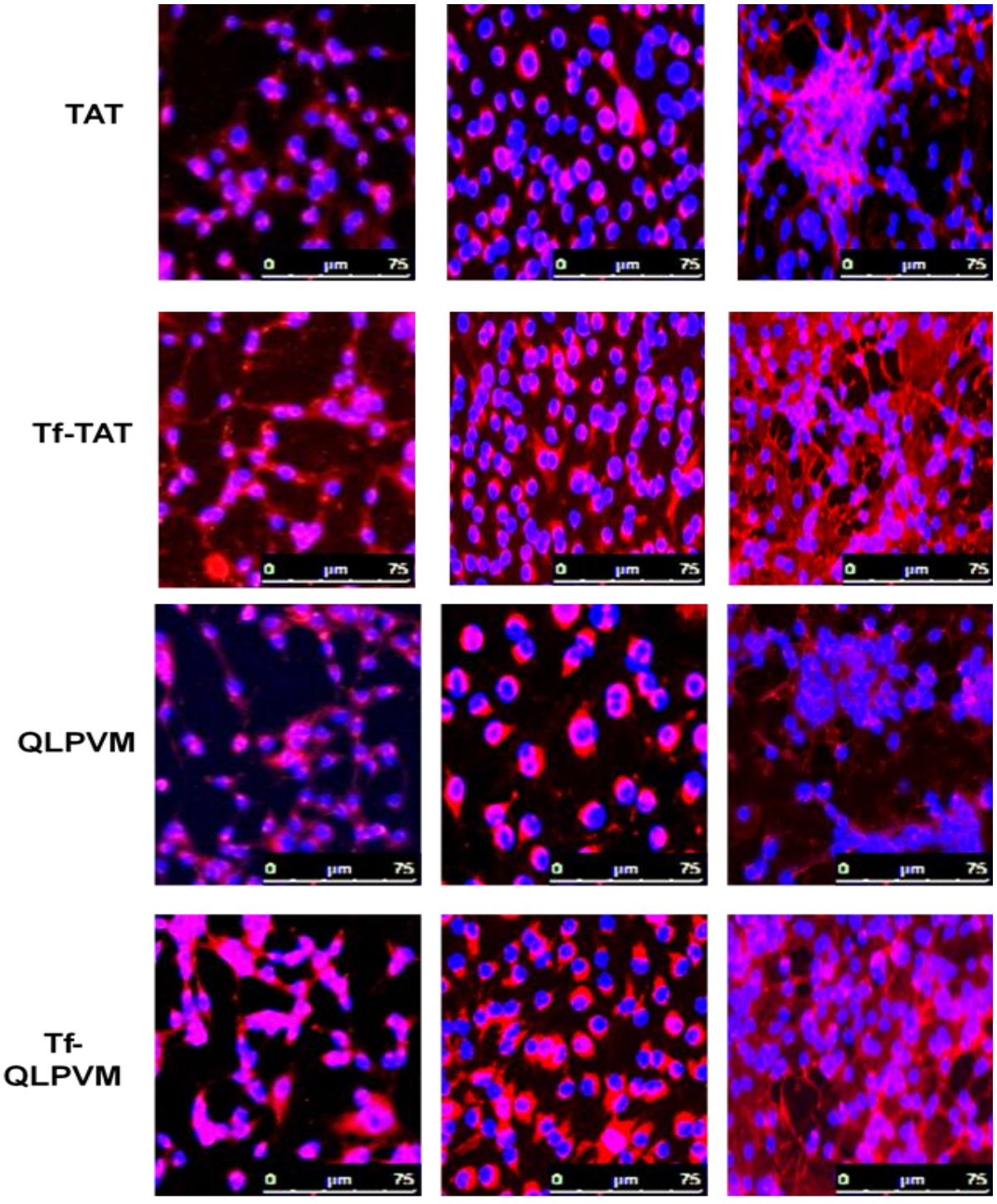

Figure 9. Fluorescence images showed uptake of lissamine rhodamine labeled liposomes after 2 h incubation in U87, bEnd.3 and Glial cells (red; excitation/emission wavelengths: 560/583 nm) (continued). Nuclei were stained with Hoechst 33342 (blue; excitation/emission wavelengths: 350/461 nm). Scale bar: 75 µm

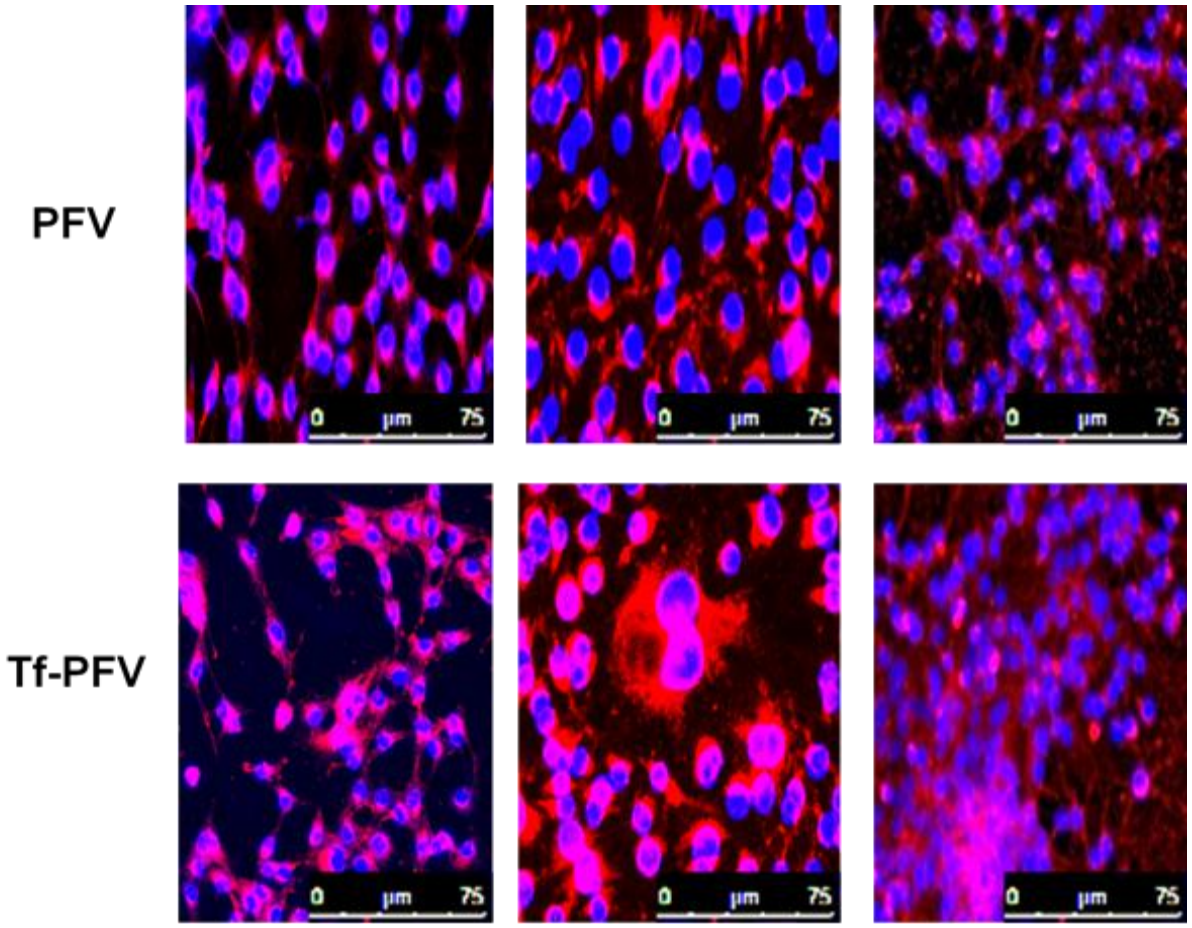

Figure 9. Fluorescence images showed uptake of lissamine rhodamine labeled liposomes after 2 h incubation in U87, bEnd.3 and Glial cells (red; excitation/emission wavelengths: 560/583 nm) (continued). Nuclei were stained with Hoechst 33342 (blue; excitation/emission wavelengths: 350/461 nm). Scale bar: 75 µm

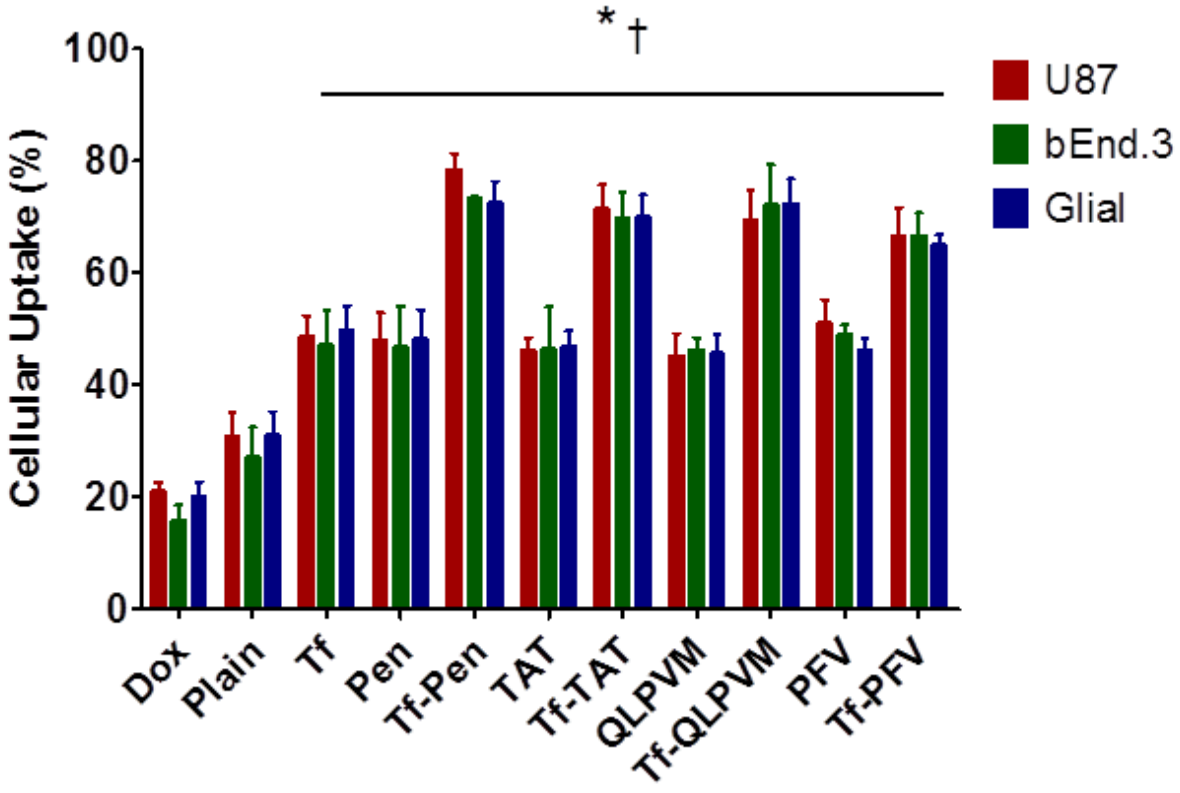

Figure 10. The graph represents the cellular uptake of doxorubicin from various liposomes in U87, bEnd.3 and Glial cells after 2 h incubation. Data represented as mean ± SD, (n=4). Statistically significant ($p < 0.05$) differences between different formulation groups are shown as (*) with plain liposomes, with (†) Dox. There is no significant difference between all three cell types in a particular treatment group.

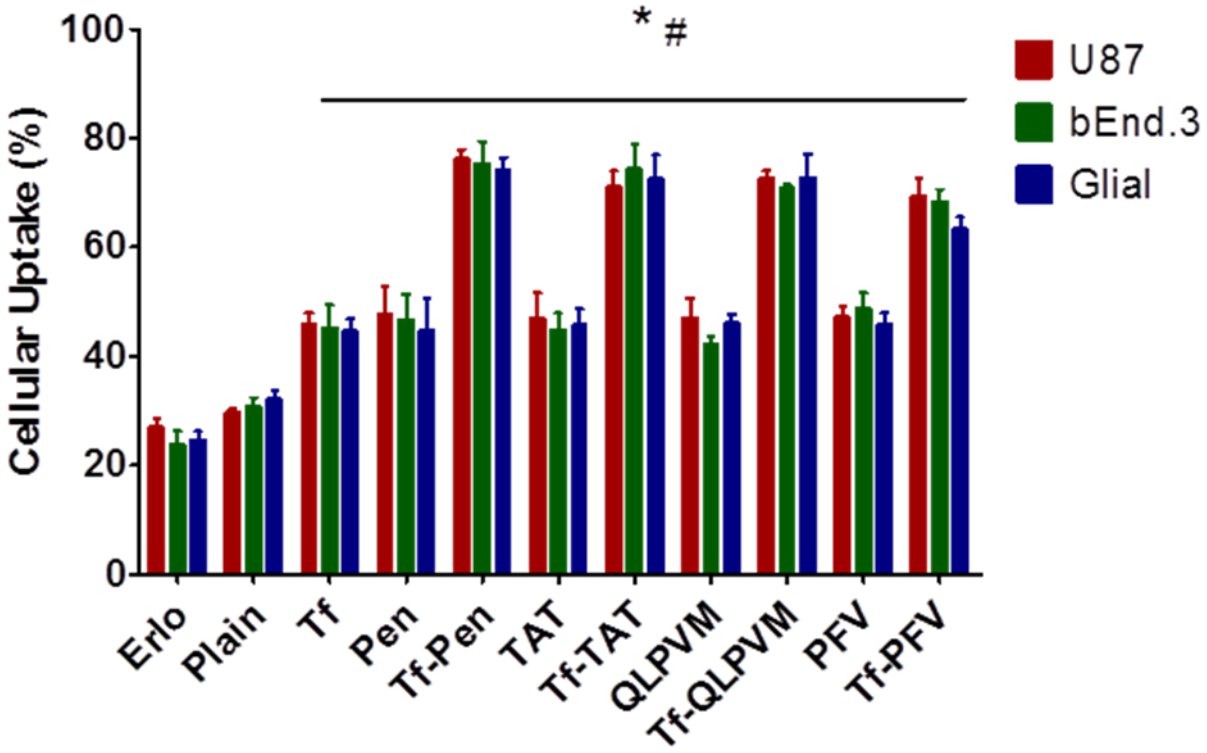

Figure 11. The graph represents the cellular uptake of doxorubicin from various liposomes in U87, bEnd.3 and Glial cells after 2 h incubation. Data represented as mean ± SD, (n=4). Statistically significant ($p < 0.05$) differences between different formulation groups are shown as (*) with plain liposomes, with (#) Erlo. There is no significant difference between all three cell types in a particular treatment group.

3.4. Apoptosis assessment

The induction of apoptosis in U87 cells is demonstrated in Figure 12. The total percentage of apoptosis in U87 cells was found to be 68.7 ± 9.36%, 35.42 ± 2.92%, 35.82 ± 4.76%, 24.55 ± 0.86%, 23.3 ± 2.62%, and 10.82 ± 2.56% for Tf-Pen, Tf, Pen, plain liposomes, free 5-FU, and control, respectively (Figure 12). Whereas the total percentage apoptosis in U87 cells after treatment with Tf-PFV, Tf, PFV, Plain liposomes, Free Dox-Erlo was about 60.87 ± 6.57, 45.67 ± 1.99, 45.62 ± 1.28, 36.02 ±1.41, 24.32 ± 2.78 and 11.87 ± 0.71, respectively (Figure 13). The *in vitro* cytotoxicity study revealed the apoptotic effects of drug loaded liposomes via induction of apoptosis leading to cell death, therefore proving the anticancer potency in U87 cells. The higher

uptake of Tf-CPP liposomes showed greater apoptotic effects as compared to single ligand or plain liposomes of the cells induced by the various formulations.

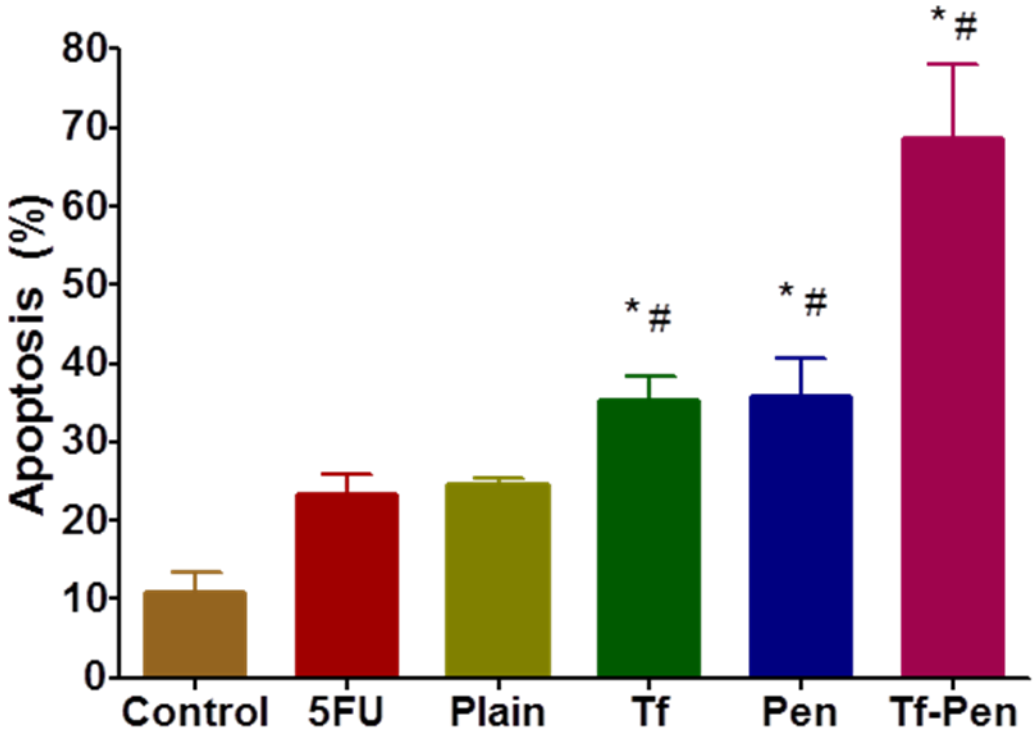

Figure 12. Graph shows the percentage of apoptosis in U87. Data represented as mean ± S.D. (n=4). Statistically significant ($p < 0.05$) differences is shown as (*) with plain liposomes and (#) with free 5-FU.

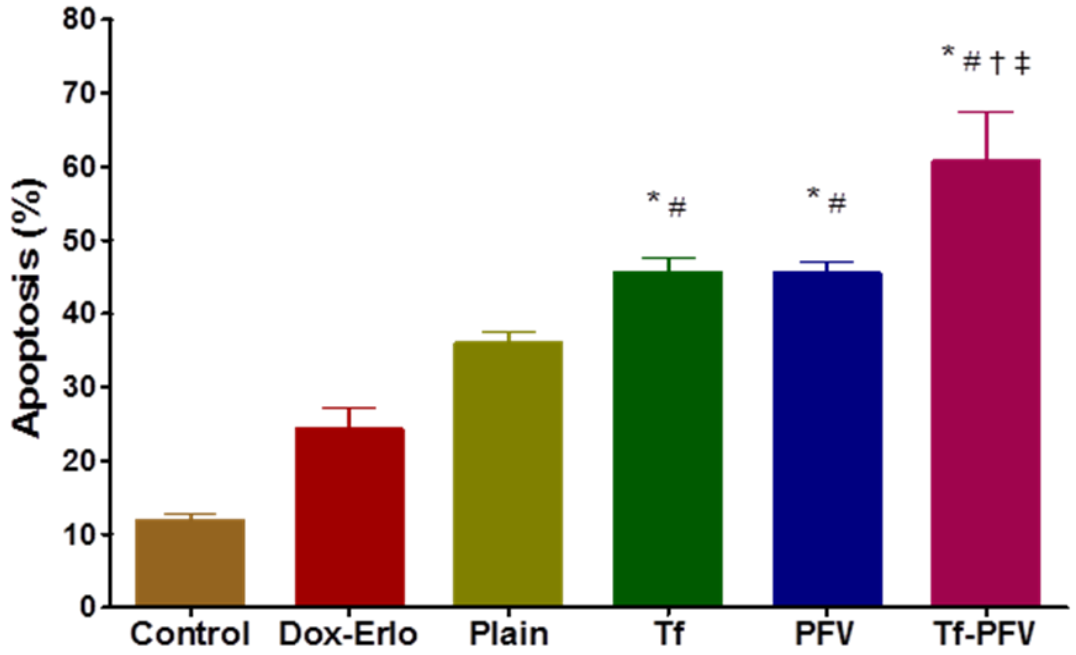

Figure 13. Graph shows the proportion of apoptosis in U87 cells after treatment with Dox and Erlo encapsulated liposomes and free Dox -Erlo for 5 h. Statistically significant ($p < 0.05$) differences is shown as (*) with plain liposomes, (#) with free Dox-Erlo, (†) Tf-liposomes, and (‡) PFV-liposomes.

3.5. Penetration ability into U87 tumor spheroids

U87 tumor spheroids that show characteristics of glioblastoma tumor *in vivo*, was used as a model to exhibit the penetration ability of liposomes, as displayed in Figure 14. After incubation with various coumarin-6 loaded liposomal formulations, images were taken at different layers from the top to the equatorial plane of a spheroid using confocal laser scanning microscope (CLSM). Results showed that Tf-Pen liposomes displayed strongest fluorescence intensity compared to single ligand or plain liposomes. In addition, the images demonstrated the strong ability of Tf-Pen liposomes to penetrate much deeper into the core of U87 tumor spheroids as compared to single ligand or plain liposomes.

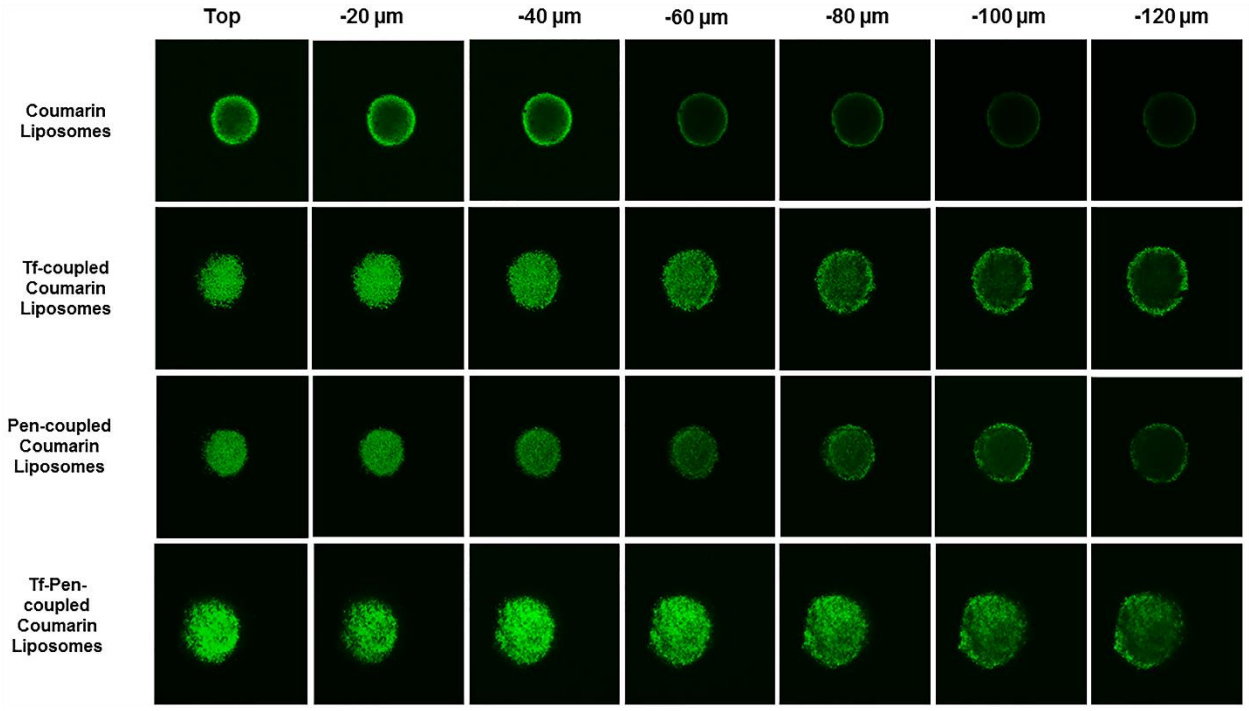

Figure 14. Penetration ability of coumarin-6 labeled liposomes into U87 tumor spheroids after 12 h. The CLSM images (10X magnification) of U87 tumor spheroids penetration of liposomes in different planes.

3.6. Hemolysis assay

The Tf-Pen-conjugated liposomes were designed to be administered into systemic circulation and therefore it is essential to determine the biocompatibility of liposomes for *in vivo* administration. The cationic charge on liposomes may initiate non-specific interactions between erythrocytes and liposomes and cause lysis of cells and a subsequent release of hemoglobin. Such interactions may lead to significant decrease in half-life, reproducibility of medication, embolization, trigger thrombosis and hemolysis, in vivo [114–117]. The hemocompatibility of the liposomes was determined by quantifying the release of hemoglobin from erythrocytes by spectrophotometer after treatment with different concentrations of phospholipids. Results demonstrated higher release of hemoglobin with increasing phospholipid concentration. Both Tf-Pen and Tf-conjugated liposomes were observed to be non-toxic and biocompatible to up to 800

nM phospholipid concentration (Figure 15). However, Pen-conjugated liposomes showed significantly higher hemolysis at the same phospholipid concentration. This can be explained by the presence of cationic charges on these liposomes, which leads to high interaction with erythrocyte membrane. On the other hand, Tf-conjugated liposomes showed minimal hemolysis due to presence of negative charges on the liposomes, thereby lesser interactions.

Similar results were obtained up on determining the hemolytic potential of Tf-CPP liposomes. Up to 10% of hemolysis is considered as non-toxic and biocompatible. As shown in Figure 16, the percent hemolysis increased with increasing in the phospholipid concentrations. Plain, Tf and Tf-Pen, and Tf-TAT liposomes demonstrated less than 9% hemolysis up to a concentration of 800 nMoles of phospholipids. However, Tf-QLPVM and Tf-PFV liposomes showed slight hemolysis at a concentration of 800 nMoles of phospholipids as compared to Tf-liposomes. This can be attributed due to the presence of more hydrophobic amino acid residues in QLPVM and PFV, thereby increasing its interaction with lipophilic erythrocytes' membrane [35]. In addition, at the same phospholipid concentration, CPP coupled liposomes demonstrated higher percent of hemolysis due to the greater interaction of cationic charged CPPs with the erythrocytes' membrane. At high phospholipid concentration, Tf liposomes demonstrated higher percent hemolysis as compared at low phospholipid concentration. This is due to the Tf protein aggregation at high concentration, thereby leading to nonspecific interactions of Tf aggregates with erythrocytes and resulting in destabilization of membrane as compared to decreased interactions of Tf and erythrocytes' membrane [114]. Thus, Tf-CPP liposomes are considered as safe, non-toxic and biocompatible for intravenous administration into mice.

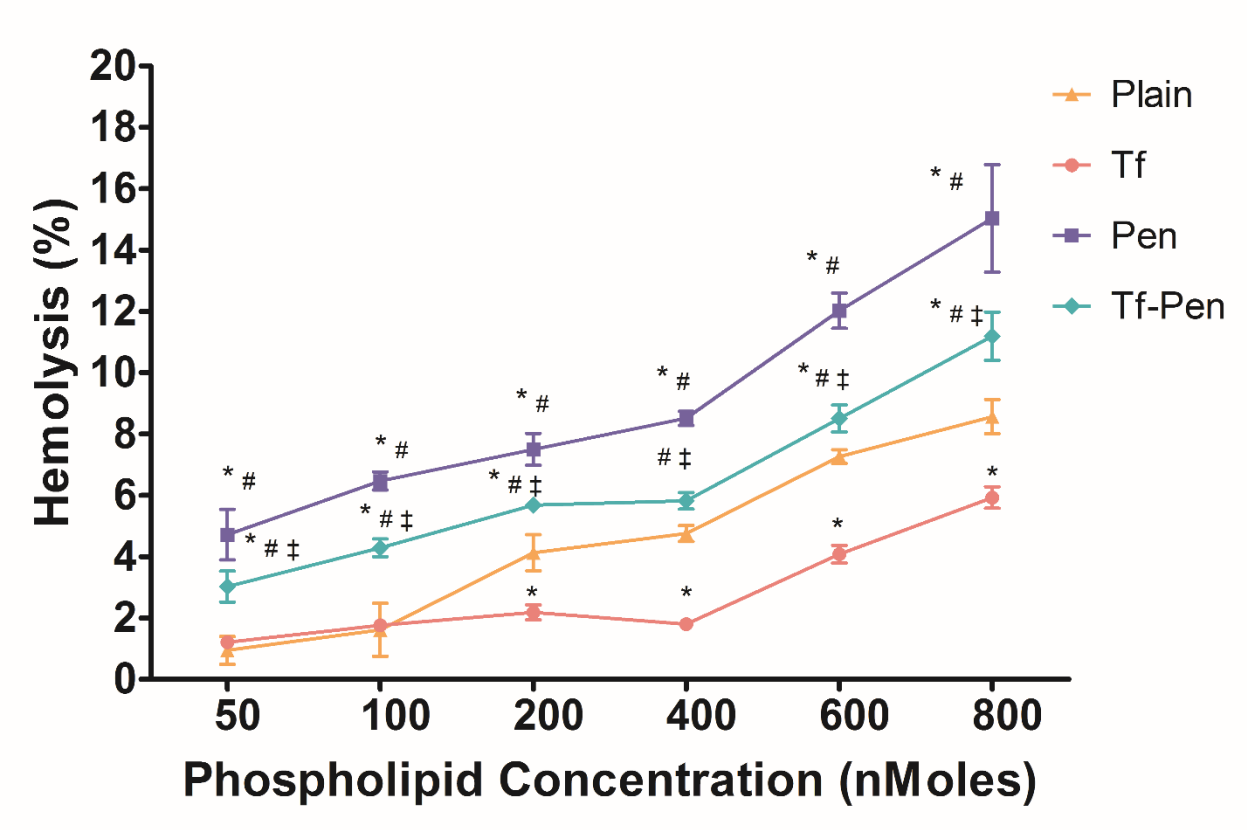

Figure 15. Hemolytic activity (%) of various liposomes. Red blood cells were exposed to different liposomes at varying concentrations. PBS and triton X-100 were used as positive and negative controls, respectively. Up to 10% hemolysis was considered non-toxic. Statistically significant ($p < 0.05$) differences is shown as (*) with plain liposomes, (#) with Tf-liposomes, and (‡) with Pen-liposomes. The data is represented as mean ± S.D. (n=4).

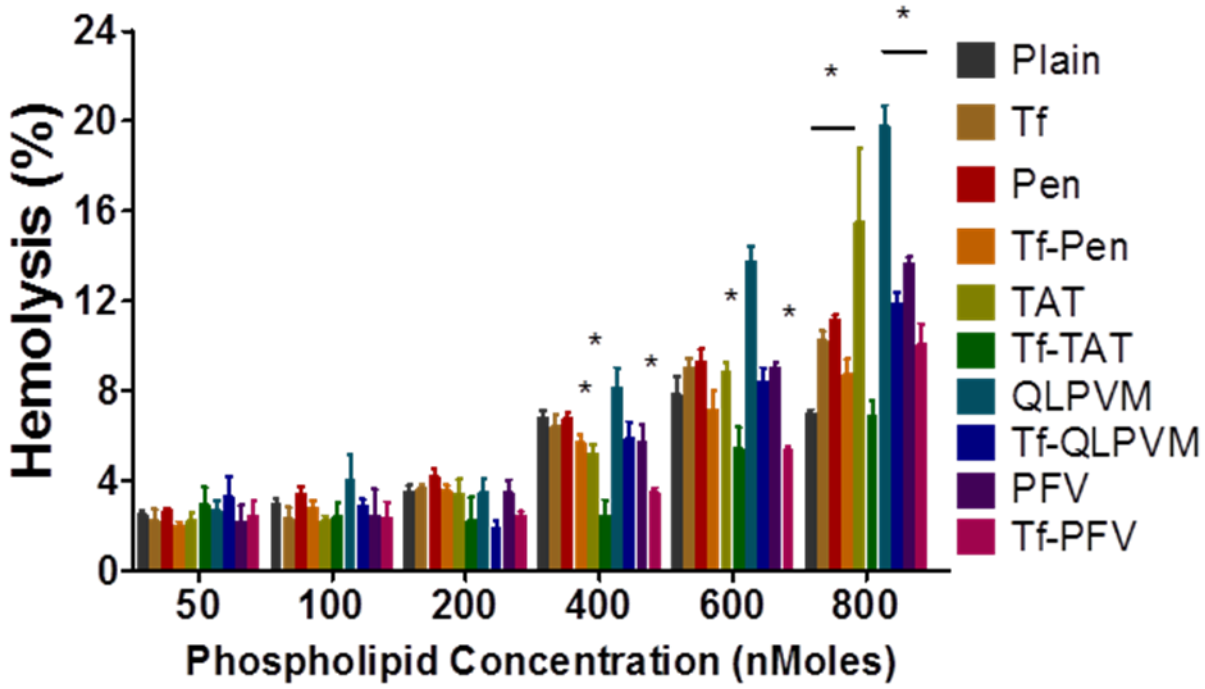

Figure 16. The graph represents the percent hemolytic activity of various liposomes on RBCs after 1 h incubation. Significant ($p < 0.05$) differences are shown as with (*) plain liposomes. The data is represented as mean ± S.D. (n=4).

3.7. Endothelial barrier layer integrity

The integrity of BBB was assessed by measuring the flux of sodium fluorescence (Na-F) and TEER across the co-culture of bEnd.3 cells and glial cells. The integrity of endothelial cells associated glial cells determined the intactness of the endothelial barrier layer. We observed significant ($p < 0.05$) decrease in the paracellular transport of Na-F across the co-culture model with bEnd.3 and glial cell ($Pe = 2.17 \times 10^{-6}$ cm/s) as compared to monolayer model ($Pe = 11.7 \times 10^{-6}$ cm/s) (Figure 17A). The lower permeability coefficient of Na-F across co-culture model attributed to the physical contact between the endothelial and glial cells, thereby showing improved complex between junctional proteins, showing the significance of glial cells in the formation of tight BBB [35,92,118,119]. Likewise, the TEER across co-culture and monolayer models was also determined to confirm the intactness of the endothelial barrier. The TEER values

of both monolayer and co-culture model were observed to be increasing with increase in the cell densities. The TEER value for the co-cultured model after 6 days of incubation period, was found to be 178.4 ± 10 Ω cm^2, significantly ($p < 0.05$) higher compared to 110.6 ± 3.5 Ω cm^2 for the monolayer model (Figure 17B). This can be explained by the up regulation of junctional proteins in the co-cultured model and supported by the presence of glial cells, which make a tighter barrier [120]. In addition, Microscopic images of hematoxylin-eosin stained scaffold sections showed gradual growth of U87 tumor cells as depicted in Figure 17C. The images of scaffold with tumor cells exhibited cellular biocompatibility. In addition, the porous nature of scaffold facilitates the attachment of tumor cells, thus supporting the tumor growth in 3-dimensional environment [121]. The percent seeding efficiency of U87 cells on porous scaffold was 31 ± 3.2 %. On day 21, the histological images of scaffold demonstrated dense growth of tumor cells inside the scaffolds. The results were in agreement with the previously published studies demonstrating the importance of using glial cells in the formation and maintenance of BBB [35,92,119,122]. Hence, the co-culture model was used to study the transport of liposomes into brain tumor cells *in vitro*.

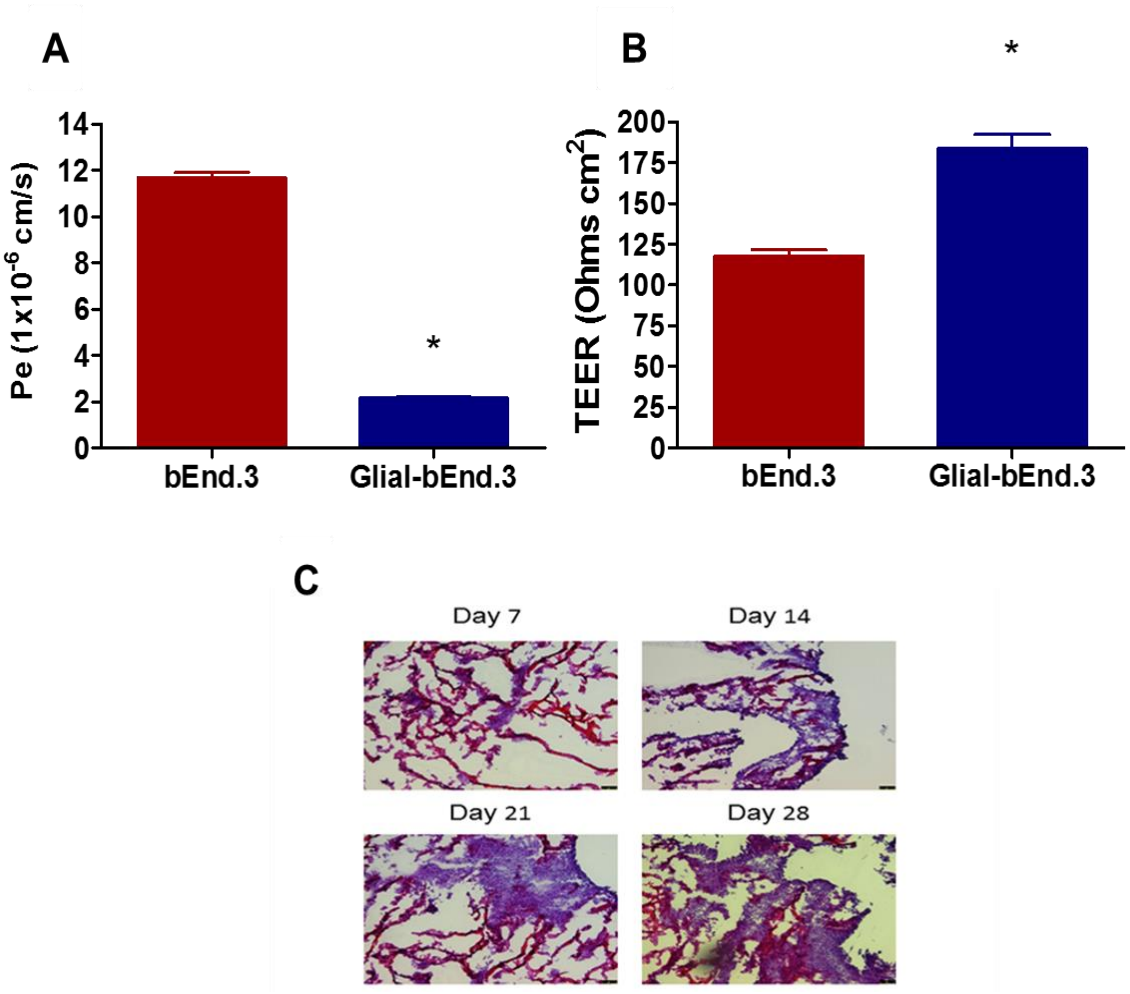

Figure 17. (A) Endothelial cell permeability coefficient (Pe, expressed in 10^{-6} cm/s) for sodium fluorescein (Na–F) of co-culture model (glial and endothelial cells) and endothelial monolayer only. The Pe values for co-culture model was observed to be significantly ($p<0.05$) lesser than endothelial monolayer (*). (B) TEER value for co-culture (glial and endothelial cells) and endothelial monolayer model only. TEER value for co-culture was observed to be significantly higher ($p < 0.05$) than endothelial monolayer (*). (C) At different time points, histological evaluation of tumor cell proliferation in PLGA-chitosan scaffold. The images show hematoxylin-eosin staining of scaffold sections with tumor cells growth (10X magnification). Data represented as mean ± S.D. (n=4).

3.8. Transport of coumarin-6 loaded liposomes across *in vitro* brain tumor model

The transport of liposomes across *in vitro* brain tumor model was evaluated through lysis of tumor cells and quantification of coumarin-6 in presence of 10% serum, which eliminates the possibility of liposomes entrapped in the endothelial barrier and thereby mimics *in vivo* conditions. The transport of coumarin-6 encapsulated Tf-Pen-conjugated liposomes was significantly higher

across the *in vitro* brain tumor model compared to single ligand or plain liposomes. The percent liposomal transport of Tf-Pen in 24 h was about 17.84 ± 0.37% while that for Tf-conjugated liposomes and Pen-conjugated liposomes were 10.02 ± 0.15% and 9.26 ± 0.50%, respectively (Figure 18B). As depicted in Figure 18A, Tf-Pen-conjugated liposomes (P_e = 4.97 x 10^{-6} cm/s) showed significantly ($p < 0.05$) higher permeability across endothelial co-culture barrier layer compared to single ligand (2.82 x 10^{-6} cm/s for Tf and 2.58 x 10^{-6} cm/s for Pen) or plain liposomes (1.16 x 10^{-6} cm/s), which was in accordance with previously published report [35]. The advantage of using *in vitro* brain tumor model over *in vitro* BBB model was that a 3-dimensional glioblastoma tumor was grown inside the scaffold, which mimicked the complex pathology of brain tumor and we studied the transport of liposomes across this brain endothelial barrier into the 3-d tumor. Overall, Tf-Pen-conjugated liposomes demonstrated higher transport as well as maximum permeability across barrier layer. However, Tf-conjugated liposomes showed higher cellular uptake, permeability and transport in comparison to Pen-conjugated liposomes, thereby demonstrating the significance of receptor mediated transcytosis over cell penetration. The electrostatic binding of cationic Pen-conjugated liposomes with negative charges on the cell membrane is postulated to facilitate cellular uptake. Moreover, a study showed that Tf-Pen and Tf-conjugated liposomes undergo clathrin-mediated uptake as the major pathway of transport, while Pen-conjugated liposomes demonstrate transport through macropinocytes and clathrin coated vesicles [35]. However, the presence of serum proteins can interfere with initial binding of the Pen-conjugated liposomes. On the contrary, Tf-conjugated liposomes specifically bind to Tf receptor, which eliminates the non-specific interaction with serum proteins. The results showed that the surface modified liposomes with Tf and Pen displayed enhanced transport across the *in vitro* brain tumor model as well as higher permeability across endothelial co-culture model.

Hence, the dual functionalized liposomes emphasized the significance of dual mechanisms of transport through receptor facilitated targeting as well as enhanced cell penetration.

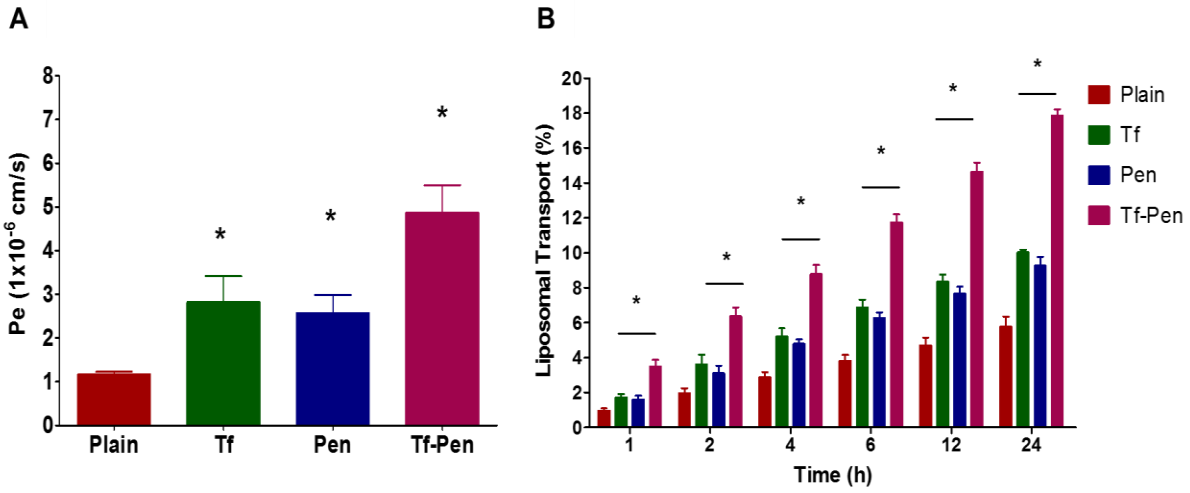

Figure 18. (A) Endothelial cell permeability coefficient (Pe, expressed in 10^{-6} cm/s) for different liposomes encapsulated with coumarin-6, across endothelial co-culture barrier model. (B) Graph shows the percent transport of different liposomes encapsulated with coumarin-6, across in vitro brain tumor model. Data represented as mean ± SD, (n=4). Significantly higher ($p < 0.05$) permeability coefficient and transport of Tf-pen liposomes in comparison to plain liposomes was observed (*).

3.9. Drug loaded Tf-CPP liposomes transport across *in vitro* brain tumor model

Liposomal transport across the co-culture endothelial barrier was evaluated using *in vitro* brain tumor model. The liposomal transport was done in the presence of 10% FBS to mimic *in vivo* like conditions. The dual functionalized liposomes demonstrated significantly ($p < 0.05$) higher transport (>12%) across the co-culture endothelial barrier in comparison to single or CPP liposomes. As depicted in the Figure 19, the percent liposomal transport for Tf-Pen, Tf-TAT, Tf-QLPVM and Tf-PFV was approximately 15.69 %, 12.72 %, 11.5 %, 12 %, respectively as compared to ~ 5.1 % and 1.3 % for plain liposomes and free dox, respectively over a period of 24 h. CPP liposomes showed the transport through adsorptive mediated transcytosis while Tf liposomes were transported *via* receptor mediated transcytosis. A comprehensive study was performed to demonstrate the uptake mechanisms using various inhibitors showed the transport of

Tf-CPP and Tf liposomes was majorly through clathrin mediated endocytosis, while for the transport of CPP liposomes was primarily *via* macropinocytes and clathrin coated vesicles [35]. The initial binding of CPP liposomes can be interfered by the presence of serum protein. However, Tf liposomes demonstrated specific binding to its receptor, thereby eliminating nonspecific interaction with serum protein. Moreover, the lower transport of plain and CPP liposomes is attributed due to the entrapment of in endothelial cell layer and absence of dual mechanisms. Therefore, Tf-CPP liposomes showed higher transport and highlighting the importance of dual mechanisms of receptor and adsorptive mediated transcytosis across the co-culture endothelial barrier. The transport of Tf-Pen liposomes across *in vitro* brain tumor model was further confirmed by incubating the model with lissamine rhodamine labeled liposomes for 24 h. The endothelial co-culture barrier was fixed with cold methanol. The z-stacks of confocal microscope demonstrated the uptake of liposomes by bEnd.3 cells (luminal side) on transwell culture insert and transported across the PET membrane or the glial cells (abluminal side). Apart from the cellular uptake of liposomes, the fluorescence of lissamine rhodamine labeled Tf-Pen liposomes demonstrated excellent evidence of transcytosis across the *in vitro* brain tumor model in comparison to plain liposomes, as depicted in Figure 20.

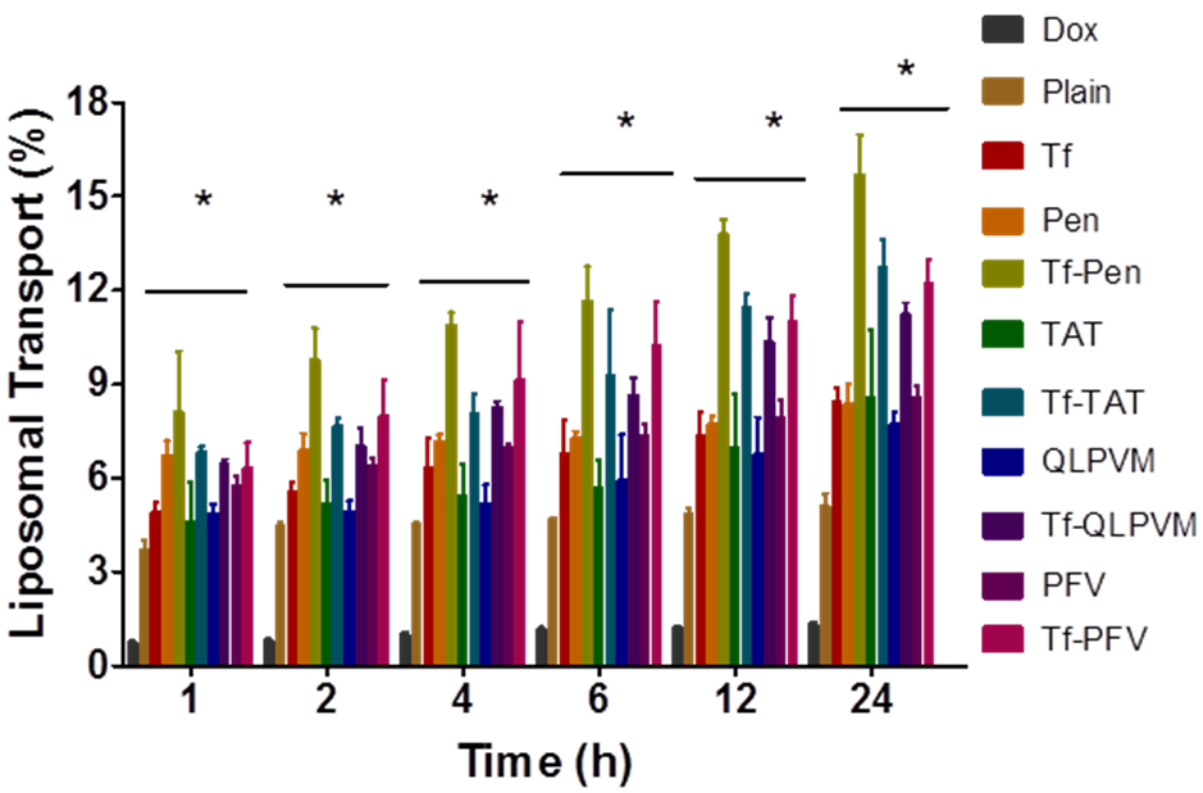

Figure 19. Plot demonstrates the percent transport of different liposomes loaded with doxorubicin, across the in vitro brain tumor model. Significant ($p < 0.05$) difference is shown in the transport of different liposomes in comparison to (*) free drug. Data represented as mean ± SD, (n=3).

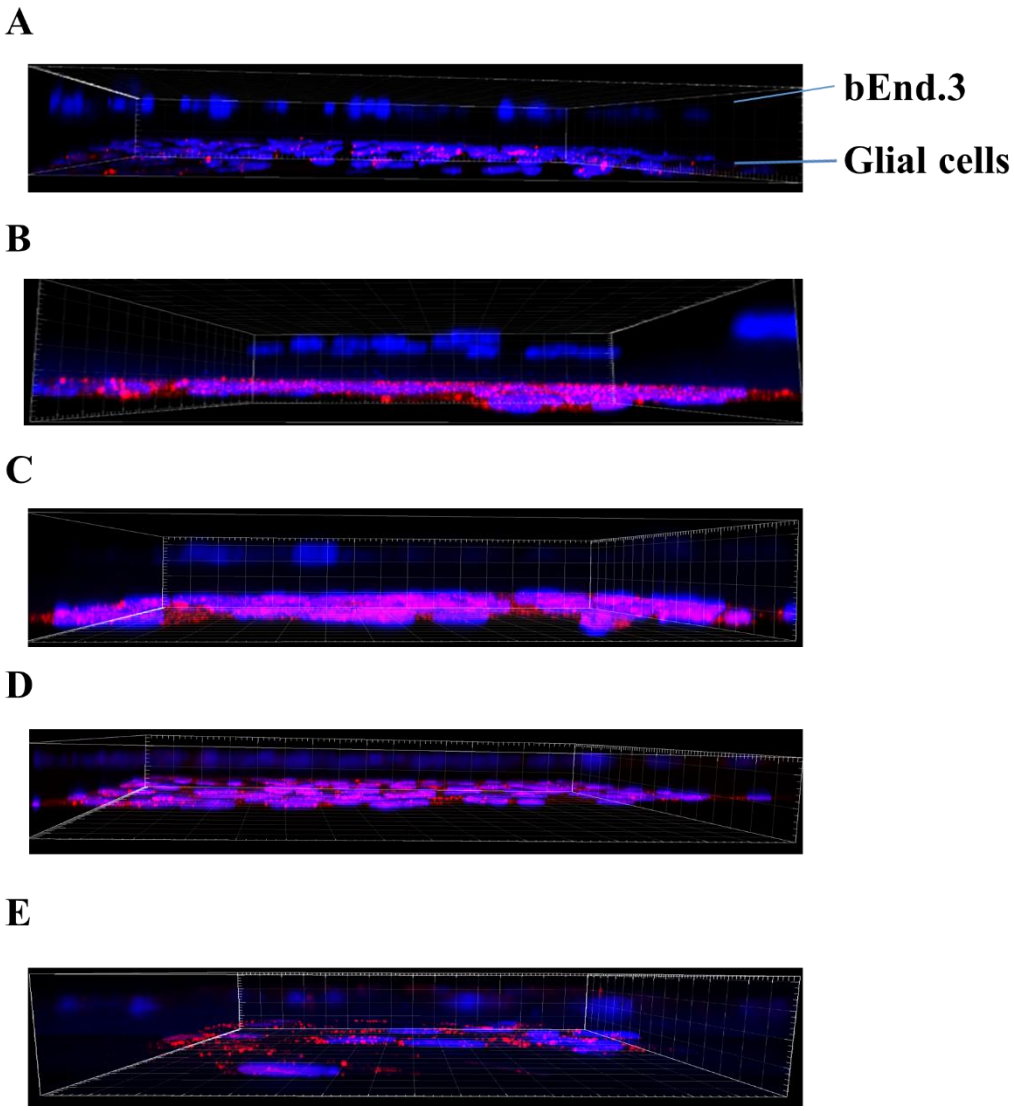

Figure 20. Confocal fluorescent images of co-culture endothelial barrier demonstrated the evidence of transport of (A) plain liposomes (B) Tf-Pen liposomes (C) Tf-TAT liposomes (D) Tf-QLPVM liposomes (E) Tf-PFV liposomes (40X magnification).

3.10. Anti-tumor efficacy of 5-FU loaded liposomes

A robust and simple *in vitro* brain tumor model was designed to evaluate the efficacy of Tf-Pen-conjugated liposomes by determining the regression of glioblastoma tumor housed inside a PLGA-chitosan scaffold. The model was constructed by placing the culture inserts carrying a tightly packed barrier of brain endothelial and glial cells on glioblastoma tumor grown inside PLGA-chitosan scaffold to mimic *in vivo* tumor environment. The porous scaffold enabled the

tumor cells to grow inside them in a 3-dimensional environment, attaching to the scaffold fibers and pores inside scaffold to form a 3-D tumor [121,123,124]. Anti-tumor efficacies of various liposomal formulations were determined by quantifying the percent tumor cell viability in the scaffold using MTT assay. After 24 h treatment, the percent tumor cell viability in the *in vitro* tumor model decreased to 88.66 ± 5.05% and 57.78 ± 1.51% for 5-FU encapsulated plain liposomes and Tf-Pen liposomes, respectively. Figure 21A shows that 5-FU encapsulated Tf-Pen-conjugated liposomes significantly decreased the percent tumor cell viability as compared to single ligand or plain liposomes. We believe that Tf-Pen-conjugated liposomes efficiently crossed the endothelial barrier *via* dual mechanisms of Tf receptor mediated transcytosis and enhanced cell penetration, subsequently reaching the tumor cells inside the scaffold and delivering the encapsulated 5-FU to the tumor cells. The anti-tumor efficacy of Tf-Pen-conjugated liposomes was also confirmed by fluorescence images of the treated scaffold sections. As depicted in the figure 21B, the tumor cells inside the scaffold subjected to Tf-Pen treatment were mostly dead, which confirmed the superior anti-tumor efficacy of these liposomes. Based on these results, it can be concluded that Tf-Pen-conjugated liposomes efficiently translocate across the brain endothelial barrier and endocytoses into the tumor cells present inside the scaffold, thereby increasing the concentration of 5-FU in the tumor cells, thus demonstrating excellent anti-tumor efficacy.

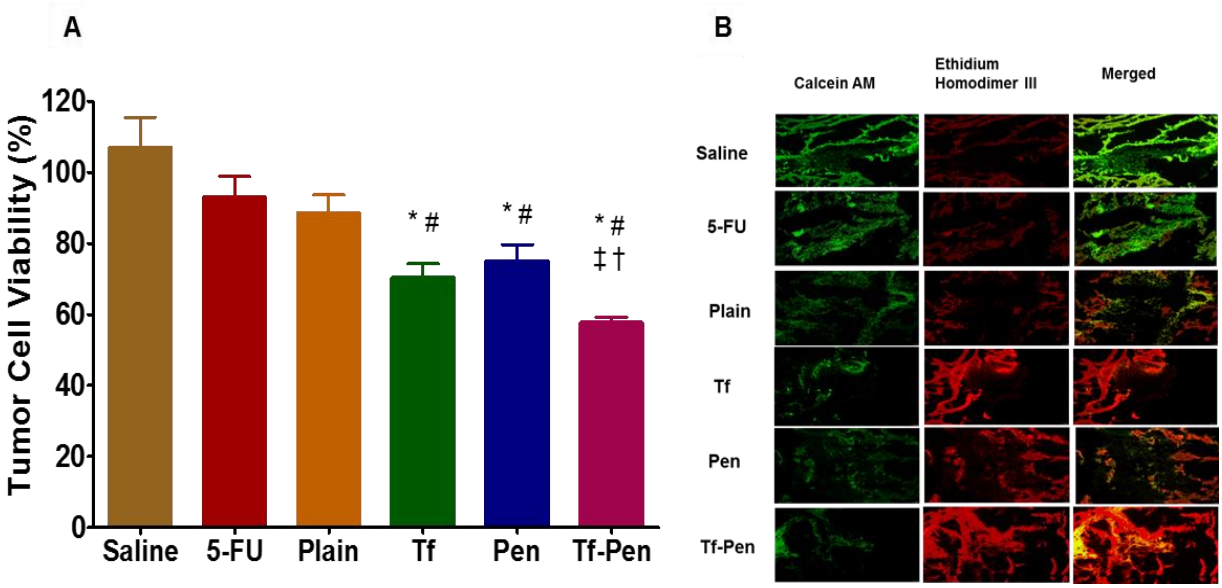

Figure 21. (A) Graph shows the percent tumor cell viability 24 h after treatment with different 5-FU encapsulated liposomes using an in vitro brain tumor model. Data represented as mean ± SD, (n=4). Statistically significant ($p < 0.05$) differences with plain liposomes (*), free 5-FU (#), (‡) Tf liposomes, and (†) Pen liposomes was observed. (B) The fluorescence images show tumor cell death in scaffold after treatment (10X magnification).

3.11. Anti-tumor efficacy of Dox and Erlo loaded liposomes

An *in vitro* brain tumor model was used to evaluate the anti-tumor efficacy of Dox and Erlo loaded Tf-CPP liposomes. The anti-tumor efficacy was evaluated in the same as in the previous section. The *in vitro* brain tumor model was treated with various Dox and Erlo loaded liposomal formulations for 24 h on day 21 of tumor inoculation. On day 28th of tumor inoculation, the treated scaffolds were quantified to evaluate the percent tumor cell viability. The percent tumor cell viability was decreased from 76.88 ± 3.80 % for Dox and Erlo loaded plain liposomes to 38.5 ± 3.3 %, 44.39 ± 1.49 %, 44.87 ± 1.86% and 47.85 ± 1.06 % for Tf-Pen, Tf-TAT, Tf-QLPVM and Tf-PFV liposomes, respectively (Figure 22). The co-delivery of Dox and Erlo to the tumor cells demonstrated the potential of combination therapy by increasing the anti-cancer effect from the delivered drugs, thereby significant decrease ($p < 0.05$) in the percent tumor cell viability. In addition, Tf-CPP liposomes revealed the excellent antitumor efficacy as compared to single ligand

or plain liposomes. Tf-Pen liposomes demonstrated significant ($p < 0.05$) difference in the percent tumor cell viability. Whereas Tf-TAT, Tf-QLPVM and Tf-PFV liposomes exhibited no significant ($p > 0.05$) difference in the percent tumor cell viability. The results showed Tf-CPP liposomes were efficiently translocated across the endothelial barrier through dual mechanisms of receptor facilitated and increased cell penetration, thereby reaching the glioblastoma tumor and co-delivering Dox and Erlo from liposomes to the glioblastoma tumor in the scaffold. In addition, the antitumor efficacy of Tf-CPP liposomes was further confirmed through live/dead cells imagining. The fluorescence images of the treated scaffold sections showed mostly dead tumor cells (Figure 23). Based on the results from this experiment, it can be concluded that the Tf-CPP liposomes demonstrated excellent antitumor efficacy by translocating across the endothelial barrier

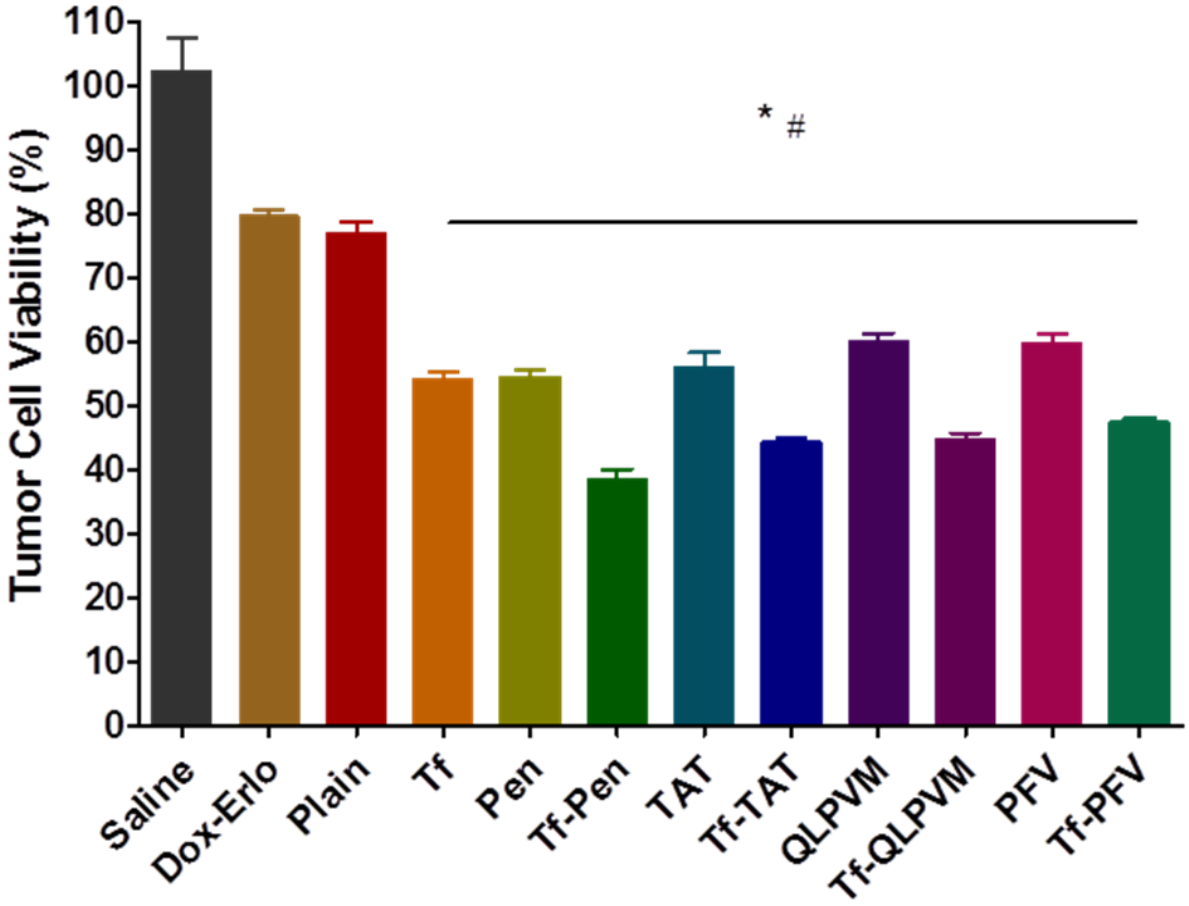

Figure 22. Plot demonstrates the percent tumor cell viability after 24 h treatment with different Dox and Erlo loaded liposomes using an in vitro brain tumor model. Statistically significant ($p < 0.05$) differences with (*) plain liposomes, (#) free Dox-Erlo were observed. Each experiment used fresh formulation. Data represented as mean ± SD, (n=4). Four separate experiments were performed for each treatment group.

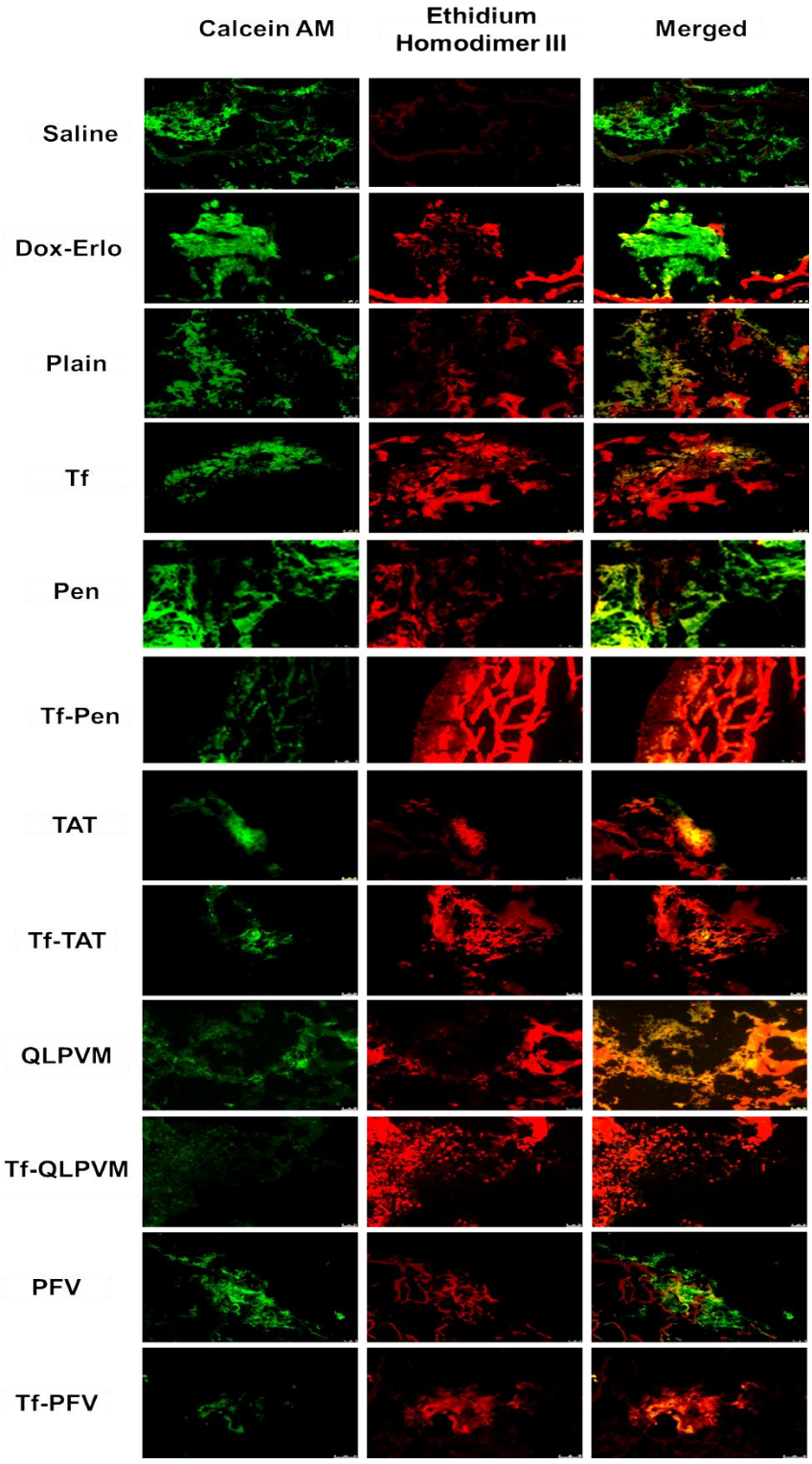

Figure 23. The fluorescence images show tumor cell death in scaffold after treatment (10X magnification).

3.12. *In vivo* biocompatibility study

Non-specific interaction and higher penetration of cell penetrating peptides have been reported toxicity in highly perfused organs [125]. Therefore, *in vivo* biocompatibility of various liposomal formulation was evaluated by histological examination of tissues. The tissue sections from the mice administered with PBS were used as a control. The tissue sections stained with hematoxylin-eosin demonstrated no evidence of change in morphological appearance. Furthermore, there were no signs of tissue necrosis, inflammation or nuclei enlargement after examining tissue sections of different organs as compared to the tissue sections from control group. Liver, spleen and heart sections were carefully examined for histological changes. The histological examination of liver showed no signs of inflammation, ballooning of hepatocytes or enlargement of nuclei while spleen sections confirmed no evidence of necrosis or apoptosis (Figure 27& 28). In addition, the histological examination of heart demonstrated no signs of myofibrillar loss and diffuse fibrosis of myocardium or disruption of cardiac muscle fibers (Figure 26). Brain histological sections were observed for loss of frontal cortex layers with capillary congestion and dilatation as well as for dark irregular stained cells with pyknotic nuclei and showed no signs of abnormality (Figure 24). Also, lung sections showed no signs of pulmonary fibrosis (Figure 25). Kidney sections were also observed for any signs of atrophy of glomerular tuft or widening of urinary space or apoptosis of epithelial cells or disruption of epithelium and demonstrated no toxicity (Figure 29). Therefore, all the organ sections were examined histologically and demonstrated no signs of toxicity, inflammation, necrosis or apoptosis. The dose of liposomes was calculated based on the *in vitro* biocompatibility study, 200 nMoles of phospholipid concentration demonstrated more than 85% of cell viability. We estimated the blood volume in mouse using Lee and Blaufox equation: $BV = 0.06 \times BW + 0.77$, Where, BV is the blood volume in mouse and BW

is the mouse body weight [126]. The blood volume was found to be in the range from 1.97 to 2.27 ml for 5 weeks old mice (20 – 25 g). The injected dose of liposomes was approximately 304 – 380 nMoles for mice weighing 20 – 25 g with approximate 2 ml of blood volume. Additionally, the results from the hemocompatibility study demonstrated that the Tf-Pen liposomes up to 800 nMoles of phospholipid concentration was observed to be safe in a volume of 1 ml of PBS with 1.5 x 10^7 erythrocytes. Therefore, the dose of the liposomes injected in mice was significantly below the hemolytic concentration of phospholipid and are suitable for *in vivo* administration. Thus, the Tf-CPP liposomes administered at a dose of 15.2 µmoles of phospholipid/kg of body weight demonstrated no signs of toxicity in any of the tissues from mice.

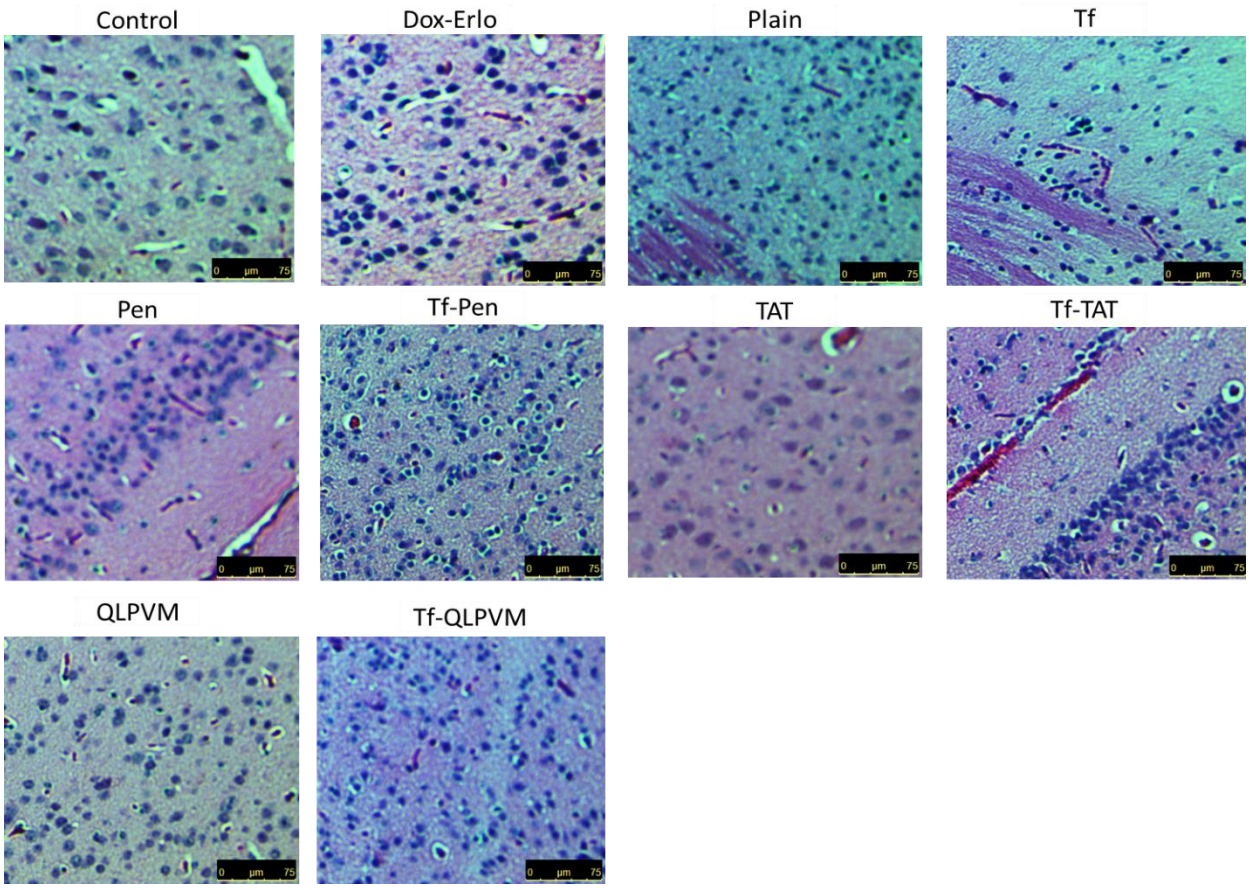

Figure 24. Histological examination of brain sections after injected with different liposomes.

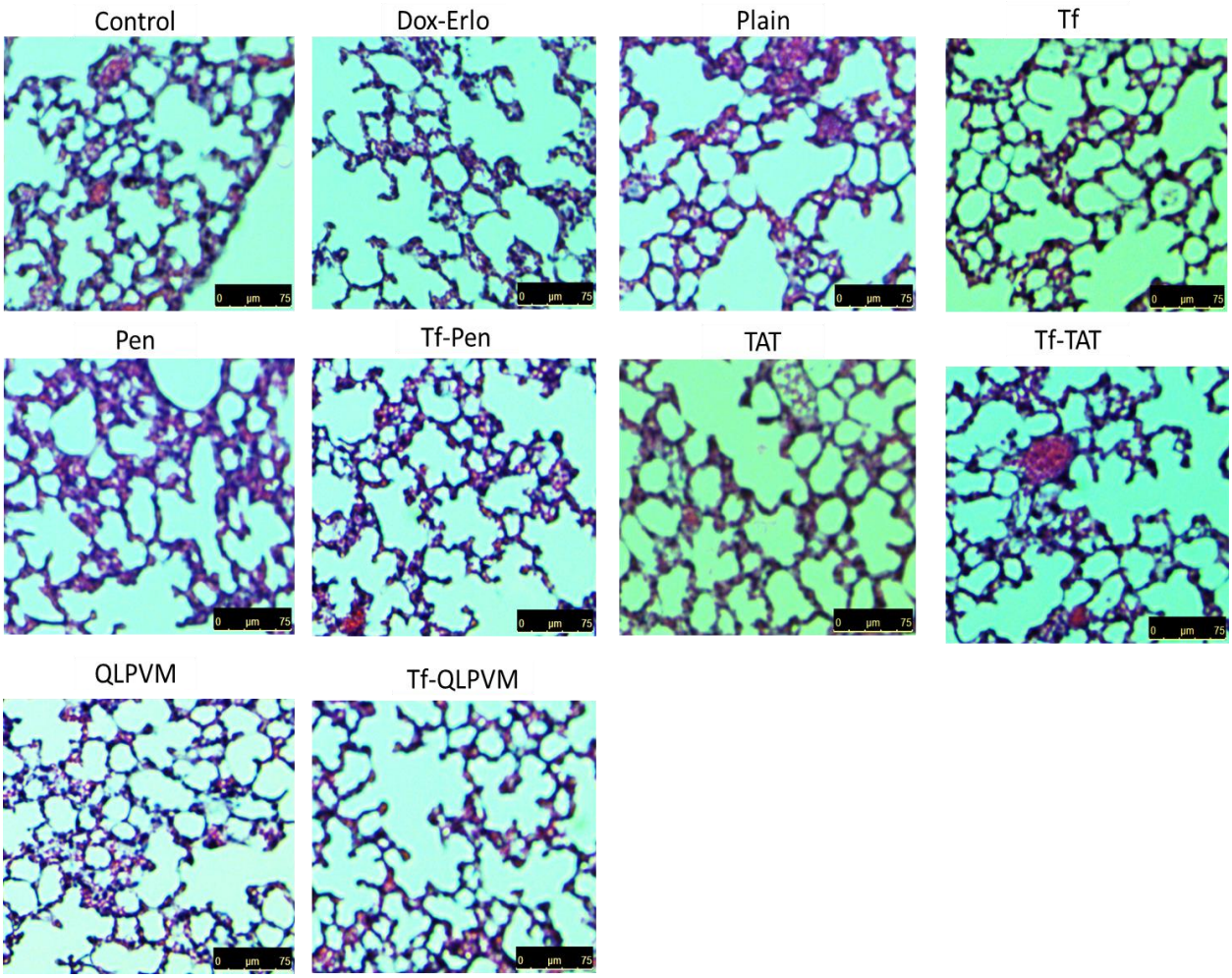

Figure 25. Histological examination of lung sections after injected with different liposomes.

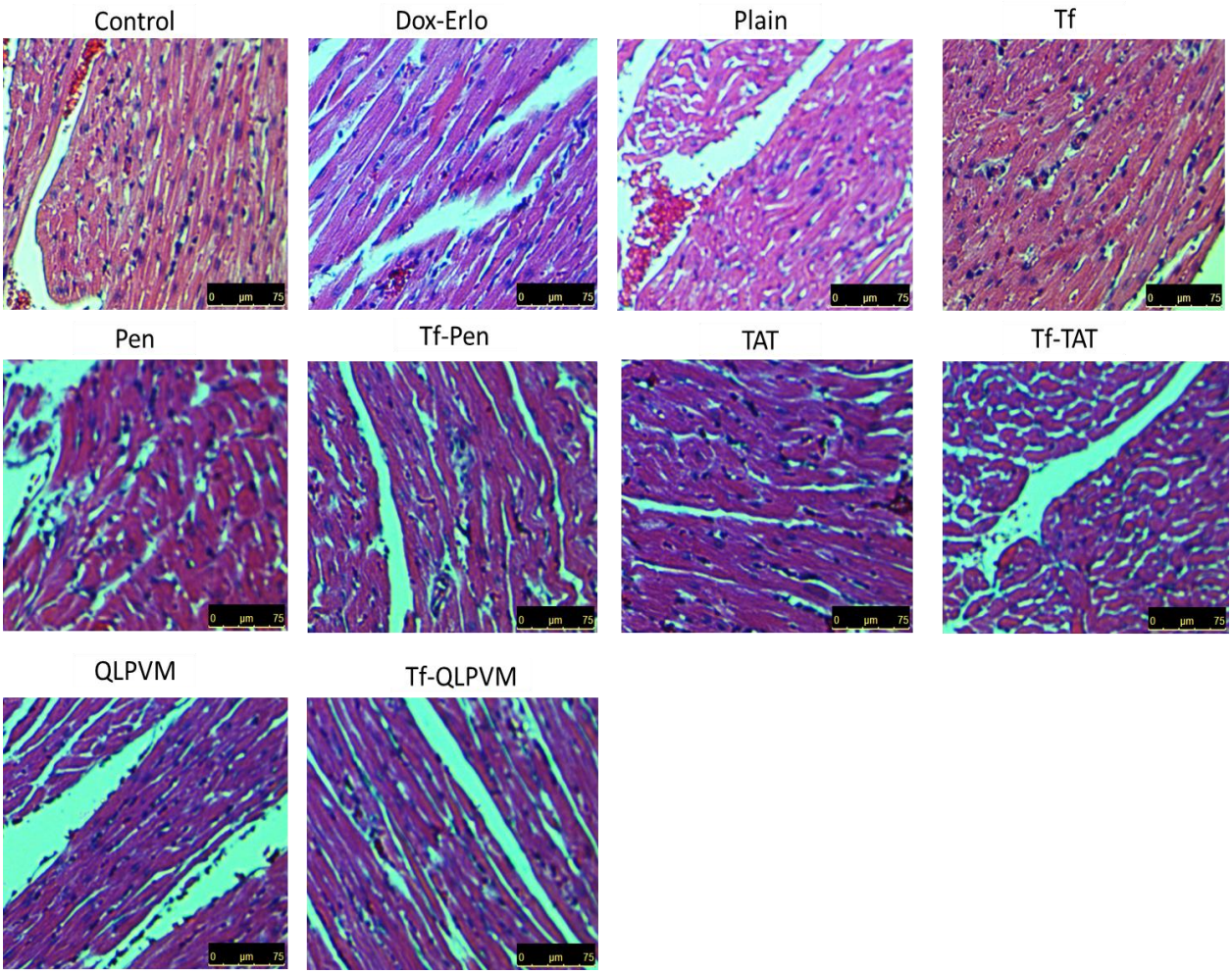

Figure 26. Histological examination of heart sections after injected with different liposomes.

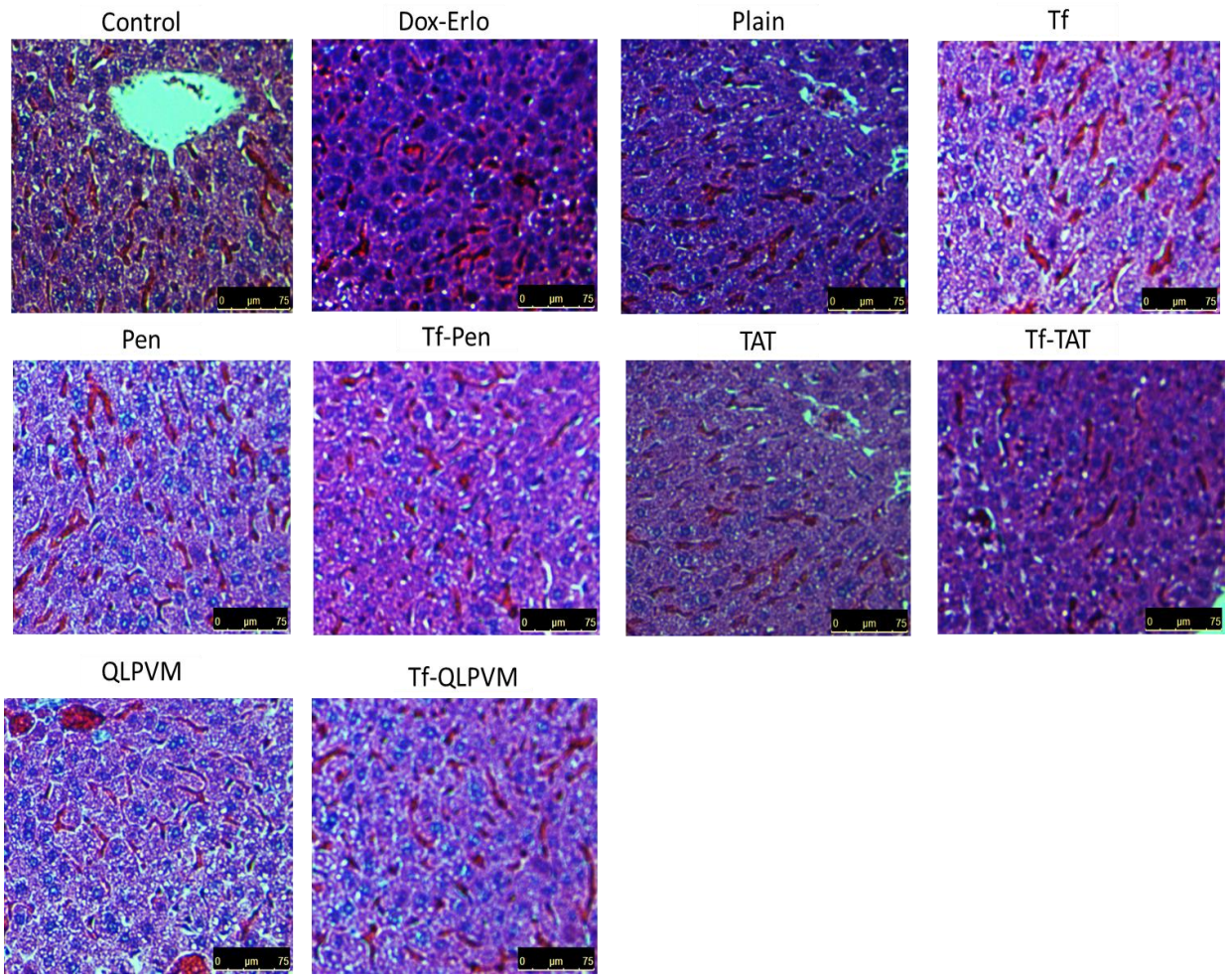

Figure 27. Histological examination of liver sections after injected with different liposomes.

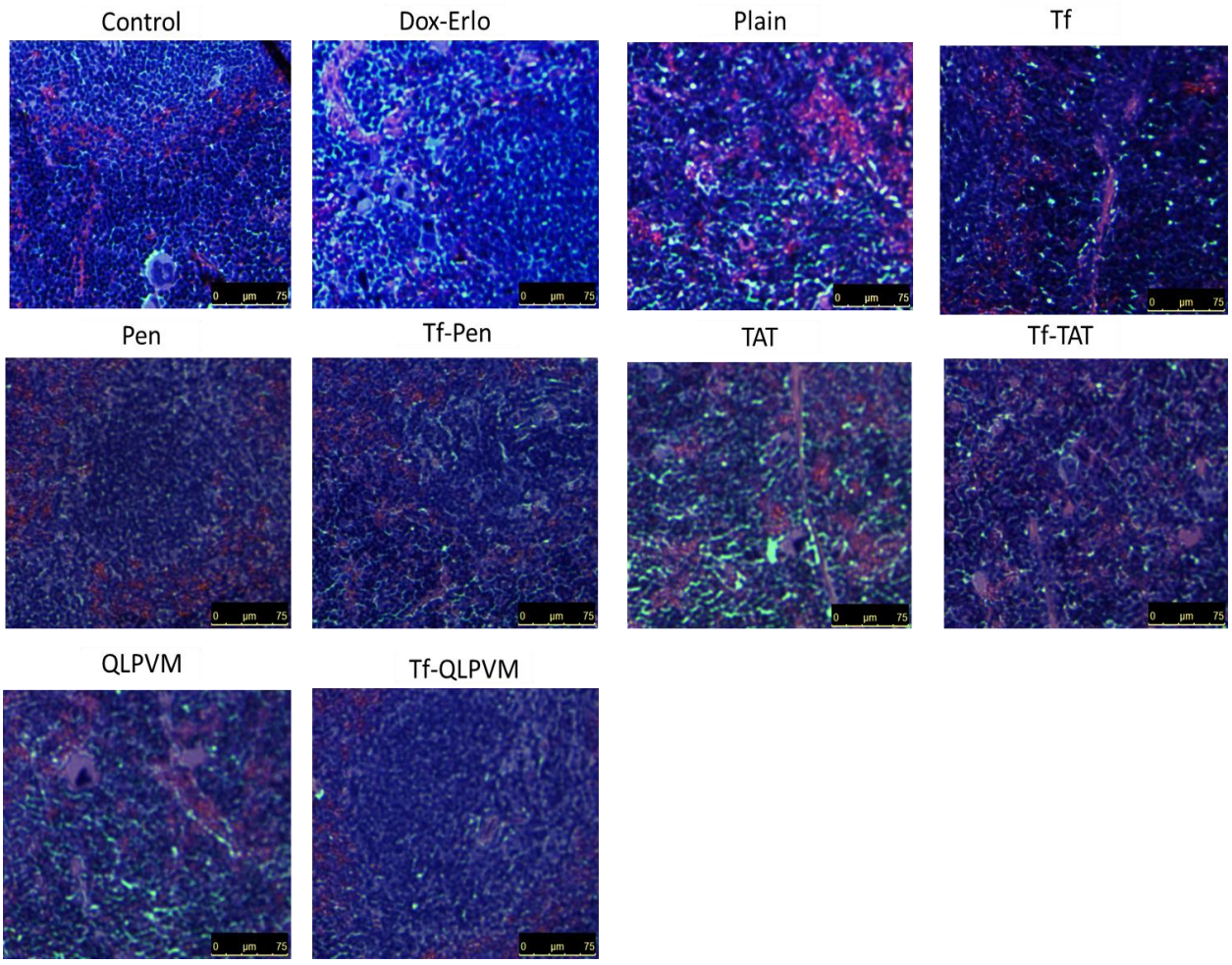

Figure 28. Histological examination of spleen sections after injected with different liposomes.

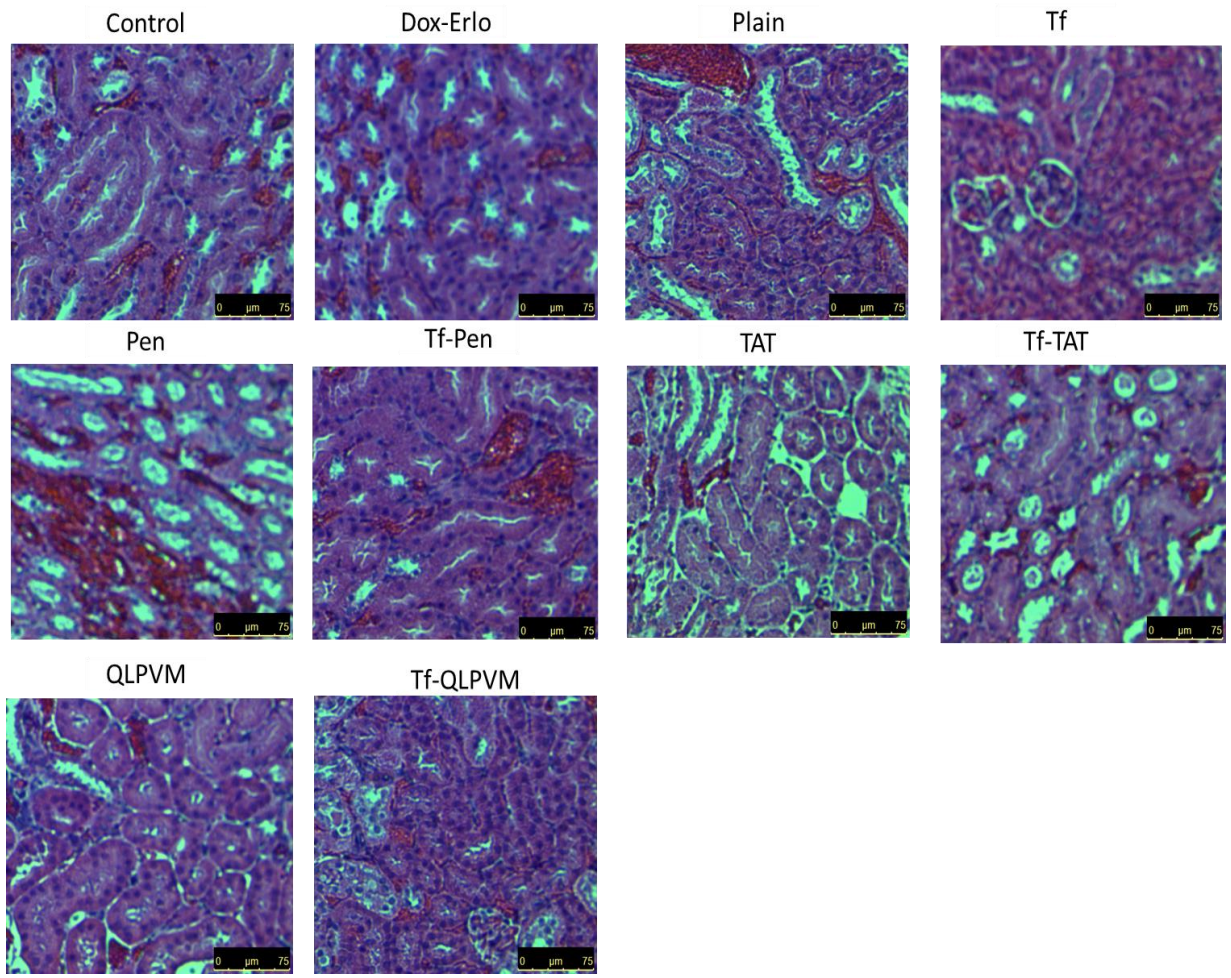

Figure 29. Histological examination of kidney sections after injected with different liposomes.

3.13. *In vivo* biodistribution of liposomes

The biodistribution of Tf-Pen liposomes was studied qualitatively as well as quantitatively after 24 h of intravenous administration of liposomes. The lissamine rhodamine labeled liposomes were tracked by an *in vivo* imaging system which images the whole mice body as well as various organs to study the biodistribution. The results from *in vivo* imaging of mice (Figure 30) showed the higher fluorescent intensity of Tf-Pen liposomes in the brain as compared to plain or single ligand liposomes which demonstrated the accumulation of liposomes. In addition, the *ex vivo* images of organs also demonstrated the strong fluorescence of Tf-CPP liposomes in the brain (Figure 31). As expected, a strong fluorescent signal was observed in liver and spleen after 24 h.

Further, the liposomes accumulation in various organs were quantified by homogenization of organs followed by extraction of drugs. Drugs loaded plain liposomes were used as a passive control. Accumulation of drugs loaded liposomal tissue samples were analyzed using HPLC. The biodistribution of Dox and Erlo loaded Tf-CPP liposomes showed more than 10 and 2.7-fold increase in Dox and Erlo accumulation in mice brain, respectively which is significantly ($p < 0.05$) higher compared to administration of free drugs (Figure 32 and 33). This showed that incorporation of CPP to liposomes significantly increased the accumulation of Tf-CPP liposomes in brain by translocating across the BBB effectively and more efficiently compared to other liposomal formulations. The Tf-CPP liposomes also showed higher accumulation in liver, spleen and heart 24 h post intravenous injection. Tf-Pen showed highest distribution in brain followed by Tf-TAT then Tf-QLPVM. Tf-TAT liposomes showed non-significantly ($p > 0.05$) higher accumulation in brain as compared to Tf-QLPVM liposomes. The Tf receptors are also present in liver, spleen and heart which triggered the uptake of Tf-liposomes in these organs [127,128]. Moreover, liver and spleen are considered to be the major macrophage organs and thus, the intravenously injected liposomes were eliminated rapidly through these organs [127,128]. However, the surface modification of liposomes with Tf and CPP improved the transport of liposomes to brain. It can be seen from the results that the negatively charged Tf-liposomes circulated longer in the blood. However, the accumulation of drugs in the brain is significantly lesser ($p < 0.05$) than Tf-CPP liposomes. CPP-liposomes were accumulated in liver and spleen due to non-specific interactions and cationic charge of CPPs. In addition, free drugs (Dox and Erlo) and plain liposomes were majorly transported to liver, spleen, kidneys and heart, and demonstrated less accumulation in brain. In conclusion, the incorporation of CPP in combination with the Tf receptor targeting ability of Tf into the Tf-CPP liposomes, resulted in higher transport across the

BBB and higher accumulation in the brain through dual mechanisms of receptor mediated transcytosis and enhanced cell penetration.

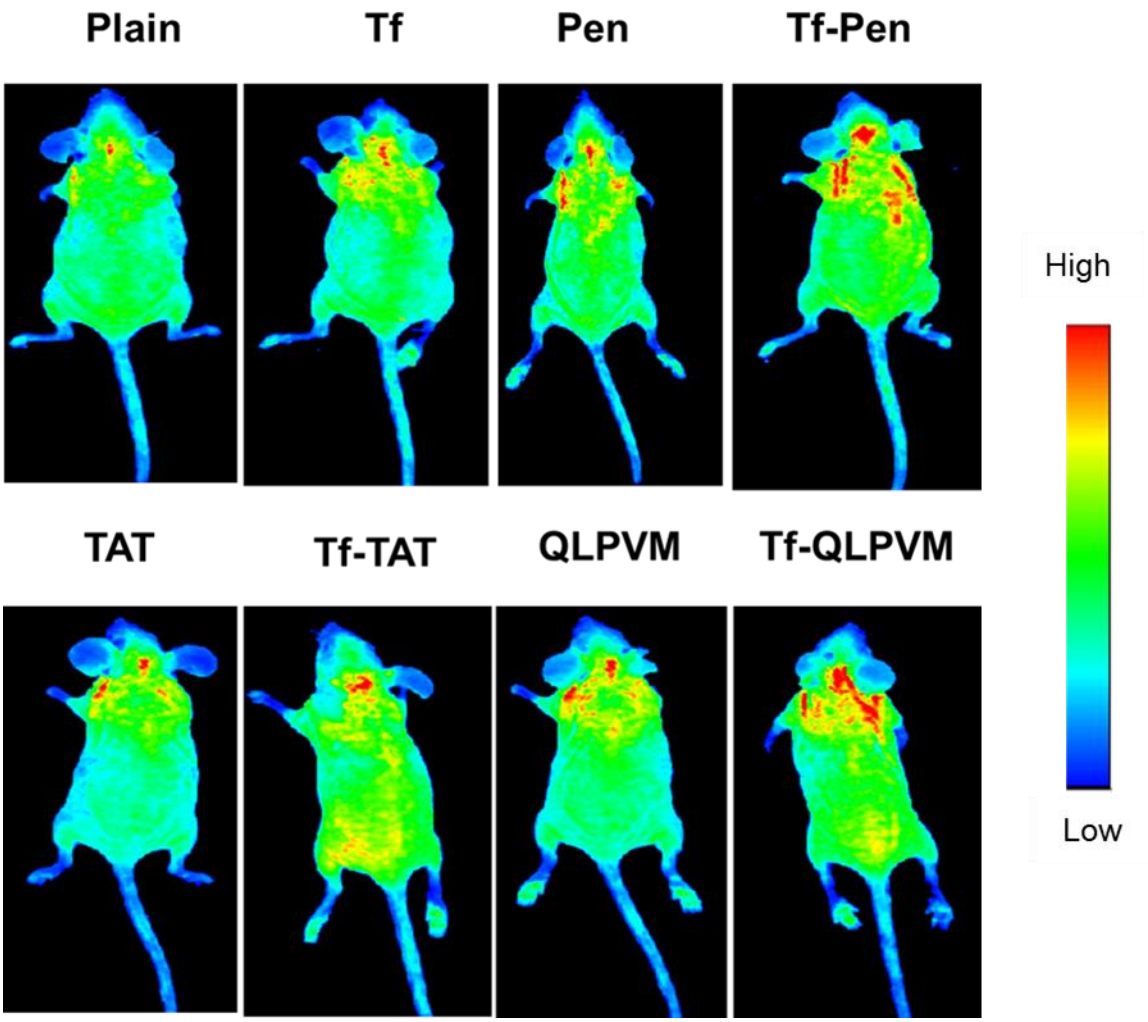

Figure 30. *In vivo* fluorescence imaging of mice at 24 h post intravenous injection.

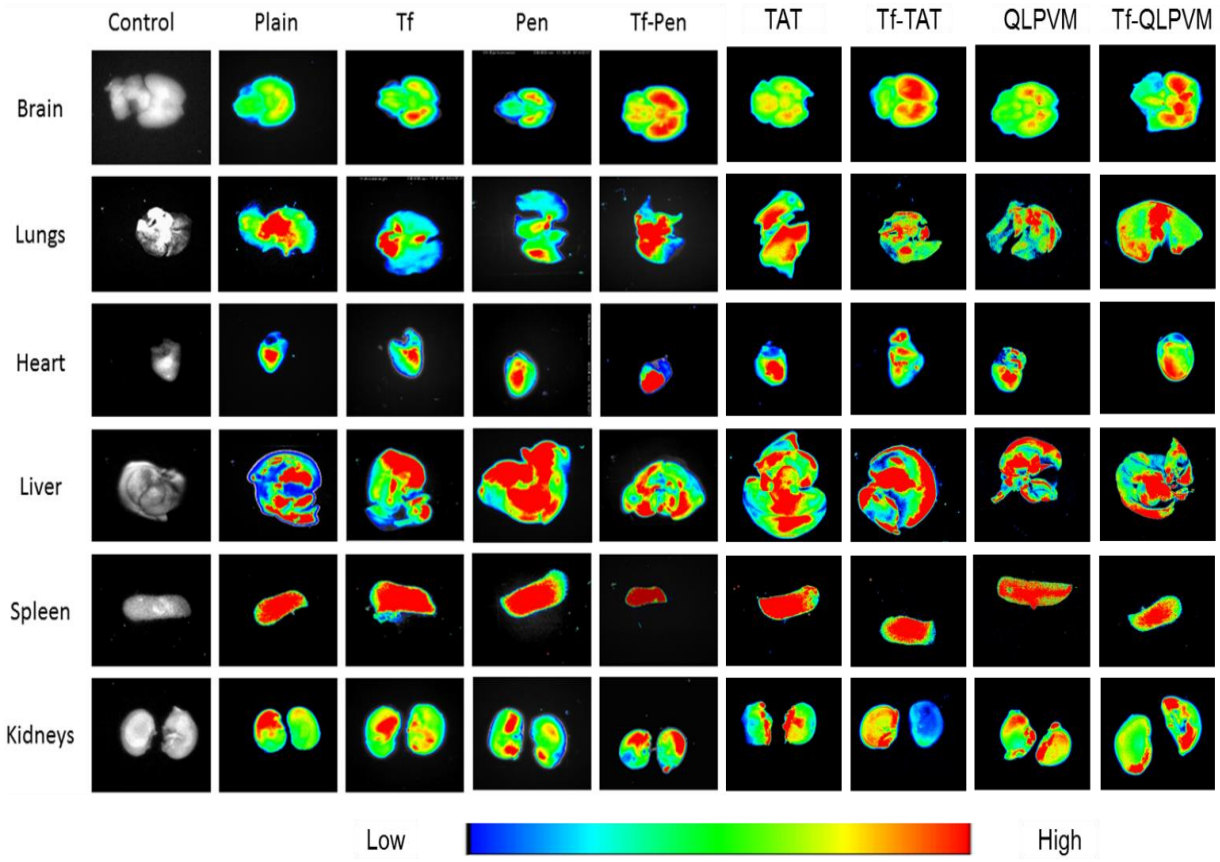

Figure 31. *Ex vivo* fluorescence imaging of different organs isolated from mice after 24 h intravenous injection.

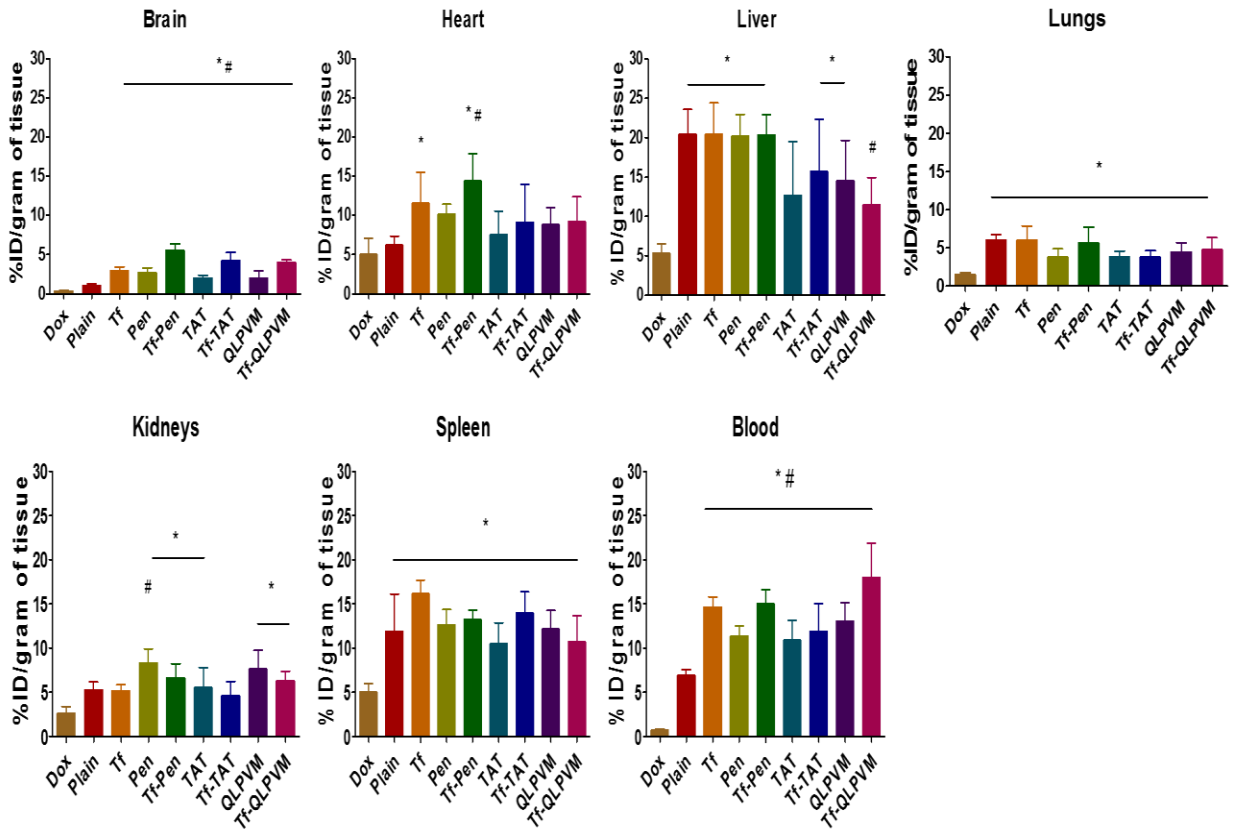

Figure 32. Bar graphs representing the biodistrubition of Dox at 24 h time point after intravenous injection in various organs. The data are expressed as percent injected dose (% ID)/gram of tissue; (mean ± SD; n = 6). Statistically significant ($p < 0.05$) differences with (#) plain liposomes, and (*) free Dox were observed.

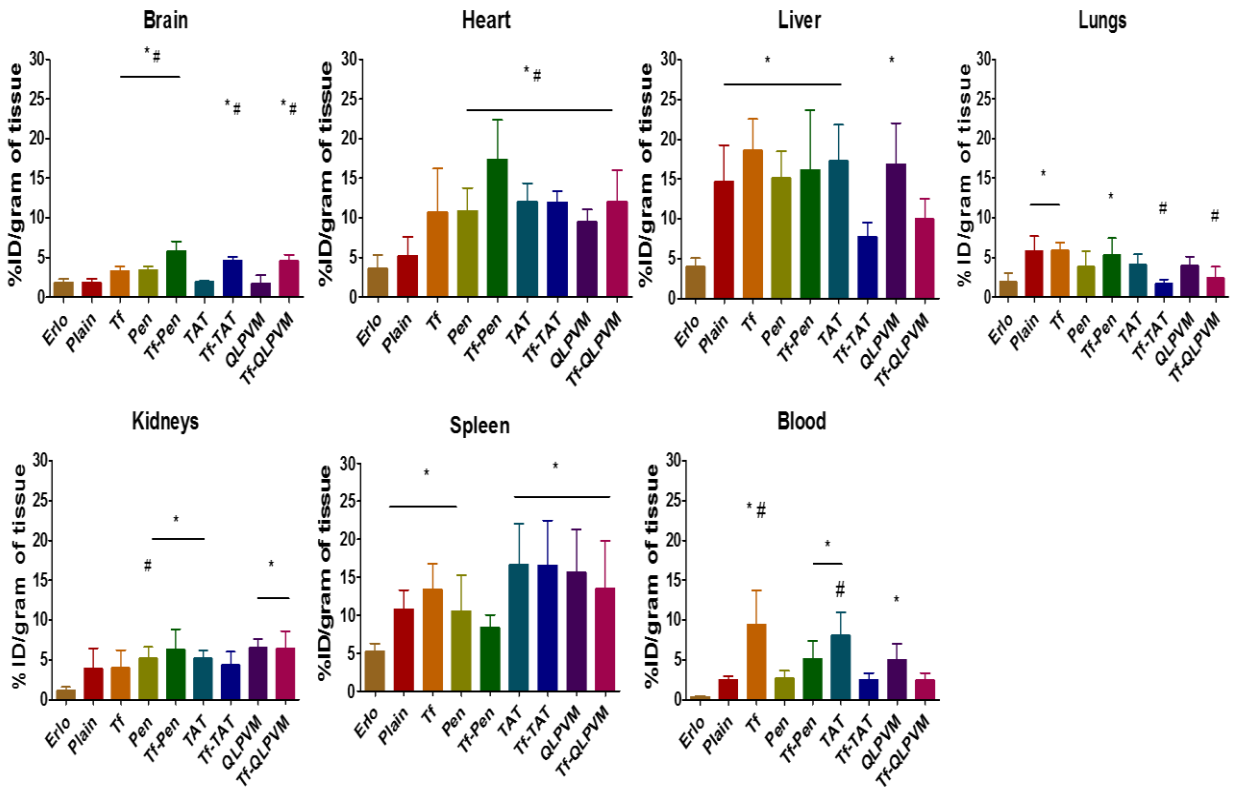

Figure 33. Bar graphs representing the biodistrubition of Erlo at 24 h time point after intravenous injection in various organs. The data are expressed as percent injected dose (% ID)/gram of tissue; (mean ± SD; n = 6). Statistically significant ($p < 0.05$) differences with (#) plain liposomes, and (*) free Dox were observed.

3.14. *In vivo* anti-tumor efficacy

The orthotopic brain tumor mice model is an appropriate and efficient model to evaluate the antitumor efficacy for targeted therapies against GBM. This model replicates both relevant signaling pathway alterations and the histopathological features of human GBM. Furthermore, in orthotopic implanted tumors the process of metastasis is efficient and mimics human metastasis [129]. Therefore, we believe that by using this model we were able to mimic human GBM and our results are likely to resemble the activity of the delivery system in patients with GBM. The antitumor efficacy of Dox and Erlo loaded Tf-Pen liposomes was evaluated in intracranial glioblastoma bearing nude mice. As shown in Fig. 34A, Dox and Erlo loaded Tf-Pen liposomes demonstrated significant ($p < 0.05$) regression of tumor area (0.54 ± 0.07 mm^2) as compared to

free drugs (3.2 ± 0.33 mm^2), plain (2.8 ± 0.28 mm^2) or single ligand liposomes (1.75 ± 0.36 mm^2 for Tf- liposomes and 1.95 ± 0.43 mm^2 for Pen-liposomes). The tumor area of mice administered with PBS was considered as a control. These results demonstrate that the Dox-Erlo loaded Tf-Pen liposomes efficiently translocated across the BBB and co-delivered drugs to glioblastoma tumor *in vivo*, thereby achieving significant reduction in tumor burden in comparison to plain or single ligand liposomes. The H&E stained tumor sections of mice brain in Figure 34B, confirmed that the Tf-Pen liposomes were more efficient in regressing tumor with a tumor inhibition of ~ 90% as compared to control (PBS). There are several published reports demonstrating therapeutic efficacy using Tf modified delivery systems to treat gliomas [130–133]. However, the translocation was limited due to receptor saturation, endosomal entrapment and loss of specificity by formation of a protein corona on ligand by other proteins present in a complex biological microenvironment, resulting in restricted transport of delivery system across the BBB [92,130,133–135]. Additionally, several other published reports with single drug loaded dual functionalized delivery systems have also shown therapeutic efficacy in treating glioblastoma [136–138]. Furthermore, they were also restricted with drug resistance in the tumor cells. Thus, we believe that the co-delivery of drugs (Dox and Erlo) through dual functionalized liposomal nanoparticulate system is superior and efficient in overcoming all the above mentioned limitations, without eliciting undesired toxicity. Moreover, the biodistribution of Tf-Pen liposomes showed more than 12 and 3.3 -fold increase in Dox and Erlo accumulation in mice brain, respectively compared to free-drugs (Fig. 32 & 33). This demonstrated that the translocation of Tf-Pen liposomes was not affected by either receptor saturation, endosomal entrapment or loss of specificity. The high translocation of Tf-Pen liposomes across the BBB was followed by their excellent targeting and penetrating ability into glioblastoma tumors which led to significant decrease in tumor burden (Fig. 34A & B).

Furthermore, the percent relative body weight of mice showed no significant difference in the treatment groups while PBS group demonstrated higher weight loss due to the aggressive invasion of GBM into the brain and deteriorating health of the animal (Fig. 34C). In addition, the results demonstrate no weight loss and maintained body conditioning, which are the signs of normal liver function regardless of high distribution of liposomes in liver [139]. Kaplan-Meier survival curve (Figure 29D) demonstrated that the median survival of mice treated with Dox-Erlo loaded Tf-Pen liposomes (36 days) was significantly ($p < 0.05$) longer as compared to Dox-Erlo loaded Tf liposomes (30 days) and Dox-Erlo loaded Pen liposomes (27.5 days). In contrast, the animals in the control group (PBS) survived only 22 days. The Dox-Erlo loaded plain liposomes (25.5days) and free drugs, Dox-Erlo (25 days) showed slight improvement than PBS group in the median survival time of mice. These results indicate the superior efficacy of Tf-Pen liposomes to achieve receptor and adsorptive mediated transcytosis across the BBB and accumulate at the glioblastoma tumor site, thereby achieving tumor control and survival in glioblastoma bearing mice. Additionally, the co-delivery of Dox and Erlo from Tf-Pen liposomes demonstrated excellent potential of combination therapy in enhancing the antitumor efficacy on tumor regression and significant ($p < 0.05$) increase in the median survival time in comparison to single drug therapy (Figure 35). The potential of combination therapy is in targeting different pathways, thereby demonstrating their effect on the proliferation and death rates of tumor cells as well as on the number of point mutations which are responsible for resistance. Thus, our results revealed the efficient targeting ability of Tf-Pen liposomes and co-delivery of Dox and Erlo appear to be an excellent strategy than single ligand or single drug approach.

Immunofluorescence staining for Ki-67 and cleaved poly (ADP-ribose) polymerase (PARP) for glioblastoma bearing mice brain sections of treated groups were also

observed for assessing tumor cells proliferation and apoptosis, respectively. As shown in Fig. 34E, glioblastoma bearing mice brain sections treated with Dox-Erlo loaded Tf-Pen liposomes showed significantly lesser Ki-67 positive cells in comparison to PBS control group demonstrating the presence of fewer number of proliferating cells. In addition, the cleaved PARP is an established marker to detect apoptosis [140,141]. The glioblastoma bearing mice group treated with Dox-Erlo loaded Tf-Pen liposomes produced significantly higher numbers of cleaved PARP apoptotic cells on the surface as well as at the core of the GBM than the control (PBS) group (Fig. 34F). These images revealed the efficient binding of Tf-Pen liposomes on tumors which resulted in effective release of drugs to tumors, thereby showing increased apoptosis with decreased proliferation of tumors as compared to single ligand or plain liposomes. Therefore, these results demonstrate the excellent antitumor efficacy of the Tf-Pen liposomes in crossing the BBB and co-delivering anticancer chemotherapeutics to brain in achieving tumor regression and survival in mice bearing glioblastoma.

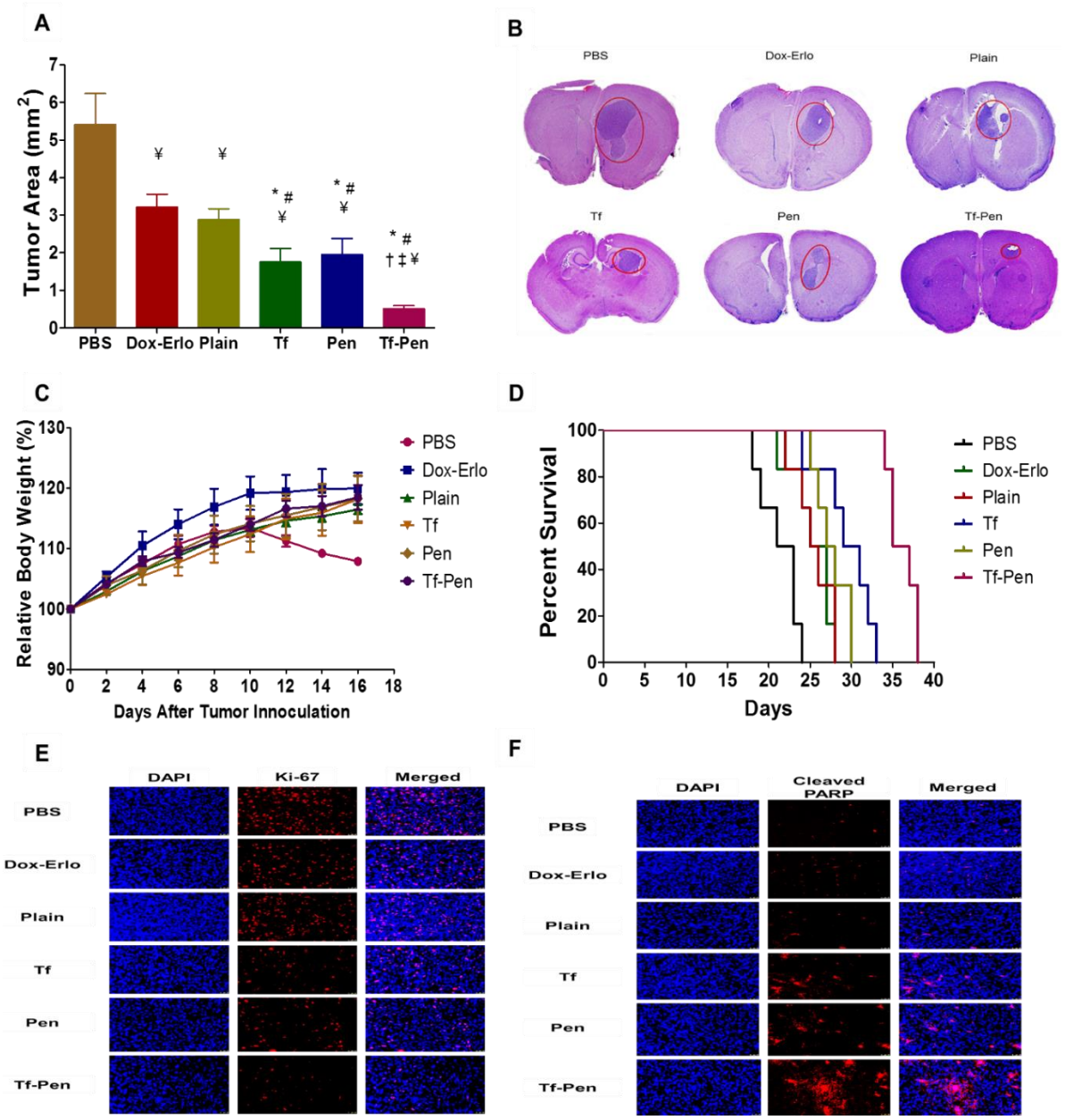

Figure 34. Anti-tumor efficacy in intracranial glioblastoma bearing nude mice**.** (A). Graph demonstrates the tumor regression in mice brain after 3 doses of treatment. Data represented as mean ± SD; n = 6. Statistically significant ($p < 0.05$) differences with (*) plain liposomes, (#) free Dox-Erlo, (‡) Tf-liposomes, and (†) Pen-liposomes were observed. (B) Histological sections of brain display the tumor regression (in red circle) after treatment. The images were taken at 20X magnification. The brain section from mice administered PBS was considered as a control. (C) Graph represents the relative body weight of mice during treatment after tumor inoculation. Data represented as mean ± SD; n = 6. (D) Kaplan-Meier survival curves of mice after treatment (n = 6). (E) Immunofluorescence staining for Ki-67 on mice brain glioblastoma site for tumor cell proliferation. (F) Immunofluorescence staining for cleaved PARP on mice brain glioblastoma site for tumor cell apoptosis. The images were taken at 20X magnification.

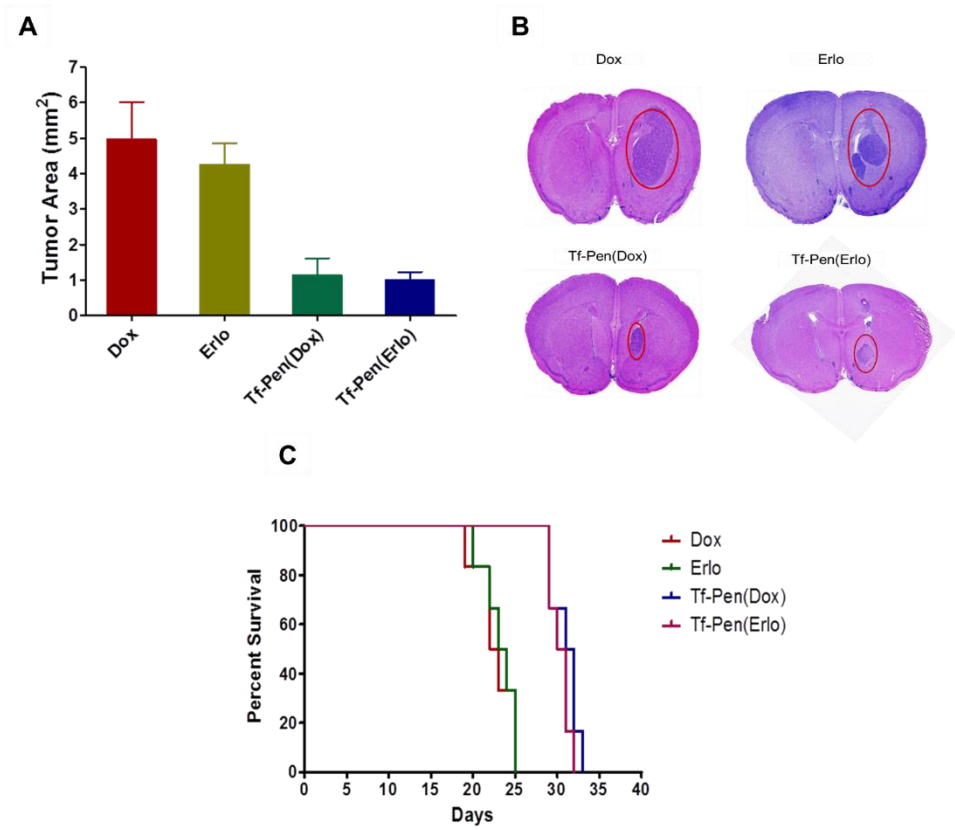

Figure 35. (A). Graph demonstrates the tumor regression in mice brain after 3 doses of treatment. Data represented as mean ± SD; n = 6. (B). Histological sections of brain display the tumor regression (in red circle) after treatment. (C). Kaplan-Meier survival curves of mice after treatment (n=6).

CHAPTER 4. SUMMARY AND CONCLUSION

Drug delivery to the brain has been a major challenge due to the presence of the blood brain barrier (BBB), which separates the blood from the cerebral parenchyma and limits the uptake of most chemotherapeutics into the brain. Therefore, there has always been a need to develop an effective delivery system to deliver chemotherapeutics drugs across the BBB to the core of the glioblastoma tumor as well as to the migratory cells in the infiltration zone. To overcome the limitation of chemotherapeutics not reaching into the brain, we put our efforts in designing a dual functionalized liposomal delivery system which can successful able to carry chemotherapeutics agents across the BBB into the brain. The liposomes were surface modified with transferrin protein for Tf receptor mediated transcytosis across brain endothelium. Moreover, these liposomes are also designed for enhanced cell penetration by coupling cell penetrating peptide. The significance of this research lies in the designing of dual functionalized liposomes for the effective delivery of anti-cancer chemotherapeutics agents across the BBB for the treatment of glioblastoma.

We investigated the influence of incorporation of various CPPs, based on their physicochemical properties to Tf-liposomes on cytotoxic potential, cellular uptake, hemocompatibility, transport and efficacy across the *in vitro* brain tumor model, *in vivo* distribution, *in vivo* biocompatibility and efficacy in glioblastoma mice model. We also illustrated the combination drug therapy for the effective treatment modalities for cancer, thereby enhancing the therapeutic efficacy. Our results demonstrated the dual functionalized exhibited excellent biocompatibility for in vivo administration. The *in vitro* cellular uptake study showed that the dual-functionalized liposomes are capable of higher cellular uptake in U87, bEnd.3 and glial cells as compared to single ligand liposomes. In addition, the dual functionalized liposomes showed significantly ($p < 0.05$) higher transport across the BBB *in vitro* and *in vivo* in mice brain. Our

results revealed that insertion of TAT and Penetratin, amphiphilic cationic CPPs on the surface of Tf liposomes increased the translocation of doxorubicin and erlotinib across the endothelial barrier *in vitro* and *in vivo*. Hydrophobic peptide QLPVM, when conjugated with Tf liposomes demonstrated increased transport across the BBB *in vitro* and *in vivo*. However, QLPVM also showed high cytotoxicity and hemolysis which restricts it use for *in vivo* administration. Tf-pen liposomes showed highest distribution in brain followed by Tf-TAT then Tf-QLPVM. Tf-TAT liposomes showed non-significantly ($p > 0.05$) higher accumulation in brain as compared to Tf-QLPVM liposomes. Tf-pen liposomes demonstrated significant ($p < 0.05$) difference in the percent tumor cell viability using *in vitro* brain tumor model. Whereas Tf-TAT, Tf-QLPVM and Tf-PFV liposomes exhibited no significant ($p > 0.05$) difference in the percent tumor cell viability. In addition, the co-delivery of dox and erlo from Tf-Pen liposomes demonstrated significantly ($p > 0.05$) lower the percent tumor cell viability as compared to 5-FU loaded Tf-Pen liposomes. Histological examination of Tf-CPP liposomes demonstrated no evidence of change in morphological appearance. Furthermore, there were no signs of tissue necrosis, inflammation or nuclei enlargement after examining tissue sections of different organs as compared to the tissue sections from control group. Additionally, the co-delivery of Dox and Erlo from Tf-Pen liposomes demonstrated excellent potential of combination therapy in enhancing the antitumor efficacy on tumor regression and significant ($p < 0.05$) increase in the median survival time in mice bearing glioblastoma. However, the manual cutting of the mice brain glioblastoma tissue sections possess a limitation which needs to be refined.

In conclusion, we successfully prepared and characterized the dual functionalized liposomes by modifying their surface with Tf for receptor targeting and CPP for enhanced cell penetration for the co-delivery of Dox and Erlo for the treatment of invasive brain gliomas.

Insertion of CPP to Tf-liposomes revealed excellent biocompatibility as well as high cellular uptake, *in vitro*. This study demonstrates the efficient translocation of the dual functionalized liposomes across the BBB, thereby showing high concentration of anti-cancer chemotherapeutic drugs in mice brain. In addition, these liposomes displayed excellent antitumor efficacy in treating invasive brain gliomas by significantly increasing the mice survival time as well as significant regression of glioblastoma tumor in mice brain. Therefore, we believe that this study would have high impact for co-delivering of chemotherapeutics across the BBB for treating patients with glioblastoma.

4.1. Future directions

This research work demonstrates the dual functionalized liposomal delivery system for the efficient co-delivery of anti-cancer chemotherapeutics across the BBB into the brain for the treatment of glioblastoma. This dual functionalized liposomes exploit the use of receptor targeting ligand and a cell penetrating peptide for enhanced cell penetration in a single delivery system. A short amino acid sequence of peptides or antibodies can be employed to surface modification of liposomes such as T7, OX-26, R17-217 for transferrin receptor mediated transcytosis, thereby preventing the competition of endogenous transferrin to bind its receptor. However, these short peptides or antibodies bind to a different site other than endogenous transferrin. Different receptors or transporters could also be exploited to deliver anticancer drugs across the BBB including Insulin, low density lipoprotein receptor (LRP1 and LRP2). In addition, it will be important to quantify the distribution of drugs in glioblastoma tumor, brain tissue and cerebrospinal fluid as well. In this research, we used combination therapy of anti-cancer chemotherapeutic drugs to target glioblastoma. It would be interesting to use a combination of a chemotherapeutic, doxorubicin and a gene, pORF-hTRAIL to target glioblastoma. The DNA damaging ability of doxorubicin could

extraordinarily synergize the benefits of tumor necrosis factor (TNF) related apoptosis-induced ligand (TRAIL), *via* regulating the expression of death receptors and stimulating apoptotic pathway. Therefore, this combination therapy of gene and chemotherapeutics is expected to achieve anti-cancer effect at lower drug doses, resulting in lower undesirable toxicities.

REFERENCES

[1] P.A. Stewart, Endothelial Vesicles in the Blood–Brain Barrier: Are They Related to Permeability?, Cell. Mol. Neurobiol. 20 (2000) 149–163.

[2] N.J. Abbott, Dynamics of CNS barriers: evolution, differentiation, and modulation., Cell. Mol. Neurobiol. 25 (2005) 5–23.

[3] W.H. Oldendorf, M.E. Cornford, W.J. Brown, The large apparent work capability of the blood-brain barrier: a study of the mitochondrial content of capillary endothelial cells in brain and other tissues of the rat., Ann. Neurol. 1 (1977) 409–417.

[4] Y. Persidsky, S.H. Ramirez, J. Haorah, G.D. Kanmogne, Blood-brain barrier: structural components and function under physiologic and pathologic conditions., J. Neuroimmune Pharmacol. 1 (2006) 223–236.

[5] M. Ramsauer, J. Kunz, D. Krause, R. Dermietzel, Regulation of a blood-brain barrier-specific enzyme expressed by cerebral pericytes (pericytic aminopeptidase N/pAPN) under cell culture conditions., J. Cereb. Blood Flow Metab. 18 (1998) 1270–1281.

[6] M. Ramsauer, D. Krause, R. Dermietzel, Angiogenesis of the blood-brain barrier in vitro and the function of cerebral pericytes., FASEB J. Off. Publ. Fed. Am. Soc. Exp. Biol. 16 (2002) 1274–1276.

[7] S. Dohgu, F. Takata, A. Yamauchi, S. Nakagawa, T. Egawa, M. Naito, T. Tsuruo, Y. Sawada, M. Niwa, Y. Kataoka, Brain pericytes contribute to the induction and up-regulation of blood-brain barrier functions through transforming growth factor-beta production., Brain Res. 1038 (2005) 208–215.

[8] J. Rip, G.J. Schenk, A.G. de Boer, Differential receptor-mediated drug targeting to the diseased brain., Expert Opin. Drug Deliv. 6 (2009) 227–237.

[9] N.J. Abbott, L. Ronnback, E. Hansson, Astrocyte-endothelial interactions at the blood-brain barrier., Nat. Rev. Neurosci. 7 (2006) 41–53.

[10] W.A. Banks, Characteristics of compounds that cross the blood-brain barrier, BMC Neurol. 9 Suppl 1 (2009) S3–S3.

[11] M.A. Deli, Potential use of tight junction modulators to reversibly open membranous barriers and improve drug delivery., Biochim. Biophys. Acta. 1788 (2009) 892–910.

[12] K. Hynynen, Ultrasound for drug and gene delivery to the brain., Adv. Drug Deliv. Rev. 60 (2008) 1209–1217.

[13] R. Stam, Electromagnetic fields and the blood-brain barrier., Brain Res. Rev. 65 (2010) 80–97.

[14] D.F. Emerich, P. Snodgrass, M. Pink, F. Bloom, R.T. Bartus, Central analgesic actions of loperamide following transient permeation of the blood brain barrier with Cereport (RMP-7)., Brain Res. 801 (1998) 259–266.

[15] D.F. Emerich, P. Snodgrass, R. Dean, M. Agostino, B. Hasler, M. Pink, H. Xiong, B.S. Kim, R.T. Bartus, Enhanced delivery of carboplatin into brain tumours with intravenous Cereport (RMP-7): dramatic differences and insight gained from dosing parameters., Br. J. Cancer. 80 (1999) 964–970.

[16] D.F. Emerich, R.L. Dean, J. Marsh, M. Pink, D. Lafreniere, P. Snodgrass, R.T. Bartus, Intravenous cereport (RMP-7) enhances delivery of hydrophilic chemotherapeutics and increases survival in rats with metastatic tumors in the brain., Pharm. Res. 17 (2000) 1212–1219.

[17] C. V Borlongan, D.F. Emerich, Facilitation of drug entry into the CNS via transient permeation of blood brain barrier: laboratory and preliminary clinical evidence from bradykinin receptor agonist, Cereport., Brain Res. Bull. 60 (2003) 297–306.

[18] E. Sanovich, R.T. Bartus, P.M. Friden, R.L. Dean, H.Q. Le, M.W. Brightman, Pathway across blood-brain barrier opened by the bradykinin agonist, RMP-7., Brain Res. 705 (1995) 125–135.

[19] J.B. Mackic, M. Stins, S. Jovanovic, K.S. Kim, R.T. Bartus, B. V Zlokovic, Cereport (RMP-7) increases the permeability of human brain microvascular endothelial cell monolayers., Pharm. Res. 16 (1999) 1360–1365.

[20] D.J. Bidanset, L. Placidi, R. Rybak, J. Palmer, J.P. Sommadossi, E.R. Kern, Intravenous infusion of cereport increases uptake and efficacy of acyclovir in herpes simplex virus-infected rat brains., Antimicrob. Agents Chemother. 45 (2001) 2316–2323.

[21] Y. Kuang, S.N. Lackay, L. Zhao, Z.F. Fu, Role of chemokines in the enhancement of BBB permeability and inflammatory infiltration after rabies virus infection., Virus Res. 144 (2009) 18–26.

[22] J. Szejtli, Introduction and General Overview of Cyclodextrin Chemistry., Chem. Rev. 98 (1998) 1743–1754.

[23] S. Tilloy, V. Monnaert, L. Fenart, H. Bricout, R. Cecchelli, E. Monflier, Methylated beta-cyclodextrin as P-gp modulators for deliverance of doxorubicin across an in vitro model of blood-brain barrier., Bioorg. Med. Chem. Lett. 16 (2006) 2154–2157.

[24] K. Hynynen, N. McDannold, N. Vykhodtseva, F.A. Jolesz, Noninvasive MR imaging-guided focal opening of the blood-brain barrier in rabbits., Radiology. 220 (2001) 640–646.

[25] R.M. Quock, F.J. Kouchich, T.K. Ishii, D.G. Lange, Microwave facilitation of domperidone antagonism of apomorphine-induced stereotypic climbing in mice., Bioelectromagnetics. 8 (1987) 45–55.

[26] L.-B. Qiu, G.-R. Ding, K.-C. Li, X.-W. Wang, Y. Zhou, Y.-C. Zhou, Y.-R. Li, G.-Z. Guo, The role of protein kinase C in the opening of blood-brain barrier induced by electromagnetic pulse., Toxicology. 273 (2010) 29–34.

[27] Tsuji, I. Tamai, Carrier-mediated or specialized transport of drugs across the blood-brain barrier., Adv. Drug Deliv. Rev. 36 (1999) 277–290.

[28] L.A. Wade, R. Katzman, 3-O-methyldopa uptake and inhibition of L-dopa at the blood-brain barrier., Life Sci. 17 (1975) 131–136.

[29] F. Hervé, N. Ghinea, J.-M. Scherrmann, CNS delivery via adsorptive transcytosis, AAPS J. 10 (2008) 455–472.

[30] M. Zorko, U. Langel, Cell-penetrating peptides: mechanism and kinetics of cargo delivery., Adv. Drug Deliv. Rev. 57 (2005) 529–545.

[31] S. Deshayes, M.C. Morris, G. Divita, F. Heitz, Cell-penetrating peptides: tools for intracellular delivery of therapeutics., Cell. Mol. Life Sci. 62 (2005) 1839–1849.

[32] G. Drin, S. Cottin, E. Blanc, A.R. Rees, J. Temsamani, Studies on the internalization mechanism of cationic cell-penetrating peptides., J. Biol. Chem. 278 (2003) 31192–31201.

[33] J.S. Wadia, R. V Stan, S.F. Dowdy, Transducible TAT-HA fusogenic peptide enhances escape of TAT-fusion proteins after lipid raft macropinocytosis, Nat. Med. 10 (2004) 310–315.

[34] M. Adenot, P. Merida, R. Lahana, Applications of a blood-brain barrier technology platform to predict CNS penetration of various chemotherapeutic agents. 2. Cationic peptide vectors for brain delivery., Chemotherapy. 53 (2007) 73–76.

[35] G. Sharma, A. Modgil, T. Zhong, C. Sun, J. Singh, Influence of short-chain cell-penetrating peptides on transport of doxorubicin encapsulating receptor-targeted liposomes across brain endothelial barrier, Pharm. Res. 31 (2014) 1194–1209.

[36] H. Xia, X. Gao, G. Gu, Z. Liu, Q. Hu, Y. Tu, Q. Song, L. Yao, Z. Pang, X. Jiang, J. Chen, H. Chen, Penetratin-functionalized PEG-PLA nanoparticles for brain drug delivery., Int. J. Pharm. 436 (2012) 840–850.

[37] S. Lakkadwala, J. Singh, Dual Functionalized 5-Fluorouracil Liposomes as Highly Efficient Nanomedicine for Glioblastoma Treatment as Assessed in an In Vitro Brain Tumor Model, J. Pharm. Sci. 107 (2018) 2902–2913.

[38] Z.M. Qian, H. Li, H. Sun, K. Ho, Targeted drug delivery via the transferrin receptor-mediated endocytosis pathway., Pharmacol. Rev. 54 (2002) 561–587.

[39] W.M. Pardridge, Blood-brain barrier drug targeting: the future of brain drug development., Mol. Interv. 3 (2003) 51,90-105.

[40] W.M. Pardridge, Drug and gene targeting to the brain with molecular Trojan horses., Nat. Rev. Drug Discov. 1 (2002) 131–139.

[41] D. Wu, J. Yang, W.M. Pardridge, Drug targeting of a peptide radiopharmaceutical through the primate blood-brain barrier in vivo with a monoclonal antibody to the human insulin receptor., J. Clin. Invest. 100 (1997) 1804–1812.

[42] C.-F. Xia, R.J. Boado, W.M. Pardridge, Antibody-mediated targeting of siRNA via the human insulin receptor using avidin-biotin technology., Mol. Pharm. 6 (2009) 747–751.

[43] S. Lakkadwala, J. Singh, Co-delivery of doxorubicin and erlotinib through liposomal nanoparticles for glioblastoma tumor regression using an in vitro brain tumor model, Colloids Surfaces B Biointerfaces. 173 (2019) 27–35.

[44] M.C. Woodle, Sterically stabilized liposome therapeutics, Adv. Drug Deliv. Rev. 16 (1995) 249–265.

[45] B. Ji, J. Maeda, M. Higuchi, K. Inoue, H. Akita, H. Harashima, T. Suhara, Pharmacokinetics and brain uptake of lactoferrin in rats., Life Sci. 78 (2006) 851–855.

[46] J.K. Vasir, M.K.R. and V.D. Labhasetwar, Nanosystems in Drug Targeting: Opportunities and Challenges, Curr. Nanosci. 1 (2005) 47–64.

[47] H. Hatakeyama, H. Akita, E. Ishida, K. Hashimoto, H. Kobayashi, T. Aoki, J. Yasuda, K. Obata, H. Kikuchi, T. Ishida, H. Kiwada, H. Harashima, Tumor targeting of doxorubicin by anti-MT1-MMP antibody-modified PEG liposomes., Int. J. Pharm. 342 (2007) 194–200.

[48] X. Li, L. Ding, Y. Xu, Y. Wang, Q. Ping, Targeted delivery of doxorubicin using stealth liposomes modified with transferrin, Int. J. Pharm. 373 (2009) 116–123.

[49] E. Markoutsa, G. Pampalakis, A. Niarakis, I.A. Romero, B. Weksler, P.-O. Couraud, S.G. Antimisiaris, Uptake and permeability studies of BBB-targeting immunoliposomes using the hCMEC/D3 cell line., Eur. J. Pharm. Biopharm. 77 (2011) 265–274.

[50] C.M. Lawrence, S. Ray, M. Babyonyshev, R. Galluser, D.W. Borhani, S.C. Harrison, Crystal structure of the ectodomain of human transferrin receptor., Science. 286 (1999) 779–782.

[51] L.C. Kühn, H.M. Schulman, P. Ponka, Iron-transferrin requirements and transferrin receptor expression in proliferating cells, in: Iron Transp. Storage, CRC Press, 1990: pp. 149–191.

[52] U. Testa, E. Pelosi, C. Peschle, The transferrin receptor, Crit. Rev. Oncog. 4 (1993) 241–276.

[53] D.R. Richardson, P. Ponka, The molecular mechanisms of the metabolism and transport of iron in normal and neoplastic cells., Biochim. Biophys. Acta. 1331 (1997) 1–40.

[54] P. Ponka, C.N. Lok, The transferrin receptor: role in health and disease., Int. J. Biochem. Cell Biol. 31 (1999) 1111–1137.

[55] K. Ulbrich, T. Hekmatara, E. Herbert, J. Kreuter, Transferrin- and transferrin-receptor-antibody-modified nanoparticles enable drug delivery across the blood-brain barrier (BBB)., Eur. J. Pharm. Biopharm. 71 (2009) 251–256.

[56] I. van Rooy, E. Mastrobattista, G. Storm, W.E. Hennink, R.M. Schiffelers, Comparison of five different targeting ligands to enhance accumulation of liposomes into the brain., J. Control. Release. 150 (2011) 30–36.

[57] B. Gupta, T.S. Levchenko, V.P. Torchilin, Intracellular delivery of large molecules and small particles by cell-penetrating proteins and peptides., Adv. Drug Deliv. Rev. 57 (2005) 637–651.

[58] M. Lewin, N. Carlesso, C.H. Tung, X.W. Tang, D. Cory, D.T. Scadden, R. Weissleder, Tat peptide-derivatized magnetic nanoparticles allow in vivo tracking and recovery of progenitor cells., Nat. Biotechnol. 18 (2000) 410–414.

[59] V.P. Torchilin, Tat peptide-mediated intracellular delivery of pharmaceutical nanocarriers., Adv. Drug Deliv. Rev. 60 (2008) 548–558.

[60] V.P. Torchilin, T.S. Levchenko, R. Rammohan, N. Volodina, B. Papahadjopoulos-Sternberg, G.G.M. D'Souza, Cell transfection in vitro and in vivo with nontoxic TAT peptide-liposome-DNA complexes., Proc. Natl. Acad. Sci. U. S. A. 100 (2003) 1972–1977.

[61] D.M. Copolovici, K. Langel, E. Eriste, U. Langel, Cell-penetrating peptides: design, synthesis, and applications., ACS Nano. 8 (2014) 1972–1994.

[62] N. Schmidt, A. Mishra, G.H. Lai, G.C.L. Wong, Arginine-rich cell-penetrating peptides., FEBS Lett. 584 (2010) 1806–1813.

[63] C. Bechara, S. Sagan, Cell-penetrating peptides: 20 years later, where do we stand?, FEBS Lett. 587 (2013) 1693–1702.

[64] F. Milletti, Cell-penetrating peptides: Classes, origin, and current landscape, Drug Discov. Today. 17 (2012) 850–860.

[65] A. Bolhassani, Non-Viral Delivery Systems in Gene Therapy and Vaccine Development, in: S.R.E.-X. Yuan (Ed.), IntechOpen, Rijeka, 2011: pp. 27–50.

[66] M. Pooga, M. Lindgren, M. Hallbrink, E. Brakenhielm, U. Langel, Galanin-based peptides, galparan and transportan, with receptor-dependent and independent activities., Ann. N. Y. Acad. Sci. 863 (1998) 450–453.

[67] N.-Q. Shi, X.-R. Qi, B. Xiang, Y. Zhang, A survey on “Trojan Horse” peptides: opportunities, issues and controlled entry to “Troy”., J. Control. Release. 194 (2014) 53–70.

[68] S.M. Farkhani, A. Valizadeh, H. Karami, S. Mohammadi, N. Sohrabi, F. Badrzadeh, Cell penetrating peptides: efficient vectors for delivery of nanoparticles, nanocarriers, therapeutic and diagnostic molecules., Peptides. 57 (2014) 78–94.

[69] E. Koren, V.P. Torchilin, Cell-penetrating peptides: breaking through to the other side., Trends Mol. Med. 18 (2012) 385–393.

[70] D. Derossi, A.H. Joliot, G. Chassaing, A. Prochiantz, The third helix of the Antennapedia homeodomain translocates through biological membranes., J. Biol. Chem. 269 (1994) 10444–10450.

[71] G. Drin, M. Mazel, P. Clair, D. Mathieu, M. Kaczorek, J. Temsamani, Physico-chemical requirements for cellular uptake of pAntp peptide. Role of lipid-binding affinity., Eur. J. Biochem. 268 (2001) 1304–1314.

[72] A. Scheller, B. Wiesner, M. Melzig, M. Bienert, J. Oehlke, Evidence for an amphipathicity independent cellular uptake of amphipathic cell-penetrating peptides., Eur. J. Biochem. 267 (2000) 6043–6050.

[73] Y. He, F. Li, Y. Huang, Smart Cell-Penetrating Peptide-Based Techniques for Intracellular Delivery of Therapeutic Macromolecules, in: R.B.T.-A. in P.C. and S.B. Donev (Ed.), Ther. Proteins Pept., Academic Press, 2018: pp. 183–220.

[74] G. Dom, C. Shaw-Jackson, C. Matis, O. Bouffioux, J.J. Picard, A. Prochiantz, M.-P. Mingeot-Leclercq, R. Brasseur, R. Rezsohazy, Cellular uptake of Antennapedia Penetratin peptides is a two-step process in which phase transfer precedes a tryptophan-dependent translocation, Nucleic Acids Res. 31 (2003) 556–561.

[75] A.D. Frankel, C.O. Pabo, Cellular uptake of the tat protein from human immunodeficiency virus., Cell. 55 (1988) 1189–1193.

[76] M. Green, P.M. Loewenstein, Autonomous functional domains of chemically synthesized human immunodeficiency virus tat trans-activator protein., Cell. 55 (1988) 1179–1188.

[77] C. Brigati, M. Giacca, D.M. Noonan, A. Albini, HIV Tat, its TARgets and the control of viral gene expression., FEMS Microbiol. Lett. 220 (2003) 57–65.

[78] S. Santra, H. Yang, P.H. Holloway, J.T. Stanley, R.A. Mericle, Synthesis of Water-Dispersible Fluorescent, Radio-Opaque, and Paramagnetic CdS:Mn/ZnS Quantum Dots: A Multifunctional Probe for Bioimaging, J. Am. Chem. Soc. 127 (2005) 1656–1657.

[79] L. Liu, S.S. Venkatraman, Y.-Y. Yang, K. Guo, J. Lu, B. He, S. Moochhala, L. Kan, Polymeric micelles anchored with TAT for delivery of antibiotics across the blood-brain barrier., Biopolymers. 90 (2008) 617–623.

[80] J.A. Gomez, V. Gama, T. Yoshida, W. Sun, P. Hayes, K. Leskov, D. Boothman, S. Matsuyama, Bax-inhibiting peptides derived from Ku70 and cell-penetrating pentapeptides., Biochem. Soc. Trans. 35 (2007) 797–801.

[81] T. Yoshida, I. Tomioka, T. Nagahara, T. Holyst, M. Sawada, P. Hayes, V. Gama, M. Okuno, Y. Chen, Y. Abe, T. Kanouchi, H. Sasada, D. Wang, T. Yokota, E. Sato, S. Matsuyama, Bax-inhibiting peptide derived from mouse and rat Ku70., Biochem. Biophys. Res. Commun. 321 (2004) 961–966.

[82] J.A. Gomez, J. Chen, J. Ngo, D. Hajkova, I.-J. Yeh, V. Gama, M. Miyagi, S. Matsuyama, Cell-Penetrating Penta-Peptides (CPP5s): Measurement of Cell Entry and Protein-Transduction Activity., Pharmaceuticals. 3 (2010) 3594–3613.

[83] D. Cai, W. Gao, B. He, W. Dai, H. Zhang, X. Wang, J. Wang, X. Zhang, Q. Zhang, Hydrophobic penetrating peptide PFVYLI-modified stealth liposomes for doxorubicin delivery in breast cancer therapy., Biomaterials. 35 (2014) 2283–2294.

[84] G. Odabaei, D. Chatterjee, A.R. Jazirehi, L. Goodglick, K. Yeung, B. Bonavida, Raf-1 kinase inhibitor protein: structure, function, regulation of cell signaling, and pivotal role in apoptosis., Adv. Cancer Res. 91 (2004) 169–200.

[85] T.J. Stuhlmiller, S.M. Miller, J.S. Zawistowski, K. Nakamura, A.S. Beltran, J.S. Duncan, S.P. Angus, K.A.L. Collins, D.A. Granger, R.A. Reuther, L.M. Graves, S.M. Gomez, P.-F. Kuan, J.S. Parker, X. Chen, N. Sciaky, L.A. Carey, H.S. Earp, J. Jin, G.L. Johnson, Inhibition of Lapatinib-Induced Kinome Reprogramming in ERBB2-Positive Breast Cancer by Targeting BET Family Bromodomains., Cell Rep. 11 (2015) 390–404.

[86] R.J. Weil, D.C. Palmieri, J.L. Bronder, A.M. Stark, P.S. Steeg, Breast Cancer Metastasis to the Central Nervous System, Am. J. Pathol. 167 (2005) 913–920.

[87] D.R. Johnson, B.P. O'Neill, Glioblastoma survival in the United States before and during the temozolomide era., J. Neurooncol. 107 (2012) 359–364.

[88] M.J. Donahue, J.O. Blakeley, J. Zhou, M.G. Pomper, J. Laterra, P.C.M. van Zijl, Evaluation of human brain tumor heterogeneity using multiple T1-based MRI signal weighting approaches., Magn. Reson. Med. 59 (2008) 336–344.

[89] A.S. Lichter, T.S. Lawrence, Recent Advances in Radiation Oncology, N. Engl. J. Med. 332 (1995) 371–379.

[90] D. Peer, J.M. Karp, S. Hong, O.C. Farokhzad, R. Margalit, R. Langer, Nanocarriers as an emerging platform for cancer therapy., Nat. Nanotechnol. 2 (2007) 751–760.

[91] S. Agarwal, R. Sane, R. Oberoi, J.R. Ohlfest, W.F. Elmquist, Delivery of molecularly targeted therapy to malignant glioma, a disease of the whole brain, Expert Rev. Mol. Med. 13 (2011) e17.

[92] G. Sharma, A. Modgil, C. Sun, J. Singh, Grafting of cell-penetrating peptide to receptor-targeted liposomes improves their transfection efficiency and transport across blood-brain barrier model, J. Pharm. Sci. 101 (2012) 2468–2478.

[93] K. Prabhakar, S.M. Afzal, P.U. Kumar, A. Rajanna, V. Kishan, Brain delivery of transferrin coupled indinavir submicron lipid emulsions-Pharmacokinetics and tissue distribution, Colloids Surfaces B Biointerfaces. 86 (2011) 305–313.

[94] S. Skarlatos, T. Yoshikawa, W.M. Pardridge, Transport of [125I]transferrin through the rat blood-brain barrier., Brain Res. 683 (1995) 164–171.

[95] J. Huwyler, D. Wu, W.M. Pardridge, Brain drug delivery of small molecules using immunoliposomes, Proc. Natl. Acad. Sci. 93 (1996) 14164–14169.

[96] S. Anabousi, M. Laue, C.-M. Lehr, U. Bakowsky, C. Ehrhardt, Assessing transferrin modification of liposomes by atomic force microscopy and transmission electron microscopy., Eur. J. Pharm. Biopharm. 60 (2005) 295–303.

[97] L. Mayer, M.B. Bally, P.R. Cullis, R.S. Ginsberg, G.N. Mitilenes, High drug:lipid formulations of liposomal-antineoplastic agents, (1988). https://www.google.com/patents/WO1988006442A1?cl=en.

[98] X. Ying, H. Wen, W.L. Lu, J. Du, J. Guo, W. Tian, Y. Men, Y. Zhang, R.J. Li, T.Y. Yang, D.W. Shang, J.N. Lou, L.R. Zhang, Q. Zhang, Dual-targeting daunorubicin liposomes improve the therapeutic efficacy of brain glioma in animals, J. Control. Release. 141 (2010) 183–192.

[99] Y. Xie, L. Ye, X. Zhang, W. Cui, J. Lou, T. Nagai, X. Hou, Transport of nerve growth factor encapsulated into liposomes across the blood-brain barrier: in vitro and in vivo studies., J. Control. Release. 105 (2005) 106–119.

[100] H. Franke, H.-J. Galla, C.T. Beuckmann, Primary cultures of brain microvessel endothelial cells: a valid and flexible model to study drug transport through the blood–brain barrier in vitro, Brain Res. Protoc. 5 (2000) 248–256.

[101] P. Thevenot, A. Nair, J. Dey, J. Yang, L. Tang, Method to Analyze Three-Dimensional Cell Distribution and Infiltration in Degradable Scaffolds, Tissue Eng. Part C Methods. 14 (2008) 319–331.

[102] S.-C. Wang, C.-F. Yu, J.-H. Hong, C.-S. Tsai, C.-S. Chiang, Radiation therapy-induced tumor invasiveness is associated with SDF-1-regulated macrophage mobilization and vasculogenesis., PLoS One. 8 (2013) e69182.

[103] D.L. Iden, T.M. Allen, In vitro and in vivo comparison of immunoliposomes made by conventional coupling techniques with those made by a new post-insertion approach., Biochim. Biophys. Acta. 1513 (2001) 207–216.

[104] J.N. Moreira, T. Ishida, R. Gaspar, T.M. Allen, Use of the post-insertion technique to insert peptide ligands into pre-formed stealth liposomes with retention of binding activity and cytotoxicity., Pharm. Res. 19 (2002) 265–269.

[105] O. Nag, V. Awasthi, Surface Engineering of Liposomes for Stealth Behavior, Pharmaceutics. 5 (2013) 542–569.

[106] V.P. Torchilin, B.A. Khaw, V.N. Smirnov, E. Haber, Preservation of antimyosin antibody activity after covalent coupling to liposomes, Biochem. Biophys. Res. Commun. 89 (1979) 1114–1119.

[107] P. Marqués-Gallego, A.I.P.M. De Kroon, Ligation strategies for targeting liposomal nanocarriers, Biomed Res. Int. 2014 (2014) 1–12.

[108] S.-H. Lee, Y. Sato, M. Hyodo, H. Harashima, Topology of Surface Ligands on Liposomes: Characterization Based on the Terms, Incorporation Ratio, Surface Anchor Density, and Reaction Yield., Biol. Pharm. Bull. 39 (2016) 1983–1994.

[109] Y. Chen, L. Liu, Modern methods for delivery of drugs across the blood-brain barrier, Adv. Drug Deliv. Rev. 64 (2012) 640–665.

[110] C. Roney, P. Kulkarni, V. Arora, P. Antich, F. Bonte, A. Wu, N.N. Mallikarjuana, S. Manohar, H.F. Liang, A.R. Kulkarni, H.W. Sung, M. Sairam, T.M. Aminabhavi, Targeted nanoparticles for drug delivery through the blood-brain barrier for Alzheimer's disease, J Control Release. 108 (2005) 193–214.

[111] S. El-Andaloussi, P. Jarver, H.J. Johansson, U. Langel, Cargo-dependent cytotoxicity and delivery efficacy of cell-penetrating peptides: a comparative study., Biochem. J. 407 (2007) 285–292.

[112] K. Saar, M. Lindgren, M. Hansen, E. Eiríksdóttir, Y. Jiang, K. Rosenthal-Aizman, M. Sassian, Ü. Langel, Cell-penetrating peptides: A comparative membrane toxicity study, Anal. Biochem. 345 (2005) 55–65.

[113] S. Trabulo, A.L. Cardoso, M. Mano, M.C.P. De Lima, Cell-Penetrating Peptides-Mechanisms of Cellular Uptake and Generation of Delivery Systems, Pharmaceuticals. 3 (2010) 961–993.

[114] G. Sharma, A. Modgil, B. Layek, K. Arora, C. Sun, B. Law, J. Singh, Cell penetrating peptide tethered bi-ligand liposomes for delivery to brain in vivo: Biodistribution and transfection, J. Control. Release. 167 (2013) 1–10.

[115] S. Antohi, V. Brumfeld, Polycation-cell surface interactions and plasma membrane compartments in mammals. Interference of oligocation with polycationic condensation., Zeitschrift Fur Naturforschung. Sect. C, Biosci. 39 (1984) 767–775.

[116] S. Zhu, F. Qian, Y. Zhang, C. Tang, C. Yin, Synthesis and characterization of PEG modified N-trimethylaminoethylmethacrylate chitosan nanoparticles, Eur. Polym. J. 43 (2007) 2244–2253.

[117] R.K. Kainthan, M. Gnanamani, M. Ganguli, T. Ghosh, D.E. Brooks, S. Maiti, J.N. Kizhakkedathu, Blood compatibility of novel water soluble hyperbranched polyglycerol-based multivalent cationic polymers and their interaction with DNA, Biomaterials. 27 (2006) 5377–5390.

[118] R.C. Janzer, M.C. Raff, Astrocytes induce blood–brain barrier properties in endothelial cells, Nature. 325 (1987) 253–257.

[119] F.E. Arthur, R.R. Shivers, P.D. Bowman, Astrocyte-mediated induction of tight junctions in brain capillary endothelium: an efficient in vitro model, Dev. Brain Res. 36 (1987) 155–159.

[120] H. Ishihara, H. Kubota, R.L.P. Lindberg, D. Leppert, S.M. Gloor, M. Errede, D. Virgintino, A. Fontana, Y. Yonekawa, K. Frei, Endothelial cell barrier impairment induced by glioblastomas and transforming growth factor beta2 involves matrix metalloproteinases and tight junction proteins., J. Neuropathol. Exp. Neurol. 67 (2008) 435–448.

[121] J. Bin Kim, Three-dimensional tissue culture models in cancer biology, Semin. Cancer Biol. 15 (2005) 365–377.

[122] R.C. Janzer, M.C. Raff, Astrocytes induce blood–brain barrier properties in endothelial cells, Nature. 325 (1987) 253–257.

[123] E. Bell, Strategy for the selection of scaffolds for tissue engineering., Tissue Eng. 1 (1995) 163–179.

[124] A. Sourla, C. Doillon, M. Koutsilieris, Three-dimensional type I collagen gel system containing MG-63 osteoblasts-like cells as a model for studying local bone reaction caused by metastatic cancer cells, Anticancer Res. 16 (1996) 2773–2780.

[125] L.N. Ramana, S. Sethuraman, U. Ranga, U.M. Krishnan, Development of a liposomal nanodelivery system for nevirapine, J. Biomed. Sci. 17 (2010) 57–65.

[126] H.B. Lee, M.D. Blaufox, Blood volume in the rat., J. Nucl. Med. 26 (1985) 72–76.

[127] S. Deaglio, A. Capobianco, A. Cali, F. Bellora, F. Alberti, L. Righi, A. Sapino, C. Camaschella, F. Malavasi, Structural, functional, and tissue distribution analysis of human transferrin receptor-2 by murine monoclonal antibodies and a polyclonal antiserum., Blood. 100 (2002) 3782–3789.

[128] W.A. Jefferies, M.R. Brandon, S. V Hunt, A.F. Williams, K.C. Gatter, D.Y. Mason, Transferrin receptor on endothelium of brain capillaries., Nature. 312 (1984) 162–163.

[129] J.J. Killion, R. Radinsky, I.J. Fidler, Orthotopic models are necessary to predict therapy of transplantable tumors in mice., Cancer Metastasis Rev. 17 (1999) 279–284.

[130] A. Jhaveri, P. Deshpande, B. Pattni, V. Torchilin, Transferrin-targeted, resveratrol-loaded liposomes for the treatment of glioblastoma, J. Control. Release. 277 (2018) 89–101.

[131] Y. Cui, Q. Xu, P.K.-H. Chow, D. Wang, C.-H. Wang, Transferrin-conjugated magnetic silica PLGA nanoparticles loaded with doxorubicin and paclitaxel for brain glioma treatment, Biomaterials. 34 (2013) 8511–8520.

[132] C.W. Gan, S.-S. Feng, Transferrin-conjugated nanoparticles of Poly(lactide)-d-α-Tocopheryl polyethylene glycol succinate diblock copolymer for targeted drug delivery across the blood–brain barrier, Biomaterials. 31 (2010) 7748–7757.

[133] H. Chen, Y. Qin, Q. Zhang, W. Jiang, L. Tang, J. Liu, Q. He, Lactoferrin modified doxorubicin-loaded procationic liposomes for the treatment of gliomas., Eur. J. Pharm. Sci. 44 (2011) 164–173.

[134] G. Kibria, H. Hatakeyama, N. Ohga, K. Hida, H. Harashima, Dual-ligand modification of PEGylated liposomes shows better cell selectivity and efficient gene delivery, J. Control. Release. 153 (2011) 141–148.

[135] A. Salvati, A.S. Pitek, M.P. Monopoli, K. Prapainop, F.B. Bombelli, D.R. Hristov, P.M. Kelly, C. Åberg, E. Mahon, K.A. Dawson, Transferrin-functionalized nanoparticles lose their targeting capabilities when a biomolecule corona adsorbs on the surface, Nat. Nanotechnol. 8 (2013) 137–143.

[136] L. Qin, C.-Z. Wang, H.-J. Fan, C.-J. Zhang, H.-W. Zhang, M.-H. Lv, S.-D. Cui, A dual-targeting liposome conjugated with transferrin and arginine-glycine-aspartic acid peptide for glioma-targeting therapy., Oncol. Lett. 8 (2014) 2000–2006.

[137] P. Zhang, L. Hu, Q. Yin, L. Feng, Y. Li, Transferrin-modified c[RGDfK]-paclitaxel loaded hybrid micelle for sequential blood-brain barrier penetration and glioma targeting therapy., Mol. Pharm. 9 (2012) 1590–1598.

[138] X. Wei, J. Gao, C. Zhan, C. Xie, Z. Chai, D. Ran, M. Ying, P. Zheng, W. Lu, Liposome-based glioma targeted drug delivery enabled by stable peptide ligands., J. Control. Release. 218 (2015) 13–21.

[139] F.C. Lam, S.W. Morton, J. Wyckoff, T.-L. Vu Han, M.K. Hwang, A. Maffa, E. Balkanska-Sinclair, M.B. Yaffe, S.R. Floyd, P.T. Hammond, Enhanced efficacy of combined temozolomide and bromodomain inhibitor therapy for gliomas using targeted nanoparticles, Nat. Commun. 9 (2018) 1991.

[140] G.H. Jo, O. Bögler, Y.-J. Chwae, H. Yoo, S.H. Lee, J.B. Park, Y.-J. Kim, J.H. Kim, H.-S. Gwak, Radiation-induced autophagy contributes to cell death and induces apoptosis partly in malignant glioma cells, Cancer Res. Treat. 47 (2015) 221–241.

[141] A. Casao, M. Mata-Campuzano, L. Ordas, J.A. Cebrian-Perez, T. Muino-Blanco, F. Martinez-Pastor, Cleaved PARP-1, an Apoptotic Marker, can be Detected in Ram Spermatozoa., Reprod. Domest. Anim. 50 (2015) 688–691.